Gamma Radiation Shielding Analysis of Clay doped with Fe_2O_3-rich additive complemented with Alucobond panels: A study of Am241, Cs137 and Co-60

By

Daniel Nii Adjei (10358534)

M.Phil. Applied Nuclear Physics (2012)

B.Sc. Physics (KNUST), 2009

This thesis is submitted to the University of Ghana, Legon

In partial fulfillment of the requirements for the award of

PhD. Applied Nuclear Physics Degree.

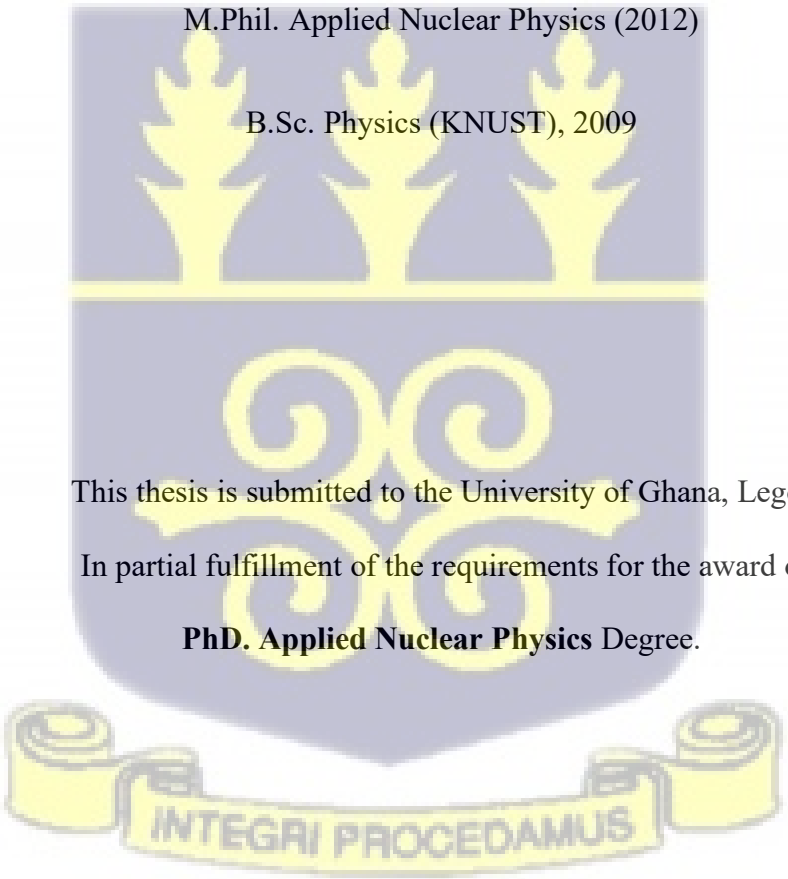

September, 2024

DECLARATION

This is to certify that this thesis is the result of research undertaken by Daniel Nii Adjei towards the award of the Doctor of Philosophy degree in the Department of Nuclear Sciences and Applications, School of Nuclear and Allied Sciences, University of Ghana.

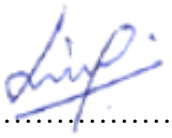

17-12-2025

Daniel Nii Adjei (Candidate) — Date

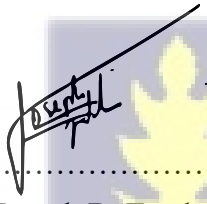

18-12-2025

Dr. Joseph B. Tandoh (Supervisor) — Date

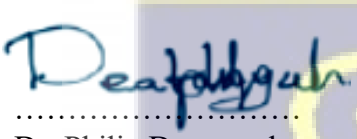

18/12/2025

Dr. Philip Deatanyah (Co-supervisor) — Date

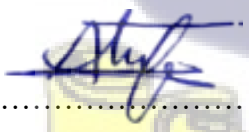

18/12/2025

Dr. Amos Forson (Co-supervisor) — Date

ABSTRACT

Clay from six known clay deposits in Ghana, namely Oframase and Amperkrom in the Eastern region, Okyreko and Assin Fosu in the Central region, and Abokobi and Kinbu in the Greater Accra Region have been studied for their gamma shielding properties against Am-241, Cs-137 and Co-60 representing lower, middle and large photon energy ranges respectively. Their shielding performance was investigated when they were undoped (X0 series), and then doped at 5% wt (X1 series) and 10% wt (X2 series) of an Fe_2O_3-rich additive and subsequently coupled to Aluminium composite panels (Alucobond) to evaluate the overall performance.

The samples, both doped and undoped exhibited a range of densities, with values spanning from 1.651 g/cm³ (FOS-X0) to 2.069 g/cm³ (ABK-X2). It was noted that the additive, as well as the clay materials own elemental composition and the grain size distribution contributed to the density of the test pieces. With 5% by wt doping the increase in density of the samples ranged from 0.94% - 2.97%, while at 10% wt doping it improved by 3.62% - 8.76%.

For Am-241, the linear attenuation coefficients (LAC) show variability, with values ranging from 0.372 ± 0.0012 cm^{-1} (FOS-X0) to 0.596 ± 0.0022 cm^{-1} (ABK-X2), reflecting differences in the clays' ability to attenuate radiation. The mass attenuation coefficient (MAC), which accounts for both the material density and the attenuation properties, follows a similar trend, ranging from 0.225 cm^2g^{-1}(FOS-X0) to 0.296 cm^2g^{-1} (OKY-X2). In the case of Cs-137, the LAC ranged from 0.116 ±0.0009 cm^{-1} (FOS-X0) to 0.145 ±0.0016 cm^{-1} (ABK-X2) while the MAC ranged from 0.0675 cm^2g^{-1}(AMK-X0) to 0.0707 cm^2g^{-1} (OKY-X2).

Similarly, considering Co-60, the LAC ranged from 0.08±0.0018 cm^{-1} (FOS-X0) to 0.107±0.0029 cm^{-1} (ABK-X2) while the MAC ranged from 0.0484 cm^2g^{-1}(FOS-X0) to 0.0517 cm^2g^{-1} (ABK-X2).

The results show that for Am-241, the dopant addition at 10% wt contributes to the 22.13% to 37.10% in LAC improvement. In the case of Cs-137 it results in 16.60% to 26.05% in LAC increase, while a 5.07% to 11.81% increase in LAC is observed for Co -60. Conversely, the increase in LAC when the clays are doped with 5% wt additive is less pronounced, not exceeding 3.5% for all the clays and photon energies investigated. LAC values in this study for the various samples were also corroborated by MCNP simulation.

The variability in LAC and MAC across the samples can be attributed to differences in their elemental and mineralogical composition, particularly the presence of elements like iron, aluminum, and silica, which influence their radiation absorption capabilities. For instance, the Al content ranges from 36,643 mg/kg (OKY-X0) to 136,386 mg/kg (FOS -X0), while Fe concentrations span from 10,166 mg/kg (FOS-X0) to 78,290 mg/kg (AMK -X2). Silicon (Si) concentrations also exhibit variation, ranging from 183,669 mg/kg (FOS-X2) to 276,740 mg/kg (ABK-X2). Other elements such as potassium (K) and titanium (Ti) are also present but in smaller quantities, although they impact the density of the clays. K concentration levels ranged from 1,406 mg/kg (OFM-X0) to 5,173 mg/kg (FOS-X1), and Ti concentrations varied between 1,524 mg/kg (FOS-X2) to 4,636 mg/kg (OFM-X0). These elements play a crucial role, especially in ceramic and material science.

These results confirm theory that density strongly correlate with linear attenuation coefficient for photon shielding which is energy dependent.

Overall, the research's finding highlights the prospect of clay doped with Fe_2O_3 for shielding low energy photons particularly for medical applications relying on ABK-X2 clay which is the densest composite clay material investigated as a case in point. If Alucobond panels which is used as wall finishing is incorporated as an extra layer, ABK-X2 clays' LAC performance will over-perform that of ordinary concrete at lower energies. This is particularly true, for the medical range of X-ray energies (30 keV to 150 keV) for purposes of diagnostic imaging such as mammography, general radiography and computed tomography (CT) scans. Consequently, all things being equal, the walls of a medical diagnostics facility can be built by using locally sourced clay particularly OKY-X2 or ABK-X2 clay which is the densest and doped at 10% wt of the Fe_20_3 oxide (71% purity) additive used in this study. The clay can safely be used in place of ordinary concrete to shield expected photon energies in such a facility which would be less than 150keV. Furthermore, adding an Alucobond panel to a fixed thickness of clay would improve the required 5 and 7 HVLs shielding performance by 7.3% and 14.1% for one surface paneling and two surface paneling respectively. The clays together with any of the Aluminum composite panels (Alucobond) defined in this study ensure that more than 99% of the initial radiation is attenuated.

Further studies on clay densification like firing at higher temperatures and the effects of addition of other dopants such as Titanium oxide to enhance shielding performance of clay is recommended.

DEDICATION

I dedicate this work to the glory of God Almighty.

And to my beloved family; my dear Evelyn Kabuky, my parents – Daniel and Comfort, and my sister Gloria as well as my very good friends and mentors for their unflinching support, sacrifice, patience and love.

And to seekers of knowledge like you who find this thesis and its contents useful.

ACKNOWLEDGEMENTS

Sincere thanks to the Almighty God for His provision and love throughout this study.

I am grateful to my supervisors, Dr. J. B. Tandoh, Dr. P. Deatanyah, and Dr. A. Forson all at School of Nuclear and Allied Sciences (SNAS), University of Ghana for their insight, contributions and successful supervision of this research.

I am also very grateful to Prof. S. B. Dampare, Prof. J.K. Amoako, Dr. E.T Glover, Prof. S. Inkoom and Prof. Kpeglo for their personal interest and pieces of advice and encouragement to complete the work. Also, to the entire Faculty of SNAS, I say thank you for their contributions to shape this work.

To the helpful team at the Ghana Geological Survey Authority, especially Mr., L. Asare, Mr. Ofori, Mr. Ahmed, Mr. T. Tenkorang, Mr. Awan Mohammed and Mr. Emmanuel Effum, thank you for your assistance during sampling, sample preparation, moulding and physical tests of clays.

To the Management and staff of Radiation Protection Institute (RPI), of the Ghana Atomic Energy Commission (GAEC), thank you for the opportunity to use your equipment and facilities for the radiation experiments. Dr. Deatanyah, thank you for your tutoring and assistance with the simulation and modelling.

To all my colleagues at the Secondary Standards Dosimetry Laboratory (SSDL) of the Health Physics Centre (HPC), as well as the Nuclear Safety and Security Centre (NSSC), all of RPI, GAEC, I say thank you. Also, to my cherished friends, including Dr. T. B. Dery and Dr. M. Pokoo-Aikins and the very many well-wishers, you have been supportive and encouraging all through the journey.

To you all I offer my sincere thanks and say God richly bless you.

TABLE OF CONTENT

LIST OF TABLES

LIST OF FIGURES

LIST OF ABBREVIATIONS

ALARA – As low As Reasonably Achievable

BS – British Standard

GAEC - Ghana Atomic Energy Commission

GGSA – Ghana Geological Survey Authority

GPS – Global Positioning System

GSD- Geological survey Department

HVL – Half Value Layer

IAEA- International Atomic Energy Agency

LAC Linear Attenuation Coefficient

MAC – Mass Attenuation Coefficient

mfp – Mean Free Path

NCRP – National Council on Radiation Protection and Measurements

NIST – National Institute of Standards and Technology

RPI – Radiation Protection Institute

TLD – Thermoluminescence Dosimeter

TVL – Tenth Value Layer

CHAPTER ONE

INTRODUCTION

1.1 Background

Clay is a natural material that has been used by humans for thousands of years in various applications. It is one of the oldest and most versatile materials known to humanity, playing a crucial role in industries such as ceramics, agriculture, construction, and even in scientific research. The term "clay" generally refers to fine-grained, natural earth materials that are plastic when wet and harden upon drying or heating. Clay materials are primarily composed of fine particles, typically smaller than 2 micrometers, and consist of mineral fragments that are rich in hydrous silicates of aluminum. The mineral composition can vary, and clays may contain other elements such as magnesium, calcium, iron, and potassium in different proportions, which contribute to their chemical and physical properties (Jackson, 1969).

Clay minerals are classified into several groups based on their structure and chemical composition. The most common types of clay minerals include kaolinite, montmorillonite, illite, and smectite. These minerals are typically composed of silicate layers (SiO_2) and alumina (Al_2O_3), with varying amounts of water incorporated into their structures. The presence of water in clay minerals gives them their plasticity, which allows them to be molded into different shapes when wet. Upon drying, clays harden, making them useful for a variety of construction and decorative purposes (Brindley & Brown, 1980).

Beyond its aesthetic and industrial uses, clay is also valued for its geotechnical properties and has been studied for its role in radiation shielding. Clays, particularly when combined with other materials such as barite or iron ore, have demonstrated promising properties for attenuating ionizing radiation, including gamma rays and neutron radiation. This has sparked interest in utilizing clays as a low-cost, environmentally friendly alternative to more traditional radiation shielding materials like lead or concrete (Isfahani, et al., 2018).

In construction, clay is used extensively in the form of bricks, tiles, and other building materials. The porosity and density of clay-based products can vary depending on their composition and the method of manufacture. Clays with higher mineral content, such as kaolinite, are often used in fine ceramics, while other types, such as bentonite or montmorillonite, are valued for their absorbent properties and use in sealing and construction materials (Murray, 2007).

In addition to its widespread use in building and industrial applications, clay also has environmental and ecological importance. As a natural material, clay is abundant and often locally sourced, which reduces the carbon footprint associated with its transportation and production. Moreover, its natural occurrence and biodegradability make it a more sustainable material in contrast to synthetic alternatives. Recent advancements in material science have explored enhancing the properties of clays to improve their performance in specific applications, such as in radiation protection and waste management (Elsafi,., 2021).

.

Clay-based materials are particularly attractive in radiation shielding applications due to their low cost, availability, and ease of modification. As the global demand

for radiation shielding materials grows, especially in nuclear facilities, hospitals, and other settings dealing with radiation, there is a growing interest in materials that can provide effective protection without the environmental and economic drawbacks of traditional shielding options. Studies on the attenuation properties of clay have demonstrated that with proper composition and treatment, clay-based materials can provide significant protection against harmful radiation, particularly gamma rays and neutrons. This makes clay not only an essential material in construction and ceramics but also a promising candidate for sustainable and effective radiation shielding in various industries (Khattari, et al 2023)

Radiation interacts with matter in various ways, and the impact of radiation on a material depends on the energy, type, and properties of the radiation involved. Ionizing radiation, which includes gamma rays, x-rays, neutrons, and charged particles -alpha and beta, carries sufficient energy to ionize atoms in its path, causing molecular damage that can result in harmful biological effects (Harrison & Muirhead, 2003).

Gamma radiation, in particular, is a significant concern because it can penetrate most materials and is potentially dangerous to humans if not properly shielded. Gamma rays, being high-energy photons, can travel through materials without significant attenuation unless they interact with matter through processes such as photoelectric absorption, Compton scattering, or pair production (Glasstone & Sesonske, 2004). As a result, shielding materials must possess high density and atomic number (Z) to be effective in attenuating gamma rays. Dense materials,

such as lead, concrete, and steel, are commonly used to provide effective shielding against gamma radiation.

In contrast, neutron radiation, which includes fast neutrons and thermal neutrons, requires different shielding strategies. Neutrons interact with matter primarily through elastic scattering with light nuclei, such as hydrogen, making materials rich in hydrogen (e.g., water or polyethylene) ideal for neutron shielding (Lamarsh & Baratta, 2001). However, gamma rays and neutrons are not the only types of radiation that pose a hazard. Alpha and beta particles, while they have limited penetration abilities and are mostly a concern for internal exposure, can be shielded easily by materials such as paper or clothing.

1.2 Statement of the Problem

A significant problem with using ordinary concrete for photon shielding, especially in Ghana and Africa, is its high environmental impact and resource demand in production.

Cement a major component of concrete production releases about 0.93 tons of CO per ton produced, contributing to 8% of global CO emissions, which is a major concern for Africa's low-carbon development programme (Sullivan & Olson 2022; Kullman, 2023). Additionally, the major raw materials used to produce concrete; cement has its major constituent clinker imported straining scare foreign exchange. Generally, high-quality aggregates that can enhance the density of concrete are often scarce in some regions of Ghana as well as other African regions, leading to reliance on imported materials, which can increase

concrete costs by up to about 30% due to transportation and logistics (Adinkrah-Appiah, et al 2015; Danso & Obeng-Ahenkora,(2018). Ordinary concrete's composition is not easily modified to enhance photon shielding, making it less flexible than other materials, like modified clay or specialized concrete mixes, which can incorporate heavy elements for better radiation protection. Beyond ordinary concrete, lead is also a well establish photon shielding material, however, it is known to have high toxicity when internalized coupled to its minimal production in Ghana. These challenges highlight the need for alternative, and environmentally sustainable materials for photon shielding.

Considering that clay is also a building material and Ghana has abundant clay deposits, it is important to study its shielding properties to check their suitability as photon shielding.

1.3 Objective(s)

The main objective of the study is to investigate the impact of Fe_2O_3-rich oxide dopant and Alucobond panels on Am-241, Cs-137 and Co-60 gamma radiation shielding effectiveness of selected clays sourced from Ghana.

1.3.1 Specific Objectives

The study specially seeks to

i. Carry out elemental composition analysis and physico-mechanical tests (i.e. density, porosity and grain size distribution) of the selected clay samples to investigate their influence on some physical and shielding parameters of selected clays.

ii. Carry out shielding performance assessment by radiation transmission tests on sample test pieces – both doped and undoped with the addition of Alucobond panels to obtain shielding parameters. i.e. Linear Attenuation Coefficient (LAC), Mass Attenuation Coefficient (MAC), Half value Layer (HVL), Tenth Value Layer (TVL), mean free path (mfp) Build up factor (B).

iii. Perform MCNP simulation to compare with some of the shielding parameters (i.e. LAC and B).

iv. Demonstrate the feasibility and suitability of using locally sourced raw materials such as clays for photon shielding and radiation protection purposes.

1.4 Relevance and Justification

Fired clay bricks offer a sustainable, cost-effective solution for photon shielding especially in areas, where clay is locally abundant, reducing transportation costs to compared to imported concrete (Al-Asadi, (2022); Nzivulu et al. (2024).). Fired clay bricks have embodied CO_2 of about 0.22 kg CO_2 per kg, compared with about 0.13 kg CO_2 per kg for normal concrete. When clay is locally sourced and fired efficiently, clay masonry can still contribute to Africa's low-carbon development goals (Alexander & Mindess, 2015; Asdrubali, et al (2023).). Enhanced with iron oxides, fired clay bricks achieve comparable photon attenuation to ordinary concrete, making them suitable for shielding in essential facilities like hospitals (Mori et al., 2020). Furthermore, fired clay bricks have a

lower embodied energy of 2.5-3.0 MJ/kg versus concrete's (cement's) 5.0-7.0 MJ/kg, reducing the environmental footprint significantly (Mahboob, et al., (2021); Asdrubali, et at., (2023)).

Ghana has large clay deposits. Clay a as material is versatile and has many uses both domestically and industrially. Interestingly, in Ghana currently, there are several applications of nuclear and radioactive materials for which there are numerous plans to expand applications of these materials. It is also planned that Ghana will introduce nuclear power into its energy mix. Therefore, these current and future radioactive and nuclear materials utilized or to be utilized in the country have to be safely and securely stored or transported whiles in the country.

This study, has demonstrated the potential of developing and improving upon existing material composites to aid the enhancement of radiation protection, nuclear safety and security.

1.5 Scope of work

In this work, properties such as, elemental composition, attenuation coefficient, half- value layer tenth value layer of three radionuclides emitting photon energies, density, mechanical strength of the prepared shielding material have been carried out. These properties have been chosen because they adequately describe a good shielding material. Clay has been chosen because when fired, it compares very well with concrete in terms of density.

Selection of the sampling sites for the clay were based on some considerations. These include areas with proven large deposits of clay, areas with clay-based industry, areas that are readily accessible within the south-eastern regions of

Ghana. The photons studied are Americium (Am241) as cesium (Cs-137) and cobalt (Co-60) which are two of the most widely used gamma emitting radioisotopes.

This study focuses on clay sourced from Ghana and their suitability for developing composite radiation shielding material. The work entails the performance of theoretical calculations, performance of computer simulations and the conduct of experiments where possible.

The project will culminate in a comparative study of the clay composite materials.

1.6 Theoretical and Conceptual Framework

This study is grounded in an interdisciplinary theoretical and conceptual framework that integrates radiation interaction physics, material science, clay mineralogy, Monte Carlo radiation transport modeling and sustainable materials engineering implemented through a combination of experimentation, simulation and theoretical analysis where applicable. Together, these frameworks guide the investigation of how Ghanaian clays -modified with Fe_2O_3-rich dopants and Alucobond panels -attenuate gamma radiation from Am-241, Cs-137, and Co-60.

The study is underpinned and synthesized considering the following:

i. **Radiation–Matter Interaction Theory**

The attenuation of gamma photons is described by the Beer–Lambert law, where interaction mechanisms - photoelectric absorption, Compton scattering, and pair production - depend on the density, atomic number, and electron structure of the

shielding material. This theory provides the basis for determining shielding parameters such as LAC, MAC, HVL, TVL, mean free path, and buildup factors.

ii. **Material Science and Composite Engineering**

The study relies on the principle that the physical and structural properties of materials (density, porosity, grain size, elemental composition) directly influence their radiation attenuation performance. Incorporating Fe_2O_3-rich oxides and Alucobond panels is theoretically supported by composite material frameworks which predict improved density, effective atomic number, and structural stability.

iii. **Clay Mineralogy**

Clay's microstructure, mineral composition (e.g., kaolinite, montmorillonite, illite), and firing behavior affect its density and porosity after processing. These mineralogical characteristics justify the use of modified Ghanaian clays as potential shielding materials.

iv. **Monte Carlo Transport Theory (MCNP)**

MCNP simulations model photon transport and validate experimental attenuation results based on probabilistic interaction cross-sections. This theoretical approach ensures alignment between measured and simulated shielding behaviors.

v. **Sustainability and Local Resource Utilization**

This framework emphasizes the environmental and economic benefits of using locally sourced clay with low embodied energy and reduced carbon

footprint as an alternative to concrete or lead in Ghana's radiation protection needs.

Overall Integrated Conceptual Framework:

Material modification (i.e. Fe_2O_3 addition coupled with Alucobond layering) alters the physico-mechanical and microstructural properties of Ghanaian clays, which in turn influences gamma photon attenuation performance. Experimental measurements, supported by MCNP simulations and sustainability analysis, determine the suitability of modified clays as viable photon shielding materials.

1.7 Structure of thesis

This thesis is presented in five chapters.

Chapter one introduces the work carried out in the research. It gives a background and states the necessity for the research and also defines its scope.

The second chapter is a review of the relevant literature to establish a foundation for the work and support an effective understanding of the research. It provides the context for this research work.

Chapter three lays out the methodology used. It describes and explains the various equipment, experimental procedures and analytical techniques used in the research.

The next chapter, is devoted to results obtained and their discussions within the context of available scientific literature.

Chapter five concludes the writeup and contains a summary of the work done. Additionally, it highlights the implication and relevance of the results based on

which recommendations are made. Following chapter five are references and appendices.

CHAPTER TWO

LITERATURE REVIEW

This chapter is a review of relevant literature on the study.

2.1 Clay

Clay is a natural, fine-grained material composed primarily of minerals that form through the weathering of rocks, particularly silicate-rich rocks such as granite. It has been used throughout human history for a variety of purposes, ranging from pottery and brick-making to modern applications in construction, medicine, and environmental management. The diversity of clay types, properties, and potential uses has generated considerable academic interest. This literature review synthesizes research on the various properties, applications, and advancements in the study of clay, with a focus on its physical, chemical, and environmental characteristics.

2.1.1. Properties of Clay

2.1.1.1 Mineralogical Composition

Clays are primarily composed of phyllosilicate minerals, which include kaolinite, illite, smectite, and vermiculite. The differences in these mineral types significantly affect the clay's behavior and applications. For example, kaolinite, a common clay mineral, is characterized by a relatively low plasticity, making it ideal for porcelain production. In contrast, smectite clays, such as

montmorillonite, are highly plastic and can absorb large amounts of water, making them suitable for drilling muds and other industrial applications (Murray, 2007).

2.1.1.2 Physical Properties

Clays exhibit a wide range of physical properties, including plasticity, shrinkage, and porosity. These properties are influenced by the mineral content, particle size distribution, and water content. Plasticity, in particular, is a key characteristic, influencing the moldability of clay for uses such as ceramics and construction. Shrinkage occurs when clay dries, which can lead to cracking if not managed properly (Andrade, et al (2011). Furthermore, clay's porosity and ability to adsorb water make it a vital material in environmental and geotechnical engineering applications (Bergaya & Lagaly, 2013).

2.1.1.3 Chemical Properties

Clay's surface charge and ion-exchange capacity are crucial for its interactions with other substances, such as water, salts, and organic compounds. The surface charge is primarily negative, which allows clays to adsorb cations, such as sodium, calcium, and potassium, from surrounding environments. This property is essential in understanding the behavior of clays in natural systems, such as soils and groundwater (Barrett et al., 1951).

2. 1.2. Applications of Clay

2.1.2.1 Ceramics and Pottery

One of the oldest and most well-known uses of clay is in the production of ceramics. The ease of shaping and firing clays into durable objects has made them indispensable in the creation of pottery, bricks, and tiles. Research has focused on optimizing the properties of clay bodies, such as their plasticity, firing temperature, and color, to improve the quality and efficiency of ceramic products (Hughes, 1985).

2.1.2.2 Construction Materials

Clay has long been a fundamental material in construction, particularly in the form of bricks, tiles, and adobe. The energy-efficient properties of clay in terms of thermal insulation, moisture regulation, and acoustic performance have prompted extensive studies into improving its use in green building practices. For instance, rammed earth construction, which utilizes compacted clay, has gained popularity as a sustainable building method (Mitsch, & Gosselink, 2007).

2.1.2.3 Environmental Remediation

Clays are increasingly used in environmental engineering, especially in the containment and remediation of hazardous materials. Their ability to adsorb and immobilize pollutants, including heavy metals and organic contaminants, has been the subject of extensive research. For example, smectite clays, due to their high surface area and ion- exchange capacity, have shown promise in the removal of toxic substances from water and soil (McBride, 1994).

2.1.2.4 Medicine and Health

Clay minerals have been utilized in medicine, particularly in the form of medicinal clay or "therapeutic clay" for various health-related treatments. Studies have demonstrated that certain clays possess antimicrobial properties and are used in wound healing, detoxification, and skin care (Tisserand & Young, 2014). Additionally, some clays have been investigated for their use in drug delivery systems due to their ability to encapsulate and release substances in a controlled manner (Massaro, et al. ,2018).

2.1.2.5 Geotechnical Engineering

Clays play a critical role in geotechnical engineering, particularly in the study of soil behavior and stability. The interaction between clays and water significantly affects the engineering properties of soils, such as shear strength, consolidation, and settlement. Research in this field focuses on understanding the mechanisms of clay-water interactions, especially in the context of foundation engineering, landslides, and soil stabilization (Das, 2007).

2.1.3 Recent Advances in Clay Research

2.1.3.1 Clay Nanomaterials

In recent years, research has focused on the use of nanoclays in various technological and industrial applications. Nanoclays, which are clays that have been reduced to the nanoscale, possess unique properties such as increased surface area, enhanced mechanical strength, and improved chemical reactivity (Uddin, et al., (2024). These properties make nanoclays useful in a variety of applications,

including in nanocomposite materials, drug delivery systems, and as catalysts in chemical reactions.

African researchers are actively exploring the potential of clay nanomaterials in various fields. For instance, a study from Nigeria investigated the use of kaolin-based nanocomposites for the development of lightweight, strong, and heat-resistant materials for the automotive industry (Mokwa, et al., (2019)). This innovation could lead to the production of more sustainable materials in African industries.

2.1.3.2 Clay in Wastewater Treatment

Recent research has focused on the development of clay-based materials for the treatment of wastewater. The use of clays in filtration, adsorption, and catalytic processes has been widely studied for the removal of contaminants, such as dyes, heavy metals, and organic pollutants. Studies have explored methods of modifying clay surfaces to enhance their efficiency in removing specific contaminants (Dhar et al., (2023)).

2.1.3.3 Clay and Climate Change Mitigation

Clays have been examined for their role in mitigating the impacts of climate change, particularly in carbon sequestration. Clays have the potential to adsorb carbon dioxide, and research is investigating their use in enhanced weathering processes as a means of capturing atmospheric CO_2 (Ciotta & Tassinari 2024). This has led to an emerging field of study regarding the use of clays in sustainable climate change mitigation strategies.

2.2 Radiation

2.2.1 Radiation Types and Their Shielding

Radiation shielding is an essential approach in protecting people and the environment from the potential harmful effects of exposure to radiation that may arise from hospitals, industrial settings and nuclear power plants. Radiation, which is energy in motion either as a particle or a wave can be categorized into different types based on the energy and particles involved. The different types of radiation interact with matter in distinct ways. Thus, the shielding materials required to protect against each differ in their physical and chemical properties.

2.2.1.1 Types of Radiation

The types of radiation can be grouped into two main categories- ionizing and non-ionizing. Ionizing radiation refers to radiation that has enough energy to remove tightly bound electrons from atoms, creating ions. On the other hand, non-ionizing radiation is only capable of causing excitation but not ionization.

2.2.1.1.1 Ionizing radiation

Alpha particles, beta particles, gamma rays, x-rays, and neutrons are the major types of ionizing radiation. They are differentiated by their physical properties and interactions with materials, influencing the choice of shielding materials.

2.2.1.1.1.1 Alpha Particles (α)

Alpha particles, consist of two protons and two neutrons and are emitted from the nucleus of heavy elements like uranium and radon. Due to their relatively large mass and charge, alpha particles have a very low penetrating ability. They can be

stopped by a sheet of paper, the outer layers of skin, or a few centimeters of air. They are highly dangerous when ingested. They are best shielded by materials with very low atomic numbers (low-Z materials) like paper, plastic, or clothing.

2.2.1.1.1.2 Beta Particles (β)

Beta particles on the other hand are high-energy, high-speed electrons or positrons emitted from the nucleus of radioactive atoms during beta decay. They are smaller than alpha particles and penetrate materials better than alphas, but nonetheless lose their energy relatively quickly when interacting with matter. The penetration ability of beta particles depends on their energy, and they can be stopped by materials like glass, plastic, or a few millimeters of aluminum. Similar to alphas, they can be hazardous if the radioactive material is inside the body, since beta particles can penetrate the outer skin layers and cause internal damage Beta radiation can be shielded by materials like plastic, aluminum or glass. The thickness of the material depends on the energy of the beta particles. For higher energy beta particles, thicker or denser materials may be needed to absorb more energy and prevent penetration.

2.2.1.1.1.3 Photons - Gamma Rays (γ) and X-rays

Gamma rays and X-rays are both forms of electromagnetic radiation (photons), but come from different sources. Gamma rays are emitted by the nucleus of radioactive atoms, whereas X-rays are produced by electrons outside the nucleus. Both types of radiation have extremely high energy and can penetrate through most materials. Gamma rays, in particular, are very dangerous due to their ability to penetrate human tissue and cause significant damage to cellular DNA. They can pass through

large distances of air and solid materials, requiring dense materials to effectively reduce their intensity.

They best shielded using dense materials, like Lead (Pb), concrete, steel or iron which can absorb or scatter the high-energy photons. Common shielding materials include: The gamma energy dictate the thickness of the shield that will be required to bring the radiation intensity to desirable levels.

2.2.1.1.1.4 Neutron Radiation (n)

Neutrons are uncharged particles. Unlike charged particles like alpha and beta particles, they do not interact electromagnetically with matter. However, they can cause nuclear reactions like activation in certain materials, making them quite dangerous in some application like nuclear reactors and accelerators. Neutrons can penetrate through materials and can even travel long distances through air. Neutron interactions with nuclei in materials can lead to the emission of gamma rays, which make shielding them more complex requiring a multifaceted approach to shield against them.

Unlike photons, lead is not a good material for shielding neutrons. Hydrogen-rich materials water or polyethylene serve as the best neutron shields since hydrogen atoms are effective at slowing down fast neutrons through elastic scattering. Once neutrons are slowed down to lower energies, they are more likely to be absorbed by materials like borated polyethylene, boron, or lithium. Concrete mixed with boron or other neutron-absorbing compounds can also serve as effective neutron shields.

2.2.3 Fundamental Concept and Principle of Radiation Shielding

Radiation shielding is a critical field in both health physics and engineering, focused on protecting people, equipment, and the environment from the harmful effects of ionizing radiation. The fundamental concept of radiation shielding is based on the principle of reducing the intensity of radiation by placing an absorbent material between the radiation source and the exposed entity. The effectiveness of shielding depends on several factors, including the type of radiation, the energy of the radiation, and the material properties of the shielding substance.

Ionizing radiation, including alpha particles, beta particles, gamma rays, and X-rays, poses various risks, and each type requires specific shielding strategies. Alpha particles, which have a relatively large mass and charge, can be effectively blocked by a thin sheet of paper or even human skin. Beta particles, being smaller and more penetrating, require denser materials like plastic, glass, or aluminum to stop them. Gamma rays and X-rays, which are highly penetrating electromagnetic radiation, demand much denser and thicker shielding materials, typically made of lead or concrete, to attenuate their energy (Martin & Harbison, 2013)

2.2.4 Factors Affecting Shielding Efficiency

The efficiency of shielding depends on several factors, including the type of radiation, its energy, and the chemical properties like atomic number of constituent elements and of the physical properties such as density shielding material. As well the thickness of a particular radiation type influences the shielding effectiveness.

There are several factors that influence the effectiveness of radiation shielding. Material density is one of the most important properties, as denser materials contain more atoms per unit volume, which increases the probability of radiation interaction. For example, lead is a commonly used material for gamma and X-ray shielding because of its high atomic number and density, which enhances its ability to absorb radiation. The energy of the radiation also plays a significant role in shielding effectiveness; higher-energy radiation requires thicker or denser materials to achieve the same level of attenuation.

In addition to material properties, the geometry of the shielding is important. The distance between the radiation source and the shield, as well as the angle at which the radiation interacts with the shielding material, affects the amount of protection provided. Increasing the distance from the source is an effective secondary strategy, as radiation intensity decreases with the square of the distance from the source, known as the inverse square law (Hall & Giaccia, 2018).

2.2.5 Radiation Shielding Materials and Their Effectiveness

In radiation protection, various materials are used to reduce the energy of radiation interacting with matter. The effectiveness of these materials in attenuating radiation depends on their atomic number, density, and the type of radiation they are intended to shield against. According to recent research, shielding materials can be broadly categorized into three groups based on their primary function: gamma radiation attenuation, neutron moderation, and neutron capture. Gamma rays, being highly penetrating, require dense materials to effectively reduce their energy. Heavy or moderately heavy elements, such as lead or tungsten, are commonly employed for this purpose, as they can attenuate gamma radiation

through processes like photoelectric absorption and Compton scattering (Ahmad, et al 2024). These materials are particularly effective in shielding fast gamma rays but are less efficient for thermal neutrons.

For neutron protection, materials rich in hydrogen, such as polyethylene, are frequently used. Neutron shielding requires moderation, or slowing down of fast neutrons, and hydrogen-rich materials are highly effective at moderating neutrons through elastic collisions. Neutrons with energies above approximately 1 MeV can be slowed down to thermal energies by repeated collisions with light nuclei, like hydrogen (Chang, et al., 2023). These materials are particularly useful for reducing neutron flux in nuclear reactors, where neutrons are produced as byproducts of fission reactions.

The third category of shielding materials includes those with high neutron capture cross -sections, such as boron or lithium. These materials are particularly effective at absorbing neutrons, especially in environments with high neutron flux. Boron, often used in the form of borated polyethylene, has a high thermal neutron capture cross- section, making it ideal for applications that require both neutron moderation and absorption (Shultis & Faw 2010)

These materials are widely used in the control rods of nuclear reactors, where they serve to absorb excess neutrons and control the chain reaction.

The most effective radiation shielding materials often combine these three properties. For example, a material might consist of a dense core to attenuate gamma radiation, surrounded by a hydrogen-rich layer to moderate neutrons, with

additional elements to capture and absorb remaining neutrons. Such composite materials are increasingly being explored in modern nuclear safety applications (Shahzad, et al., 2023). The choice of shielding material also depends on several practical considerations. The National Council on Radiation Protection and Measurements (NCRP, 1970) highlights the importance of factors such as the material's uniformity, permanence, required thickness, weight, cost, and installation challenges. Furthermore, aesthetic considerations may also play a role, particularly in the construction of radiation protection in accessible or public areas.

Common shielding materials, including concrete, water, lead, aluminum, and steel, are widely used in various applications. Concrete is often the material of choice for large- scale nuclear facilities due to its low cost and versatility. Lead is highly effective for gamma shielding but is less suitable for neutron moderation. Water, with its high hydrogen content, is an effective neutron moderator and is often used in reactor cooling systems where both radiation shielding and heat removal are necessary (Shultis & Faw 2010). Each of these materials has its strengths and weaknesses, and the optimal choice depends on the specific radiation protection requirements of a given application.

2.3 Photon Shielding

Photon shielding is a crucial aspect of radiation protection in various fields, such as nuclear medicine, radiology, space exploration, and nuclear power. In shielding photons, materials that are dense are preferred. These typically include, lead (Pb), concrete, and steel.

Concrete, particularly in its different forms, has long been studied for its effectiveness as a photon shielding material due to its availability, cost-effectiveness, and ability to attenuate radiation. Lead, on the other hand, is a well-established material for high- energy photon shielding due to its high density and atomic number. This literature review examines the recent developments in photon shielding, particularly focusing on concrete (ordinary and heavy), and lead as shielding materials, with special attention to advancements in their performance and applications.

2.3.1. Photon Shielding Principles

Photon shielding refers to the attenuation of high-energy photons (such as X-rays or gamma rays) as they pass through a material. The degree of attenuation depends on the material's atomic number (Z), density (ρ), and the energy of the photons. The relationship between photon intensity and distance traveled in a material follows the exponential attenuation law.

For photon shielding, materials with high atomic numbers and high density are often preferred because they offer higher probabilities of photon interactions.

2.3.2. Concrete as a Photon Shielding Material

Concrete is one of the most widely used materials for photon shielding, especially in the construction of radiation protection walls in nuclear facilities, radiological departments, and laboratories. Its advantages include low cost, ease of production, and the ability to provide substantial thicknesses for effective shielding.

2.3.2.1 Ordinary Concrete

Ordinary concrete, typically composed of cement, water, and aggregates (sand, gravel, or crushed stone), has a relatively moderate density (about 2.3 g/cm³) and is effective for shielding against low-energy photons (X-rays) or lower-intensity gamma rays. The shielding effectiveness of ordinary concrete is attributed to its constituent elements, mainly calcium (Ca), silicon (Si), and oxygen (O), but it is not as effective for higher energy photon attenuation compared to more specialized materials like lead or heavy concrete (Martin & Harbison 2013).

Recent studies have focused on improving the photon shielding properties of ordinary concrete by altering the mix design. The addition of heavy elements such as barite (BaSO) or magnetite (FeO) can enhance its shielding performance for gamma rays (El-Samrah, et al., 2023). However, the primary limitation of ordinary concrete is its relatively low atomic number and density, which restrict its use in applications requiring high photon attenuation, such as in nuclear reactors or high-energy radiation environments.

2.3.2.2 Heavy Concrete

Heavy concrete, also known as high-density concrete, is a modified version of ordinary concrete that incorporates heavy aggregates such as barytes, magnetite, or hematite. These materials are used to increase the overall density of the concrete, which in turn enhances its photon attenuation properties. Heavy concrete is commonly employed in applications such as radiation shielding walls, bunkers, and storage for radioactive materials. The attenuation properties of heavy concrete can be significantly improved compared to ordinary concrete. For example, concrete containing 30-40% barite has been shown to provide an attenuation

equivalent to that of lead in certain energy ranges, although it is still less effective at high photon energies (Akkurt, et al., 2010). Heavy concrete provides a cost-effective alternative to lead for environments where high- density materials are required but lead may be too expensive or difficult to handle due to its toxicity.

2.3.2.3 Recent Developments in Concrete Shielding

Recent research has explored the use of nano-materials and advanced cementitious compositions to further enhance the photon shielding effectiveness of concrete. For instance, incorporating nanoparticles such as bismuth oxide (Bi_2O_3) has been shown to improve the gamma-ray shielding properties of concrete, due to the higher atomic number of bismuth (El-Nahal, et al. (2021)). The use of hybrid composites that combine concrete with polymeric materials or other high-atomic-number substances has also been investigated to create lighter and more effective photon shielding materials for specific applications (Chang, et al., 2023)

2.3.3. Lead as a Photon Shielding Material

Lead has been the standard material for high-energy photon shielding for decades, due to its high atomic number (Z = 82) and high density (11.34 g/cm³). These properties make it highly effective at absorbing and scattering high-energy gamma rays and X- rays. Lead is commonly used in radiology, nuclear power plants, and in protective clothing for radiation workers.

2.3.3.1 Effectiveness of Lead

Lead's effectiveness in photon shielding is well-documented. It provides excellent attenuation for high-energy photons across a broad energy spectrum, including both X -rays and gamma rays. Martin & Harbison (2013) reports that for energies in the range of 100 keV to 1 MeV, lead offers superior shielding compared to other common materials like concrete. However, lead's disadvantages include its toxicity and environmental concerns, particularly in the disposal of lead-based shielding materials.

2.3.3.2 Recent Research on Lead-Based Shielding

Recent studies have focused on improving lead-based shielding through alloying or the development of lead-free alternatives. For instance, tungsten-based alloys are being considered as lead substitutes, offering similar shielding properties with reduced toxicity (AbuAlRoos, et al., 2020). Lead's high density makes it highly effective in compact shielding systems, but its environmental and health risks have led to increased interest in eco-friendly alternatives without compromising protection performance.

2.3.4. Comparative Studies: Concrete vs. Lead

The shielding effectiveness of concrete versus lead depends on several factors, including the photon energy, the application, and the required thickness of the shield. Studies comparing the two materials generally find that lead is more effective at attenuating high-energy photons, while concrete, especially heavy concrete, can be a more practical and cost-effective option for low- to medium-energy photon shielding.

Research by Abdullah *et al.* (2022) showed that at higher photon energies (>1 MeV), lead outperforms concrete in terms of shielding efficiency, but concrete remains an essential material in situations where cost, weight, and construction flexibility are priorities. Furthermore, heavy concrete's photon shielding properties can be optimized by using specialized aggregates, making it a viable option for industrial and medical radiation shielding.

2.4. Recent Trends and Future Directions

2.4.1 Advanced Materials for Photon Shielding

The future of photon shielding is likely to see the continued development of advanced materials, including composite and nanomaterial-enhanced concretes. The use of hybrid materials, such as cement mixed with nano-sized bismuth, has been shown to increase the photon attenuation properties of concrete (Saif et al., 2023). The exploration of novel lead-free alloys, polymer composites, and even 3D-printed shielding materials for use in radiological protection is expected to continue, driven by both safety concerns and technological advancements (Ogul, et al., 2024).

2.4.2 Environmental Considerations

Environmental and health concerns related to lead, particularly in the context of disposal and contamination, have spurred research into alternative shielding materials. Studies focusing on "green" radiation protection technologies aim to minimize environmental damage while maintaining shielding effectiveness, and this may lead to the development of new concrete formulations or novel materials that outperform lead in both safety and efficiency.

2.5 Clay-Based Materials for Radiation Shielding

Clay-based materials have emerged as promising candidates for radiation shielding, particularly in applications involving radioactive waste disposal. One approach to enhancing the radiation shielding properties of clay is the incorporation of boron, which is known for its neutron-absorbing properties and ability to attenuate gamma radiation. This section reviews recent studies that explore the potential of boron-enriched clay materials for radiation shielding, particularly in the context of nuclear waste storage.

2.5.1 Boron-Enhanced Clay for Radiation Shielding

A study by Akkurt & Canakci (2011). examined the photon attenuation properties of clay composites mixed with varying amounts of boron to evaluate their potential use in radioactive waste disposal applications. The study utilized gamma spectrometry to measure the linear attenuation coefficients (μ) of clay samples containing different concentrations of boron at photon energies of 662 keV, 1173 keV, and 1332 keV. These photon energies are characteristic of the gamma rays typically emitted by radioactive isotopes, such as cesium-137 and cobalt-60, commonly encountered in nuclear waste.

The attenuation coefficients were measured using gamma spectrometry, which involves the detection and analysis of gamma photons passing through the material. The study investigated how the addition of boron, a known neutron-absorber and photon attenuator, affected the shielding capabilities of the clay. Linear attenuation coefficients were calculated from the transmitted photon

intensities at each energy level, and the results were compared to those of pure clay samples.

The study found that the addition of boron significantly increased the linear attenuation coefficients of the clay for all tested photon energies. For instance, the addition of boron led to a notable increase in photon absorption and scattering at the energies of 662, 1173, and 1332 keV. This finding confirmed that boron improves the material's ability to shield against gamma radiation, primarily due to its high neutron capture cross- section and its capacity to interact with photons, thereby enhancing the overall radiation shielding performance.

Akkurt & Canakci (2011) concluded that boron-enriched clay can be a highly effective material for photon shielding, especially for radioactive waste containment. The study emphasized that boron's addition not only improves the radiation shielding properties of clay but also makes it a viable and cost-effective alternative to more conventional shielding materials, such as lead or concrete, for certain applications. The authors suggested that this composite material could play an important role in safe and environmentally friendly nuclear waste disposal.

This research also highlighted the need for further studies to optimize the boron content in clay-based materials, test the long-term stability of the shielding properties, and evaluate the mechanical and thermal durability of these materials under real-world conditions.

2.6 Effects of radiation on matter

Radiation, in its various forms, interacts with matter in complex and sometimes unpredictable ways. Its effects on materials - whether biological, chemical, or physical - depend largely on the type, energy, and duration of the exposure. Radiation is classified into two broad categories: ionizing and non-ionizing. Ionizing radiation, which includes alpha particles, beta particles, gamma rays, and X-rays, carries enough energy to remove tightly bound electrons from atoms, thereby ionizing them. Non- ionizing radiation, such as ultraviolet (UV) light, microwaves, and radio waves, does not possess sufficient energy to ionize atoms but can excite molecules and atoms. This paper focuses on the effects of ionizing radiation on matter, with particular attention to biological and material impacts, and how these can influence both living organisms and technological devices.

2.6.1 Biological Effects of Ionizing Radiation

Ionizing radiation has significant biological effects because it has the ability to break chemical bonds, leading to structural damage in cells, tissues, and DNA. When living cells are exposed to radiation, direct ionization of the atoms and molecules in the cells can lead to the formation of free radicals, which can cause further chemical damage. DNA is especially susceptible to radiation-induced damage, which may result in mutations, cancer, or cell death (Baskar et al., 2014). The damage can manifest in two ways: direct effects, where the radiation directly hits the DNA, and indirect effects, where radiation interacts with water molecules to generate free radicals, which then damage the DNA (Hall & Giaccia, 2018).

The severity of radiation damage depends on several factors, including the type of radiation, the dose, and the duration of exposure. For example, alpha particles, which have high mass and charge, are much more damaging per unit of energy than beta particles or gamma rays, but they are less penetrating and can be stopped by a sheet of paper or the outer layer of skin (Martin & Harbison 2013). Beta particles, while more penetrating, generally cause less localized damage. Gamma rays, on the other hand, are highly penetrating and can affect tissues deep inside the body. The biological effects of radiation are also influenced by the rate of exposure. Acute high-dose exposure can cause radiation sickness, while chronic low-dose exposure increases the risk of cancer over time (Hall & Giaccia 2018).

Beyond biological tissues, ionizing radiation also affects materials, particularly metals, polymers, and semiconductors. When exposed to radiation, materials can undergo physical and chemical changes that alter their structural integrity. For example, radiation can cause the formation of defects in the crystal lattice of metals and alloys, leading to embrittlement and weakening of the material (Thomas et al 2023). This process is particularly significant in nuclear reactors, where materials such as steel and zirconium are subjected to radiation-induced damage over time. In semiconductors, radiation can disrupt the electronic structure, causing malfunction in devices such as transistors and integrated circuits, which are critical components in electronic and aerospace technologies (Zhao et al., 2021).

Polymers, which are commonly used in packaging, medical devices, and various industrial applications, can undergo radiation-induced degradation. This

degradation can involve chain scission; breaking of the polymer chains, cross-linking (formation of new bonds between chains), and oxidation reactions (Chmielewski, et al (2005); Chang, et al. (2023)). These alterations can change the physical properties of the material, such as flexibility, strength, and transparency, and can ultimately lead to the failure of the material in its intended application.

The effects of radiation on matter are also of considerable concern in the field of environmental science and technology. In environmental settings, radiation can cause the alteration of soil, water, and air quality. Contamination from radioactive materials can lead to the long-term degradation of ecosystems, as radiation can kill or mutate plant and animal species. For instance, ecosystems near nuclear disaster sites, such as Chernobyl and Fukushima, have experienced significant disruptions in biodiversity, with radiation levels remaining hazardous for many decades after the initial event (Mousseau and Møller 2014).

In the field of technology, radiation shielding has become a critical aspect of nuclear power generation, space exploration, and medical applications. For example, astronauts are exposed to higher levels of cosmic radiation due to the lack of an atmosphere and magnetic field in space. Advanced materials that can shield astronauts from harmful radiation are a subject of ongoing research (Montesinos, et al. 2021).

Additionally, radiation is used in cancer treatment (radiotherapy), where controlled doses of radiation are targeted at cancerous tissues to kill or shrink tumors. This therapeutic application, however, requires precision to avoid damaging healthy tissues (Delaney et al., 2005).

2.7 Mathematical equations used in Radiation Shielding studies

The fundamental mathematical relation that underlines radiation shielding also known as the Beer-Lamberts law is given as

$$I = Ie^{-\mu x} \quad \text{.....(2.1a)}$$

$$I = BIe^{-\mu x} \quad \text{.....(2.1b)}$$

Where

I is the flux after the beam of radiation has moved through the absorbing medium

I_0 is the initial flux of the radiation

B is the buildup factor

e is exponential function

μ is the attenuation coefficient of material x is thickness of material

2.7.1. Half Value Layer (HVL) and Tenth Value Layer (TVL)

The Half Value Layer (HVL) and Tenth Value layer (TVL) correspond to the thickness of the shielding (absorber) material that will reduce photons by a one half (1/2) and a tenth (1/10) of its initial intensity respectively.

HVL and TVL values are specific to different types of materials and are different for radiation types and energies.

Mathematically according to Martin (2006) ,

$$\frac{I(x)}{I_0} = \frac{1}{2} = e^{-\mu x_{1/2}} \quad \text{.....[2.2]}$$

This can be computed as

$$x_{1/2} = HVL = \frac{ln\ 2}{\mu} \text{.....[2.3]}$$

Likewise, TVL according to Martin (2006) is obtained as

$$TVL = \frac{In\ 10}{\mu} = \frac{2.3026}{\mu} \text{.....[2.4]}$$

Where;

μ is the linear attenuation coefficient.

Equation 2.1a holds when there is good geometry between the source, absorber material and detector. In which case, every radiation that interacts with the absorber is either absorbed or scattered out of the primary beam such that all the radiation that reach the detector have all their original energy, Martin (2006).

In most practical situations however, poor or bad geometry is what pertains. Poor geometry also referred to as broad-beam geometry is when a significant fraction of the scattered radiation reaches the detector of interest in addition to unattenuated radiation that still possess all their initial energy. This makes shielding calculations complex. The anomaly can be rectified by introducing a term into Equation 2.1a called the buildup factor as in Equation 2.1b to account for broad-beam geometry Martin (2006).

2.8 The Role of Computer Codes in Radiation Shielding

In recent years, the development of advanced computer codes has revolutionized the way radiation shielding is designed, analyzed, and optimized. These computational tools allow researchers and engineers to model complex radiation environments and predict the behavior of different shielding materials under various conditions. The use of computer codes has greatly improved the efficiency of shielding design, reducing the time and cost associated with physical experimentation.

One of the most commonly used types of computer codes in radiation shielding is the Monte Carlo method, a statistical technique that simulates the random paths of radiation particles as they interact with matter. Monte Carlo simulations are particularly useful for modeling complex geometries and radiation transport, making them ideal for applications like radiation protection in nuclear reactors or space missions. For example, the MCNP (Monte Carlo N-Particle) code developed by Los Alamos National Laboratory is widely used for simulating the transport of neutrons, photons, and other particles in shielding materials (Goorley, et al. (2012).

Another popular computer code is FLUKA, which is used for both medical and industrial applications. FLUKA is capable of simulating radiation interactions at both low and high energies and is widely used in medical physics for radiation therapy planning, as well as in high-energy physics experiments (Battistoni et al., 2011). The code is particularly useful in designing shielding for radiation sources like particle accelerators, where accurate predictions of radiation dose and shielding requirements are essential.

PHITS (Particle and Heavy Ion Transport System) is another powerful code that has gained significant attention in the radiation protection field. PHITS is capable of simulating various radiation types, including photons, neutrons, and heavy ions, and is commonly used for radiation shielding in space and medical applications (Sato et al., 2015). Its flexibility in modeling complex geometries and materials makes it a valuable tool for optimizing radiation shielding in a wide range of industries.

2.9 Recent Developments in Radiation Shielding Computer Codes

Recent advancements in radiation shielding computer codes have focused on improving computational efficiency, enhancing user interfaces, and expanding the capabilities of existing models. One significant area of improvement has been the development of multi-scale modeling approaches, which combine the accuracy of Monte Carlo simulations with the efficiency of deterministic methods. These approaches allow for faster simulations of complex systems while maintaining a high level of accuracy, making them ideal for large-scale applications like nuclear power plants or space missions (Cordella, et al 2024).

Another area of focus has been the integration of machine learning algorithms into radiation shielding design. Machine learning techniques can be used to optimize material selection, predict shielding performance, and identify novel materials for radiation protection. For instance, researchers have applied machine learning to predict the attenuation coefficients of composite materials based on their

composition, which could significantly speed up the development of new shielding materials (Amin, et al., 2022).

Furthermore, the growing use of cloud computing has made it possible to perform large -scale simulations and share results more easily. Cloud-based platforms allow multiple users to collaborate in real-time, making it easier to analyze radiation shielding designs across different applications and environments. This has been particularly beneficial in collaborative research efforts, such as those focused on designing shielding for long- duration space missions or developing effective radiation protection for medical facilities (Wang, et al., 2011).

The integration of computer codes into radiation shielding design has greatly enhanced our ability to protect against harmful ionizing radiation. Advances in Monte Carlo simulations, multi-scale modeling, and machine learning algorithms have made it possible to design more effective and efficient shielding systems, reducing costs and increasing safety. As computational power continues to improve and new materials and methods are discovered, the role of computer codes in radiation shielding will only continue to expand, offering more precise and customizable solutions for a wide range of applications, from nuclear waste management to space exploration.

2.10 Validation of Experimental Results

Theoretical models, including Monte Carlo simulations, provide valuable insights into the expected photon interaction mechanisms in a material, but these

predictions must be validated with experimental data. A key challenge in the field of radiation shielding is ensuring that theoretical predictions correlate with observed experimental results. Several studies have sought to validate the performance of fired clay bricks as photon shields by comparing theoretical predictions to laboratory measurements of their attenuation coefficients.

2.10.1 Challenges in Validation

While Monte Carlo simulations are powerful tools for predicting the behavior of photons in shielding materials, several challenges remain when comparing experimental and theoretical results. One of the main challenges is the variability in the composition of fired clay bricks, which may contain different amounts of additives like iron oxide or barium sulfate. Even small variations in the proportion of these additives can significantly influence the shielding performance, leading to discrepancies between theoretical and experimental results.

Brouwers et al. (2022) emphasized that the complex microstructure of fired clay bricks, including factors like porosity and mineral composition, could lead to additional uncertainties in the experimental data. For instance, the presence of microcracks or air pockets in the brick matrix can alter photon scattering and absorption rates, making experimental results more difficult to interpret. Additionally, the resolution of gamma spectroscopy equipment and the precision of the experimental setup can also contribute to variations in the results.

Despite these challenges, the combination of theoretical simulations and experimental validation offers a comprehensive approach for optimizing fired clay bricks as photon shielding materials. By continually refining both the material

models and the experimental techniques, researchers can improve the accuracy of predictions and better understand the factors that influence photon attenuation in these materials.

CHAPTER THREE

METHODOLOGY

The chapter is broken down into thematic areas, each dealing with a major aspect of the research which are investigation of elemental composition and analysis, physico- mechanical (engineering) properties, and photon radiation shielding properties

3.1 Materials

3.1.1 List of materials

Below is a list of the apparatus and equipment used for the experiments in this work

- Global Positioning System (GPS) equipment – (GPSMAP 64s manufactured by GARMIN)
- Maps
- Sampling bags
- Pick axe
- Shovel
- Auger
- Mass balance
- Set of Sieves
- Electronic Shaker/vibrator
- Moulds
- Furnace/Oven

- Liquefied petroleum gas - LPG (commercially procured) – with purity of over 99% hydro carbons (combined propane and butane) as indicated by suppliers.
- Measuring cylinder
- Beaker
- Micrometer screw gauge
- Vernier calipers
- Pair of dividers
- Measuring rule
- Radiation detectors (Na:Tl scintillation detector coupled to a computer operating on GAMWIN SW version 2.00) from NuviaTech Instruments
- Survey meter – Radiagem 2000 (Manufactured by Mirion Technologies, Inc)
- Radiation sources (Am-241, Cs-137, & Co-60)
- Modulus of rupture testing setup
- Microsoft EXCEL (data analysis and presentation software)
- Camera
- Measuring balance (Model: Adventurer-Pro AV 264)
- Mill/Mixture (Model: MM301)
- Hydraulic press (Model: Specac)
- X-ray Fluorescence Spectrometer-XRF (Model: VMR) from Olympus
- Binder (Hoechst wax)
- Examination gloves
- Acetone

3.1.2 Alucobond

According to the manufacturers, ALUCOBOND® is a composite panel comprising two aluminum cover sheets and a fire-retardant or non-combustible mineral-filled polymer core, which is suitable for a wide range of architectural applications, typically as facades due to the lightweight nature of the panel (3A Composites GmbH, 2024). It is a proprietary product produced by the manufacturer with some specifications, for example, the exact composition of the mineral-filled polymer core being regarded as trade-secrets.

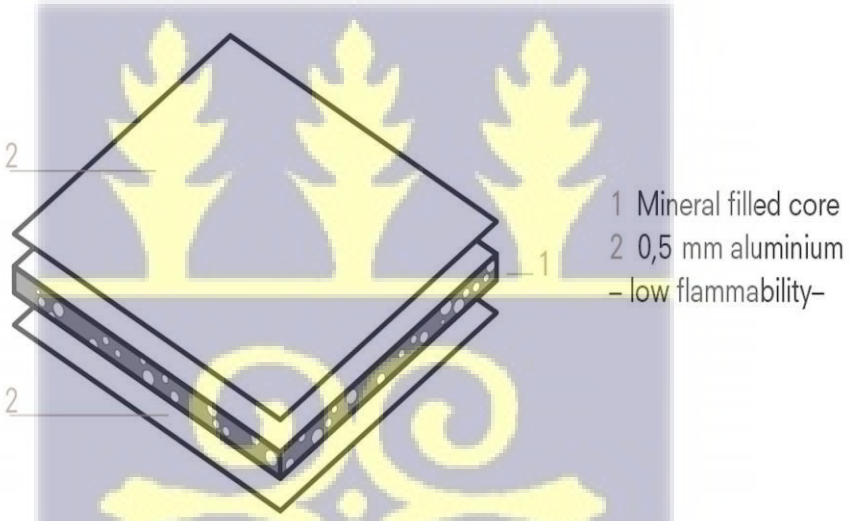

Figure 3.1: Schematic of Alucobond composite panel layering (Image Source: 3A Composites GmbH, 2024)

Table 3.1 Technical Specifications of Alucobond Panels

Parameter	Unit	Alucobond (4 mm)
Cover sheet thickness	[mm]	0.5
Weight	[kg/m²]	7.6
Production widths	[mm]	1250 / 1500
Technical properties		1.75
Section modulus	[cm³/m]	
Flexural rigidity	[kNcm²/m]	2400
Alloy temper of the cover sheets		EN AW 5005/A (AlMg1) H22 / H42
Modulus of elasticity	[N/mm²]	70.000
Tensile strength of the cover sheets	[N/mm²]	Rm ≥ 130
Proof stress (0.2 limit)	[N/mm²]	Rp0.2 ≥ 90
Elongation	[%]	A50 ≥ 2
Linear expansion coefficient		2.4 mm/m at 100 K Temperature difference
Core Mineral fillers with polymer binder		
Surface Lacquering/Coating		High-quality polymer coating systems applied using the coil coating process
▪ **Acoustic properties**		
Sound absorption factor		0.05
Rated sound reduction index	[dB]	27
dissipation factor		0.005
▪ **Thermal properties**		
Thermal resistance	[m²K/W]	0.002
Thermal conductivity	[W/mK]	1.77
Heat transition coefficient	[W/m²K]	5.80
Temperature resistance	[ºC]	-50 to +80

(Source: 3A Composites GmbH: https://www.alucobond.com/en/products/)

Data in table 3.1 is sourced from the manufacturers' (3A Composites GmbH) for the 4mm thick Alucobond.

3.2 Methods

3.2.1 Sampling

Sampling was done at six sampling sites known for clay deposits within the study area of the south-eastern part of Ghana. The sites are Okyereko and Assin Fosu in the Central Region, Abokobi and Kinbu in the Greater Accra Region and Oframase and Amperkrom in the Eastern Region were chosen at random but based on a combination of factors, including but not limited to

1. Accessibility of the sampling site.
2. A history of brick, tile, and pottery industry.
3. An existing brick, tile, and pottery industry.
4. Size of deposit
5. Type of clay (Kaolinte or montemorillonite)

Table 3.2 gives the samples codes of the clays studied; both doped and undoped. They were arranged in alphabetically order to facilitate the consistent presentation of results and discussion.

Table 3.2: Sample codes for the studied clay at various levels of doping

Deposit Abokobi	Region of Ghana deposit is located	Sample Code		
		Undoped	Doped at 5% wt	Doped at 10%wt
	Greater Accra	ABK-X0	ABK-X1	ABK-X2
Amperkrom	Eastern region	AMK-X0	AMK-X1	AMK-X2
Assin Fosu	Central region	FOS-X0	FOS-X1	FOS-X2
Kinbu	Greater Accra	KBU-X0	KBU-X1	KBU-X2
Oframase	Eastern region	OFM-X0	OFM-X1	OFM-X2
Okyereko	Central region	OKY-X0	OKY-X1	OKY-X2

In this study, the dopant used in this study is an oxide which is Fe_2O_3-rich. It was incorporated at 5% and 10% by wt to produce the X1 and X2 series of test pieces

3.2.2 Study Area and Clay Sampling Sites

Multiple points were sampled within each clay deposit in the study area. With the aid of a map, the sites for sampling were located. Subsequently, specific locations within the site were selected based on practical considerations in the view of the researcher such as access to the land, reasonable spatial distribution of locations and absence of visible source of contamination of soil from anthropogenic activities such as industry. This ensured that the clay soil collected is representative of the site and unpolluted. The positions and coordinates of these locations were determined using a GPS. The study area is shown in figure 3.2. The

base map used in plotting study area was obtained online credited to Geological Survey Department of Ghana, Ghana: http:// www.ghana-mining.org)

Table 3.3 Locations of clay deposits that were sampled

Deposit	Region of Ghana	GPS coordinate of
Abokobi	deposit is located	deposit location
	Greater Accra Region	5.730345, -0.197797
Amperkrom	Eastern Region	6.523508, -0.744452
Assin Fosu	Central Region	5.687153, -1.350261
Kinbu	Greater Accra Region	5.552147, -0.202255
Oframase	Eastern Region	6.529232, -0.727415
Okyereko	Central Region	5.414641, -0.574293

Table 3.3 shows the locations of the clay deposits that were sampled in this study. At each deposit, clay was collected from multiple points with the location.

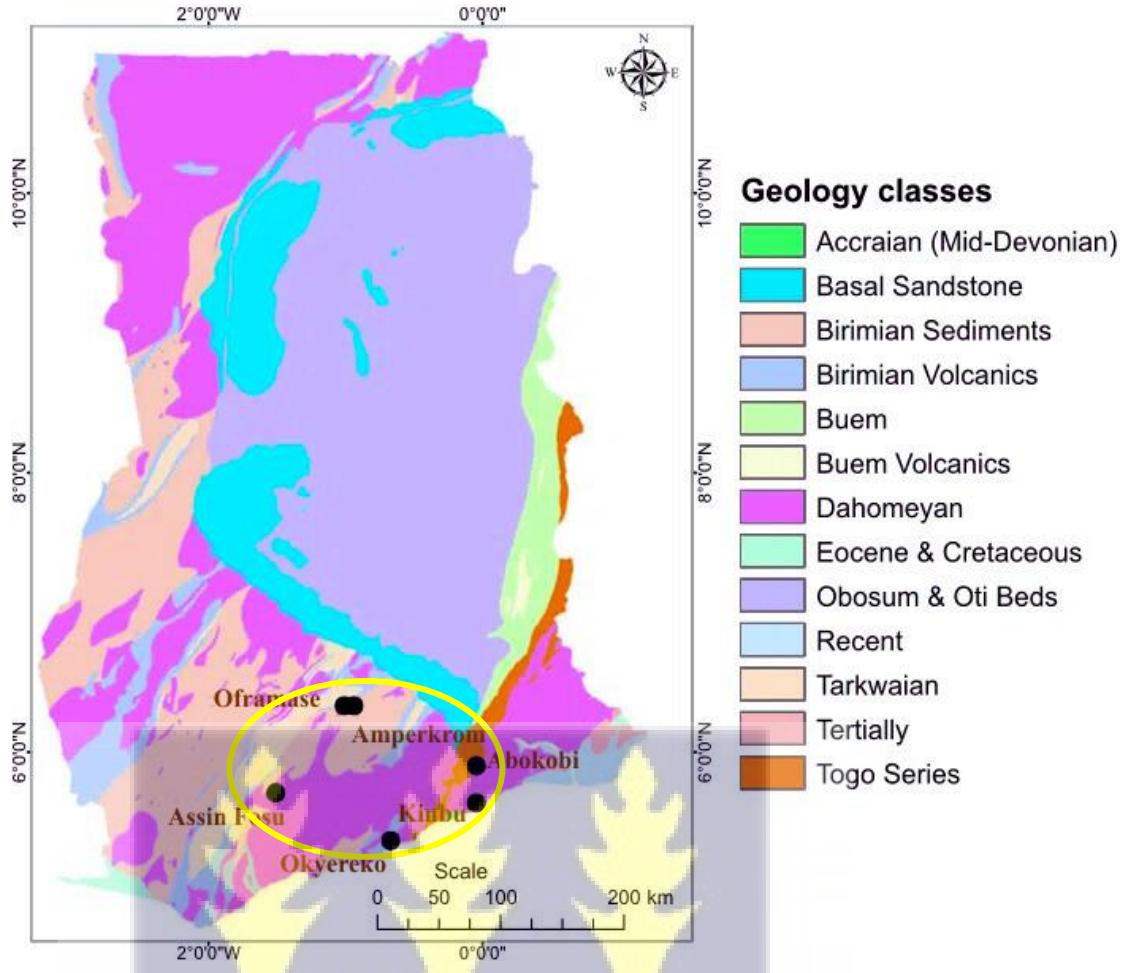

Figure 3.2: Geological map of Ghana showing study area (Source: GSD)

3.2.1.1 Clay Soil Sampling

The following procedure was adopted for sampling the clay soil. As suggested by Li, (2019), sites within each sampling area were chosen to avoid variability in soil properties which could be influenced by drainage, organic matter content, and past human activity.

The sampling area was divided into smaller grids and samples collected from each sub -unit to ensure representativeness and thereafter creating a composite sample. According to Winegardner, (1995); Tan, (2005)., a composite sample consists of several subsamples taken from different spots within the sampling site, and mixed

together to form a representative sample ((Winegardner (1995); Tan, (2005)) This is especially crucial in clay soil, where properties such as texture and compactness may vary across short distances.

By aid of hand digging implements- a combination of shovel, pickaxe and a trowel to clear the overburden, and coupled with an auger, samples were taken from about 1 - 3m depths. The soil was then stored immediately in plastic bags to avoid contamination from other samples. They were then labelled appropriately. The equipment used are cleaned with rug, brush, water and rubbing alcohol to remove any soil residues before being sent to the next sampling location that could contaminate the sample ((Winegardner (1995); Tan, (2005)). The samples were then transported promptly to the laboratory for storage, preparation and analysis.

3.2.3 Sample Preparation

The clay was properly conditioned before shaping. The conditioning involved air drying the clay, crushing, and grinding with porcelain mortar and pestle and then sieving it through BS 30 sieve in a process called clay washing for uniformity in the fine particles for all the clays. The sieved clay from the various sampling locations (points) within a sampling site was mixed and homogenized to form a composite sample representing the sampling site and sieved and bagged ready for processing. Where applicable, for the clay doping, the required percentage by weight of clay and additive (Fe_2O_3) were weighed and put in a container and was mixed thoroughly by means of an electronic mixer. Subsequently, the homogenized composite clays were then mixed with appropriate amount of water of about 500 ml to every 2kg clay to obtain a workable clay paste.

This step ensures the clay is malleable and has the right plasticity for shaping (Eramo, G. 2020). The wet clay was then kneaded and then put into various slightly oiled moulds depending on the intended use and then pressed with a hydraulic press to ensure uniform pressure in compacting. Once mixing and kneading for a particular clay or doping ratio was completed, the container and mixing apparatus were cleaned thoroughly with acetone to avoid contamination. Subsequently, various sizes of test pieces were made, in particular, for the shielding test, each clay type had transmission test slabs of dimensions 10 cm x 10 cm x 1 cm.

3.2.3.1 Drying the Shaped Clay

After shaping, the clay was dried to remove excess moisture before firing. It is essential to allow the clay to dry slowly and evenly to prevent warping or cracking. The drying process was done at ambient temperature and humidity, and the clay was placed in a dry, dust-free environment in line with the procedures suggested by Eramo (2020). The air drying was carried out for at least 48 hours.

3.2.3.2 Firing the Clay

Firing is the final step in the preparation of clay samples, and it involves heating the clay in a kiln to a high temperature. This process transforms the clay into a durable, hardened material with improved mechanical properties.

3.2.3.2.1 Temperature Control and Firing Curve

According to Guerrero Gómez, et al., (2022), a key consideration during firing is controlling the kiln's temperature. The firing curve, which describes the rate of

temperature increase and holding times at specific temperatures, plays a crucial role in the properties of the final product. For example, fired clay used in radiation shielding may need to be fired at higher temperatures to enhance its structural integrity (Guerrero Gómez, et al., 2022). The firing temperature must be chosen based on the clay's composition and the desired properties of the fired sample. High temperatures improve the density and hardness of the clay, which can enhance its suitability for various applications, including building materials and radiation shielding. In this work, the test pieces were fired at a temperature of 1,000 ±30 °C in an LPG fired kiln

3.2.3.2.2 Cooling the Fired Clay

After firing, the clay samples were cooled gradually. Rapid cooling can cause thermal shock, leading to cracking or structural failure. The cooling process was controlled by allowing the clay to cool in the kiln at a slow rate. Typically, the samples were allowed to cool naturally over several hours, usually overnight before removal from the kiln (Eramo, 2020).

3.2.3.2.3 Post-Firing Analysis

Once the clay test pieces were cooled, their shrinkage was checked by measuring the length along diagonal marks that were made on dedicated test pieces to ascertain the degree of reduction in the size of the fired test piece form the dimensions of molding, dimensions after air drying-dry shrinkage and dimensions after firing- fired shrinkage. The porosity and density were then determined. These are particularly relevant to radiation shielding, where the density and porosity of fired clay affect its attenuation of gamma rays.

3.2.4 Grain Size Distribution (Sieve Analysis)

3.2.4.1 Grain Size Distribution Tests

The grain size distribution (GSD) of clay soil is a crucial characteristic that influences its behavior in various engineering and environmental applications. The GSD provides valuable information on the texture, porosity, and permeability of the soil, which in turn affects its suitability for several applications including construction, and serving as part of composites for radiation shielding.

Since clay particles are typically small (less than 0.002 mm in diameter), the methods used to determine the grain size distribution of clay soils differ from those used for coarser materials like sand or gravel. Standard procedures are employed to analyze both the fine and coarse fractions of clay soil, ensuring accurate and reproducible results.

Clay soils are characterized by their fine particles, which have a diameter smaller than 0.002 mm. This fine-grained material typically exhibits cohesive properties, which are in contrast to the granular nature of sandy soils. The grain size distribution of clay soils is typically presented as a cumulative percentage of the total sample that passes through a given sieve size. This distribution can be plotted as a curve, which provides a detailed view of the soil's particle size distribution. Sieves of mesh size 0.85 mm. 0.71 mm, 0.5 mm, 0.30 mm, 0.212 mm, 0.150 mm, and 0.106 mm were weighed to determine their initial mass. They were then stack on top of each other and placed on a pan. In the staking, the smallest mesh size was at the bottom and arranged in ascending order. Subsequently, 400g of the

dried and crush clay soil sample was poured into the topmost and largest mesh size, and then covered.

The setup was place on a mechanical sieve shaker for 10 minutes. Then the mass of each sieve is measured and recorded. The difference between this mass and the sieve's initial mass is computed to determine the mass of soil retained by the sieve in order to calculated what percentage has passed through each sieve using Equation 3.2.1. The results of this analysis are presented on a semi log graph.

After each sample grain size distribution test, a brush was used to clean the sieves thoroughly before the next sample was analyzed.

$$\%\, reatined = \frac{mass\ of\ sample\ retained\ sieve}{mass\ of\ initial\ sample} \times 100 \quad \text{.....[3.2.1]}$$

3.2.5 Density

Density is defined as the mass per unit volume of a material. It is one of the most important physical properties of fired clay, as it influences various characteristics such as mechanical strength, thermal conductivity, and radiation shielding. In the context of fired clay materials used in construction, understanding the density is crucial for ensuring optimal performance. Additionally, the density of fired clay influences the attenuation of radiation, with denser materials often providing better shielding properties.

In fired clay, the density can vary depending on several factors, including the clay composition, firing temperature, and firing duration. Density is typically expressed in units of grams per cubic centimeter (g/cm^3) or kilograms per cubic

meter (kg/m³). The bulk density of the test pieces were determined using water displacement method This method involves measuring the volume of water displaced when the clay sample is immersed in water.

3.2.5.1 Procedure for Bulk Density Measurement

1. The sample is dried in an oven at 105 – 110°C to remove any moisture.
2. The dry weight of the sample is recorded using the balance.
3. The dried sample is submerged in water in the graduated cylinder, ensuring that no air bubbles are trapped.
4. The volume of water displaced by the sample is recorded. This volume corresponds to the volume of the fired clay sample. 5. The bulk density is calculated using the formula:

$$\rho = \frac{W_d}{W_s - W_{ss}} \quad \text{.....[3.2..2]}$$

Where;

W_d is the weight of the dry test piece

W_s is the weight of the soaked test piece

W_{ss} is the weight of the soaked and suspended test piece in water

3.2.6 Determining the Porosity of Fired Clay

Porosity refers to the fraction of the volume of a material that is occupied by voids or pores, and it is typically expressed as a percentage of the total volume. In fired clay bricks, porosity can significantly impact mechanical strength,

thermal insulation, and radiation attenuation properties, making it a crucial parameter to measure.

3.2.6.1 Porosity of Fired Clay

In radiation shielding, the porosity of fired clay can influence the attenuation of different types of radiation, including gamma and neutron radiation. Materials with high porosity typically have lower density, which can make them less effective for shielding high-energy photons such a as gamma rays. On the contrary, a higher density (lower porosity) tends to provide better attenuation. Understanding the relationship between porosity and other physical properties of fired clay is therefore essential for optimizing its use as a construction material and in other specialized applications.

The Archimedes' principle was relied upon for measuring the porosity of fired clay. This technique involves determining the volume of voids by measuring the water displaced when the clay sample is submerged. The principle behind this method is that the volume of water displaced by the sample is equal to the volume of the pores (voids) within the material.

1. The fired clay sample was first dried in an oven at 105°C to 110°C until it reaches a constant weight. This step ensures that any moisture in the clay is removed.
2. The weight of the dry sample (W1) is recorded.

3. The sample was then completely submerged in distilled water in a graduated cylinder. Care should be taken to ensure no air bubbles are trapped in the sample, as this would lead to inaccurate readings.
4. The weight of the sample while submerged in water (W2) is measured. The buoyant force (the difference in weight between the dry and submerged sample) corresponds to the volume of water displaced.
5. The porosity was then computed using Archimedes' principle,

$$\%\ Apparent\ Porosity = \frac{W_2 - W_1}{W_2 - W_3} \times 100 \ldots\ldots [3.2..3]$$

Where ;

W_1 is dry weight of briquette

W_2 is the soaked weight of briquette

W_3 is the weight of the suspended (immersed) briquette

For Grain Size Distribution, as well as Porosity and Density analysis, the American Standard - ASTM D6913 (for Sieve Analysis) and ASTM C373 (for bulk density, apparent porosity) respectively were adopted (ASTM International 2017; ASTM International 2018).

3.2.7 Determination of Elemental Composition of clay using a Handheld XRF device in the Laboratory

X-ray fluorescence (XRF) is a non-destructive analytical technique used to determine the elemental composition of materials, including clays.

In this study, a dried, pulverized, and homogenized sample was sieved through 75µm sieve and readied for analysis. 4.0 g of the sieved sample was portioned out and well-mixed together with 0.9 g of a binder (Hoechst Wax) which is a tableting aid in a mill and pressed with 15 tons (13.61 kg) to make a 32 mm pellet. To prevent contamination in the analytical process, in particular, the sample preparation and handling, gloves are worn. Acetone was also used to clean the mixing containers.

The prepared pellet was then placed into the irradiation chamber of the model VMR of OLYMPUS VANTA M-Series XRF equipment for an energy-dispersive polarizing X- ray fluorescence (XRF) spectrometry analysis. The tube rating was set at 50 kV, 0.2 mA. To calibrate the system and validate the procedure, a National Institute of Standards & Technology (NIST) Standard Reference material 2711a of Montana II Soil was used.

All sample preparations and analyses were performed at the Ghana Geological Survey Authority laboratory in Accra. Laboratory temperature was kept at 20 ºC during the analysis.

3.2.8 Investigation of radiation shielding properties

The clay slabs were placed mid-way between a radiation source and a detector that were 1m apart with all three centrally aligned in a straight line along one axis. The mid-point placement of the slabs ensured that minimal scattered radiation reached the detector in order not to introduce or increase build up. To detect the photon radiations from the sources, a scintillation detector coupled to a computer interface counter was used

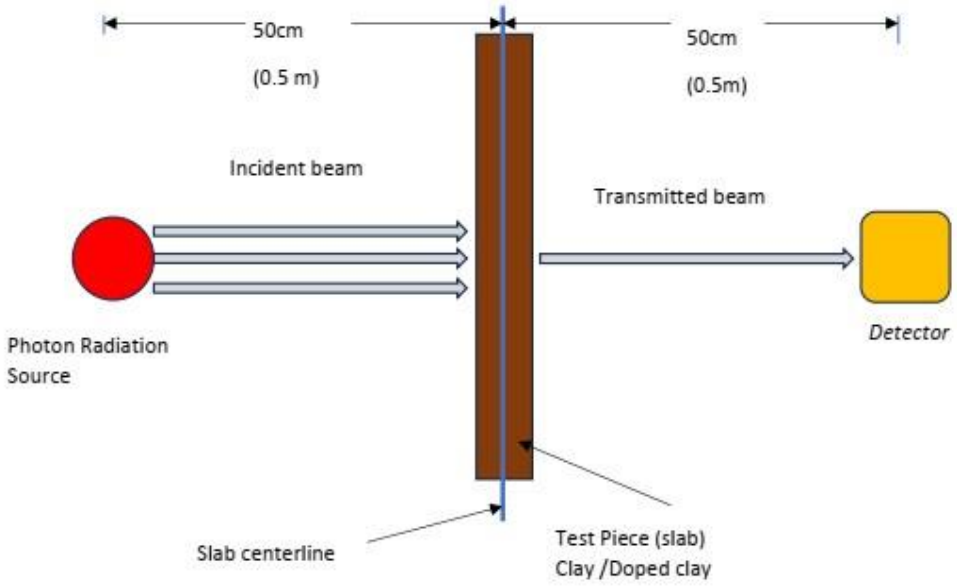

Figure 3.3. Schematic diagram of the set up for shielding test.

In order to verify and validate the experimental procedure and the reliability of the instruments and apparatus, standard absorber materials of Al, Pb, Cu and Fe were also taken through the procedure to determine their linear attenuation coefficient. The following equations were used in the calculation of shielding parameters:

3.2.8.1 Linear Attenuation Coefficient (LAC) in cm^{-1}

$$I = BI_0e^{-\mu x} \quad \text{.....[3.2.4]}$$

Where;

I_0 is initial radiation intensity

I is radiation intensity after passing through absorber

B is the build-up factor

X is absorber thickness

μ is the linear attenuation coefficient

For multilayer shield materials, the equation become

$$I = I_0(B_1 e^{-\mu_1 x_1}).(B_2 e^{-\mu_2 x_2}) \dots \dots (B_n e^{-\mu_n x_n}) \quad \text{.....[3.2.5]}$$

Where;

I_0 is initial radiation intensity

I is radiation intensity after passing through absorber

B_1, B_2, B_n are the build-up factors in the 1st , 2nd and nth layers

X_1 X_1 and X_n are absorber or shield thickness of layers 1st, 2nd and nth layers

μ_1 μ_2 and μ_n are the linear attenuation coefficient of layers 1st,2nd and nth layers

3.2.8.2 Mass Attenuation Coefficient (MAC) in cm^2g^{-1}

$$\mu_m = \frac{\mu}{\rho} \quad \text{.....[3.2.6]}$$

Where;

μ_m is mass attenuation coefficient in cm^2/g

μ is the linear attenuation coefficient in cm^{-1} ρ is the density of the clay absorber in g/cm^3

3.2.8.3 Half Value Layer (HVL) in cm

The thickness of the clay that will reduce the intensity of the incident radiation by one half.

$$HVL = \frac{Ln\ 2}{\mu} \quad \text{.....[3.2.7]}$$

Where;

HVL is the half value layer in cm

μ is the linear attenuation coefficient in cm^{-1}

3.2.8.4 Tenth Value Layer (TVL) in cm

The thickness of the absorber that will reduce the intensity of the incident radiation to one-tenth.

$$TVL = \frac{Ln\ 10}{\mu} \quad \text{.....[3.2.8]}$$

Where;

TVL is the half value layer in cm

μ is the linear attenuation coefficient in cm^{-1}

3.2.8.5 Mean free path in (cm)

The mean free path quantifies the mean distance a photon travels in an absorber before it undergoes absorption or scattering that removes it from the initial beam completely Martin (2006). This is calculated by equation 3.2.9.

$$mfp = \frac{1}{\mu} \quad \text{.....[3.2.9.]}$$

Where;

mfp is the mean free path in cm

μ is the linear attenuation coefficient in cm^{-1}

3.2.9 Using MCNP to Determine the Linear Attenuation Coefficient of Clay and Buildup factor

The Monte Carlo N-Particle (MCNP) transport code was used for simulating the interactions of radiation- photons with matter. Parameters from the output (output tally) was used to calculate the linear attenuation coefficient (LAC) of the clay material.

To determine the LAC of clay using MCNP, the following general procedure and methodology can be applied:

3.2.9.1 Problem Definition and Simulation Setup

The goal of using MCNP was to simulate the attenuation of photons through fired clay at different energies, in order to compute the linear attenuation coefficient for the material.

3.2.9.1.1 Material Definition

For MCNP simulations, clay was defined as a homogeneous mixture of its constituent elements (i.e., silicon, aluminum, oxygen, iron, titanium, calcium, magnesium, zirconium, etc.). The elemental composition and density of fired clay was defined in the simulation.

3.2.9.1.2 MCNP Model Setup

In MCNP, the model used consisted of the following parameters:

i. The geometry of the clay sample was defined as a solid object with a given size and shape (e.g., a rectangular).

ii. A photon source was placed at a defined position and distance similar to the experimental setup,

iii. The energy and intensity of the photon was also specified

iv. Using the material card, the elements in clay were specified, including their atomic composition, and density.

v. Using MCNP's tallying feature the flux and energy deposition of Photons passing through the material was calculated.

3.2.9.2 Running the Simulation

After defining al the input files (e.g. geometry, material, photon source, and tallies), the code was run in MCNP for the simulation. The programme performed a Monte Carlo simulation, calculating how photons interact with the fired clay and estimating the attenuation properties.

3.2.9.2.1 Comparison with Theoretical and Experimental Data

The experimentally obtained LAC, was compared to that of the MCNP-calculated values to validate the simulation model.

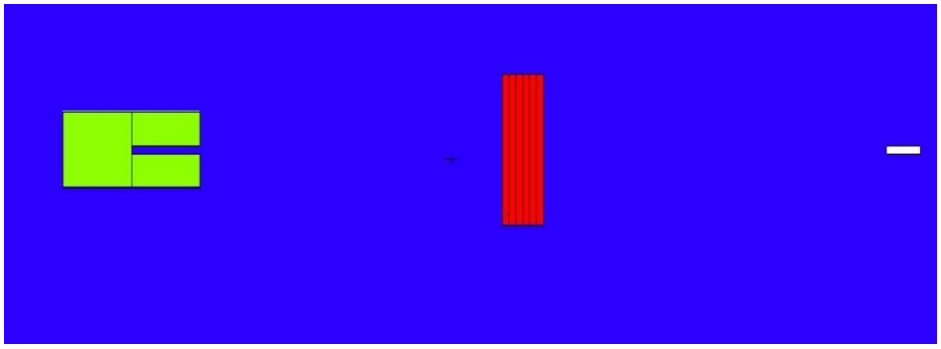

Figure 3.4.1 Schematic of MCNP simulation geometry showing orientation of shielded source, shield material and detector from left to right

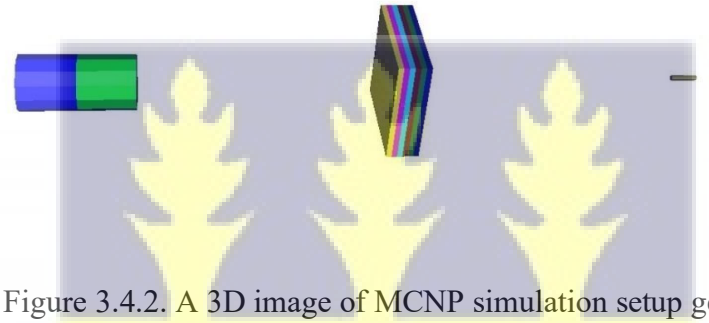

Figure 3.4.2. A 3D image of MCNP simulation setup geometry

Figure 3.4.3. A 3D image of MCNP simulation setup geometry

3.2.10 Uncertainty (Error) estimation

In order to minimize uncertainty associated with the results, multiple readings were taken for each measurand under consideration. The arithmetic mean (average) $\bar{x}$ of these were taken to represent the best value of the measurand for that set of measurement.

The standard deviation, s which specifies the range of the values was also calculated. Uncertainty estimation is a fundamental aspect of statistical treatment in scientific analysis, providing insight into the precision and reliability of measurement results. In any experimental setup, uncertainty refers to the degree to which a measured value deviates from the true value, and it can arise from various sources, such as instrument limitations, environmental conditions, or human error.

Uncertainty is typically classified into two types: systematic and random errors. Systematic errors are consistent and repeatable, often resulting from flaws in the measurement system or experimental procedure. These errors can be minimized or corrected with proper calibration or experimental design. Random errors, on the other hand, vary unpredictably with each measurement, stemming from factors like fluctuations in the environment or limitations of the measuring device. These errors are usually quantified using statistical methods, such as calculating the standard deviation of repeated measurements.

To estimate uncertainty, a common approach involves calculating the standard deviation (σ) or standard error (SE), which represent the variability of data. The confidence interval provides a range within which the true value is likely to fall,

given the uncertainty. For multiple measurements, the mean is often reported alongside the uncertainty, providing a more comprehensive understanding of the data's reliability (Bevington & Robinson, 2003). Thus, uncertainty estimation helps researchers interpret results with a quantifiable level of confidence, ensuring the validity of scientific conclusions.

The arithmetic mean, $\bar{x}$ was calculated using equation (3.2.10a)

$$\bar{x} = \frac{\sum_{i=1}^{n} x}{n} \quad \text{.....[3.2.10a]}$$

Where;

x is the measured quantity

n is the number of measurements

The standard deviation, s is given by

$$s = \sqrt{\frac{\sum_{i=1}^{n}(x_i - \bar{x})^2}{n-1}} \quad \text{.....[3.2.10b]}$$

Were,

x_i is an individual measurement of the variable x

$\bar{x}$ is average of the measurements of x

n is the number of measurements of x

The standard error (uncertainty), SE is given by equation 3.3.1c

$$SE = \frac{s}{\sqrt{n}} \quad \text{.....[3.2.10c]}$$

Where;

s is the standard deviation of the measurements

n is the number of measurements (sample size)

Unless otherwise stated, the values in this work are quoted as (mean ± SE).

3.3 Results Validation

The major results obtained in this study were compared to results from standards taken through the experimental procedure or published results of similar materials or with computer simulations for purposes of validating the experimental results.

CHAPTER FOUR

RESULTS AND DISCUSSION

The results from this study have been presented in this chapter and discussed within the context of information from literature and other works done in the field.

4.1. Elemental Composition Analysis

4.1.1 Elemental composition of samples using XRF

Shielding of radiation is dependent on elemental concentration just as it also depends on material structure, density, and how these elements are bound in the matrix. X-ray Fluorescence (XRF) is a powerful analytical tool for determining the elemental composition of materials, with advantages such as rapid analysis, minimal sample preparation, and the ability to analyze a broad range of elements. However, its limitations, such as difficulties with low atomic number elements, matrix effects, and elemental interferences, should be borne in mind when using XRF.

Notwithstanding, with respect to earthy materials such as clay, XRF serves as an important and widely used tool for characterizing the materials according to their elemental composition.

The results obtained presented in Figure 4.1a, Figure 4.1b as well as Tables 4.1a, 4.1b, and 4.1c show elemental compositions for six different clay samples (coded as ABK, AMK, FOS, KBU, OFM, and OKY) under three variations or series (doping conditions), represented as "X0", "X1", and "X2". These materials, sourced from geological formations, contain a variety of elements such as aluminum (Al), silicon (Si), potassium (K), calcium (Ca), iron (Fe), and trace

elements like titanium (Ti), manganese (Mn), copper (Cu), zinc (Zn), and zirconium (Zr). The primary aim of analyzing these materials is to assess their suitability for radiation shielding, with specific emphasis on their potential to attenuate gamma radiation.

In this aspect of the study, the trends in elemental composition, the role of density in shielding performance is analysed.

From the elemental composition data across three series for six clay samples, it is seen that each sample includes major elements such as aluminum (Al), silicon (Si), potassium (K), calcium (Ca), iron (Fe), and trace elements like titanium (Ti), manganese (Mn), copper (Cu), zinc (Zn), and zirconium (Zr).

The major elements like S, Fe, and Al show substantial variation across the samples. The samples from FOS-X1 have the highest percentage of aluminum (150,766mg/kg), while ABK-X0 contains the highest silicon content (276,740mg/kg).

These variations in elemental composition directly affect their potential for radiation shielding, with those containing heavier elements like iron typically offering better attenuation of gamma rays.

The elemental composition of materials plays a significant role in their radiation shielding capabilities. In particular, elements with high atomic numbers (Z) tend to be more effective in interacting with and attenuating gamma radiation.

Elements such as iron (Fe), aluminum (Al), and silicon (Si) and titanium (Ti) are of primary interest in this study.

Silicon (Si) is abundant in most of the samples and ranges from 183,669 mg/kg (FOS-X2) to 276,740 mg/kg (ABK-X0). While silicon itself is not the most effective at shielding against high-energy gamma radiation, its high electron density means it will still contribute to photon absorption. ABK-X0, with its high silicon content, is expected to perform reasonably well in shielding low-energy gamma radiation.

On the other hand, iron (Fe) with an atomic number of 26, is one of the most effective elements for shielding gamma radiation due to its high atomic mass and density. In this study, the iron content is highest in KBU-X2 (97,110 mg/kg) and OFM-X2 (87,758 mg/kg). Studies have shown that iron-rich materials are excellent for shielding gamma rays, particularly at higher energies. These samples would be expected to provide effective shielding for both medical and industrial radiation shielding applications. This trend indicates that as iron content increases, the material's potential for shielding high-energy gamma radiation improves confirming studies of Mori, et al., (2020).

Incidentally, while aluminum has a lower atomic number (13) compared to iron, it is still a commonly used material in radiation shielding, especially for low-energy gamma radiation. FOS-X1 contains the highest percentage of aluminum (150,766mg/kg), which may give it an edge in applications where very low-energy gamma radiation is a concern.

With respect to trace elements (Ti, Mn, Zn, Cu, Zr): These elements, although present in trace amounts, may also contribute to shielding properties Ti, for instance, with an atomic number of 22, is often used in radiation shielding, particularly in alloys. Manganese (Mn), copper (Cu), and zinc (Zn) have lower atomic numbers but can still contribute to radiation shielding However, their impact in this study is less significant compared to iron and silicon.

On the other hand, calcium (Ca) and manganese (Mn) concentrations show significant variation across the samples, with calcium content peaking in OKY-X2 (6,531mg/kg) and manganese content increasing in AMK-X1 (357mg/kg). Calcium and manganese are generally not as effective at shielding gamma rays but may play a role in neutron shielding (Zhao et al., 2021).

The use of natural and locally sourced materials for radiation shielding is a growing area of research, particularly in developing countries where access to commercial radiation shielding materials may be limited. Several studies have examined the potential of iron-rich materials, as well as silicon-based materials, for radiation shielding. Zhao et al. (2021) explored the use of iron and silicon compounds for gamma radiation shielding and found that materials with higher iron content performed significantly better. This supports the trend observed in KBU-X2 and OKY-X2, where higher iron content correlates with better shielding performance (Zhao et al., 2021).

Furthermore, Sathish, et al (2023) found that all other things being equal, aluminum-based materials are also relatively effective at shielding low-energy gamma rays, which is consistent with the higher aluminum content in FOS-X0.

These findings from other studies support the hypothesis that iron and aluminum, along with other elements like silicon, could be effective in low-cost, locally sourced radiation shielding applications.

Figure 4.2.1a show the elemental composition of the iron-rich dopant oxide. The XRF results on the dopant oxide concentrations presents a list of elements typically used to modify the properties of materials for various industrial applications. The concentrations are expressed in parts per million (mg/kg), with key elements including Fe, Al, Si, K, Ca, Ti, Mn, Zn, and Zr. Each of these elements contributes unique properties when added to materials, particularly in ceramics, semiconductors, and structural alloys.

Aluminum (Al) for example which 13,498 mg/kg in this sample is a common dopant in oxide materials, particularly for improving the strength and thermal stability of ceramics and glasses. Its relatively high concentration in the sample suggests a potential use in high-strength materials or those requiring improved resistance to high temperatures (Silva, et al 2021). The role of Silicon (Si) at 41,375 mg/kg concentration in the dopant oxides is also well-established, particularly in the semiconductor industry, where silicon dioxide (SiO_2) is a key material. The high concentration of silicon indicates potential applications in materials requiring high thermal stability (Lin & Wu (2018)).

For Iron (Fe) at a concentration of 498,991 mg/kg has a dominant presence with a normalized concentration at about 80% in the sample suggests its role in structural applications, likely as a strengthener or for improving corrosion resistance. Iron oxide (FeO) is commonly used in catalysts and coatings, and its abundance here could imply a focus on material durability in addition to its density improving properties. On the other hand, Calcium (Ca) – 52,052 mg/kg is widely used in ceramic and cementitious materials for enhancing strength and improving the material's mechanical properties. Its high concentration here suggests it may be used to stabilize the structure or modify the melting point of the oxide matrix (Silva, et al., (2021)).

Similarly, for other elements such as Potassium, Titanium, Manganese, Zinc, and Zirconium (K, Ti, Mn, Zn, and Zr) are present in trace amounts and may contribute to specific properties such as catalytic activity, corrosion resistance, or high-temperature stability radiation shielding, etc. For instance, titanium and zirconium are often used to improve the mechanical properties and resistance of materials under extreme conditions (Dana, et al. (2023).

The dopant oxide sample is rich in elements that enhance structural strength, thermal stability, density and resistance to corrosion, suggesting its use in industrial applications like ceramics, construction materials, and high-temperature alloys.

This analysis has highlighted the potential of clay materials for use in radiation shielding applications. High-density materials like ABK and OKY series, with significant iron and silicon content, show promise for gamma radiation shielding,

particularly in low-cost and sustainable applications. The application of these materials in developing countries could provide affordable, locally sourced solutions to radiation protection challenges.

Table 4. 1a: Elemental constituents of the undoped clay.

Element	Elemental composition- Major elements (mg/kg) **ABK - X0**	**AMK- X0**	**FOS - X0**	**KBU- X0**	**OFM - X0**	**OKY - X0**
Al	46845	60711	136386	90305	80006	63643
Fe	20458	50535	10166	59226	49398	39271
Si	276740	246286	224531	213016	229821	209417

Element	Elemental composition - Minor elements (mg/kg) **ABK - X0**	**AMK- X0**	**FOS - X0**	**KBU- X0**	**OFM - X0**	**OKY - X0**
Ca	341	4089	n.d	n.d	1162	2080
Cr	n.d	113	n.d	62	109	57
K	2173	4722	5673	4883	1406	4441
Mg	n.d	n.d	n.d	n.d	n.d	n.d
Mn	130	90	0	37	72	362
Pb	15	4	26	18	0	12
S	n.d	n.d	n.d	n.d	n.d	n.d
Sr	17	174	41	53	54	95
Ti	4726	4016	1970	3943	4636	4517
V	n.d	63	n.d	20	51	33
Zn	24	52	24	24	78	53
Zr	304	81	118	225	86	243

n.d: not detected

Table 4. 1b: Elemental constituents of the 5% wt doped clay.

Elemental composition- Major elements (mg/kg)						
Element	**ABK -X1**	**AMK-X1**	**FOS - X1**	**KBU-X1**	**OFM-X1**	**OKY -X1**
Al	35043	77823	150766	61773	59710	78651
Fe	44682	61783	36257	79925	68456	60874
Si	270811	239179	228401	186921	215561	243020

Elemental composition - Minor elements (mg/kg)						
Element	**ABK -X1**	**AMK-X1**	**FOS - X1**	**KBU-X1**	**OFM-X1**	**OKY -X1**
Ca	3034	4058	218	2756	4870	3893
Cr	n.d	80	n.d	76	196	82
K	1812	4814	3319	4440	1983	4769
Mg	n.d	n.d	n.d	n.d	n.d	n.d
Mn	153	357	40	102	89	292
Pb	15	15	14	20	n.d	16
S	n.d	243	n.d	n.d	n.d	479
Sr	19	103	18	51	129	102
Ti	4262	4421	1704	3293	3647	4479
V	n.d	56	n.d	37	43	53
Zn	27	60	18	21	64	59
Zr	296	273	133	196	78	254

n.d: not detected

Table 4. 1c: Elemental constituents of the 10% wt doped clay.

Element	Elemental composition- Major elements (mg/kg) ABK - X2	AMK- X2	FOS - X2	KBU- X2	OFM - X2	OKY - X2
Al	38448	70562	91378	79623	70811	62572
Fe	62582	78290	58010	97110	87758	82574
Si	250955	225081	183669	210938	238380	217994

Element	Elemental composition - Minor elements (mg/kg) ABK - X2	AMK- X2	FOS - X2	KBU- X2	OFM - X2	OKY - X2
Ca	3320	5453	4472	3223	5932	6531
Cr	n.d	74	n.d	45	92	53
K	2221	4429	4332	4338	2247	4457
Mg	n.d	n.d	n.d	n.d	5225	n.d
Mn	164	334	73	156	120	323
Pb	16	13	20	17	n.d	16
S	n.d	411	n.d	n.d	n.d	514
Sr	20	94	38	49	122	99
Ti	4314	4132	1524	3468	3564	3867
V	20	35	0	36	50	40
Zn	28	61	19	20	68	53
Zr	270	227	106	191	81	246

n.d: not detected

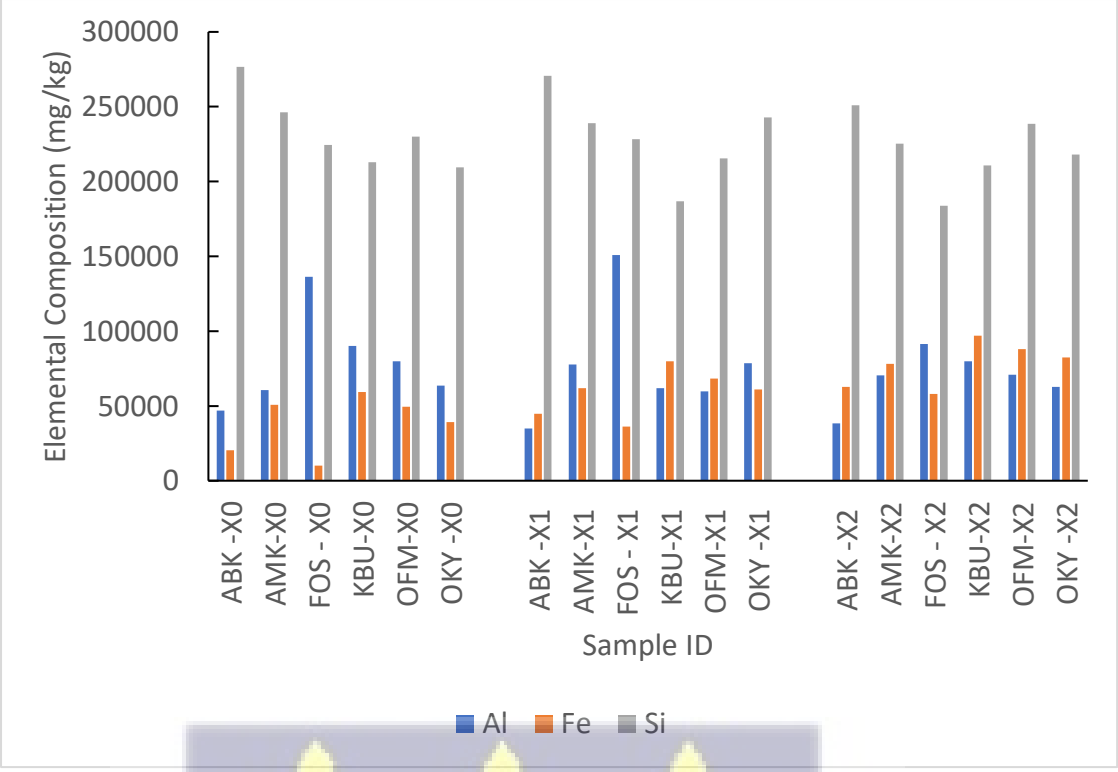

Figure 4.1a: Comparison of elemental composition of major elements of the clays

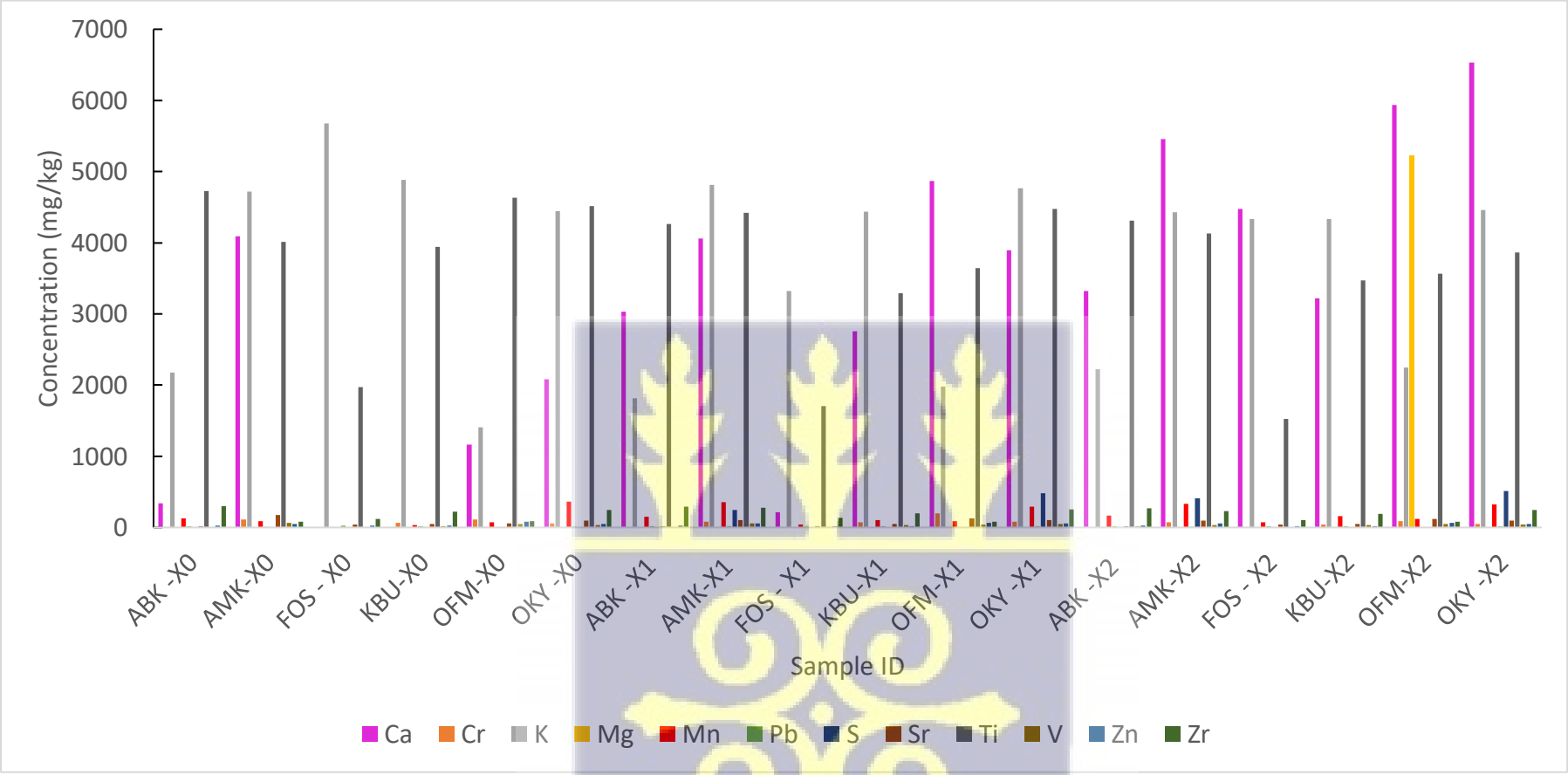

Figure 4.1b Comparison of elemental composition of minor elements present in the clays

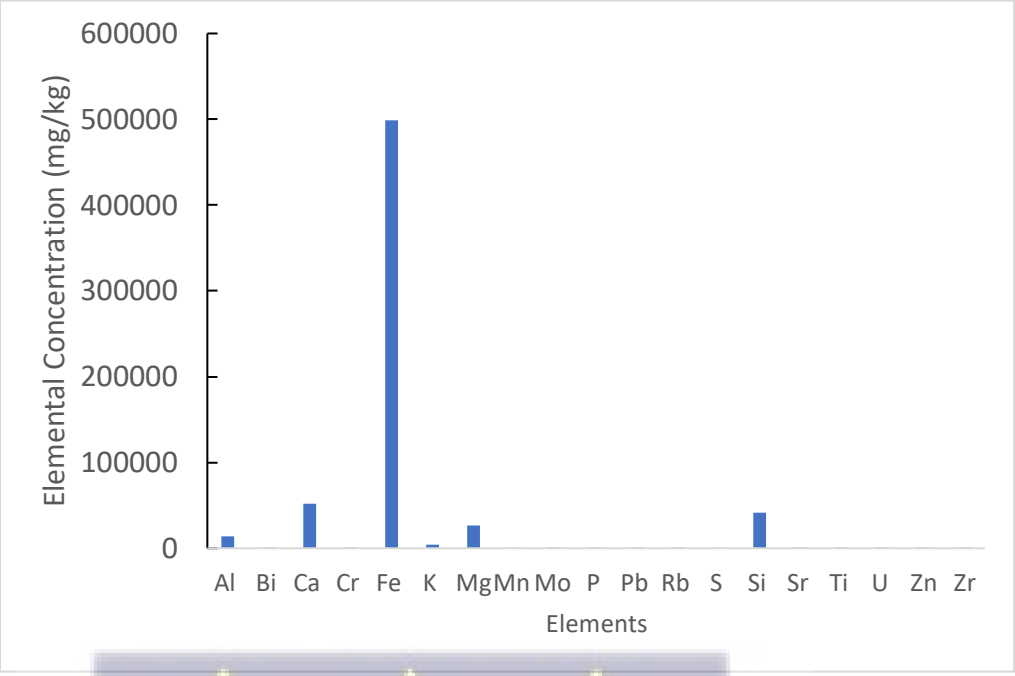

Figure 4.2.1a A graph showing the constituent of the dopant

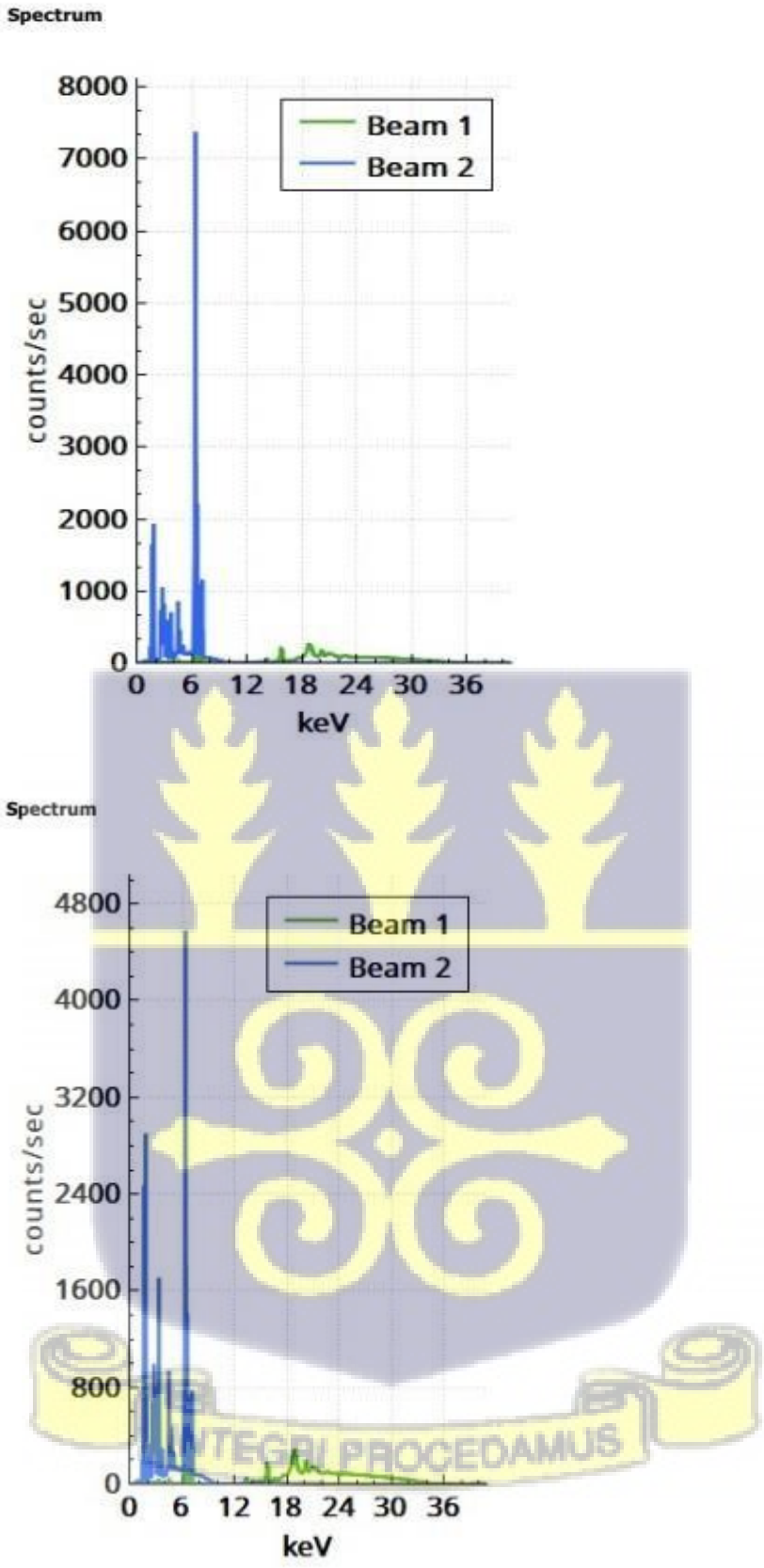

Figure 4.2.2 a: An example of spectra from the XRF analysis of the samples

4.1.2 Relationships between some key elements in clay and the densities of the clay's samples

In this section, the densities of fired clay samples doped with varying amounts of iron- rich oxide by weight addition, focusing on how key elements—silicon (Si), aluminum (Al), iron (Fe), and titanium (Ti) and how they contribute to the density of the samples is presented and discussed. The samples are grouped into three series: X0 series (0% doping), X1 series (5% doping), and X2 series (10% doping), where the doping refers to the incorporation of iron oxide-rich into the matrix.

The data reveals a clear trend indicating that as the iron oxide doping increases, the density of the fired clay samples also increases. This can be summarized as follows:

For Series X0 (0% doping), density values in this series range from 1.651 g/cm³ (FOS -X0) to 1.995 g/cm³ (ABK-X0). The FOS-X0 sample shows the lowest density, which suggests a more porous or less compacted structure. Other samples, such as ABK-X0 and OKY-X0, show higher densities, indicating a denser, more compact mineral composition.

The results reveal that for series X1 (5% doping) of iron oxide, the densities increase across the samples, ranging from 1.679 g/cm³ (FOS-X1) to 1.949 g/cm³ (OKY-X1). The increase in density is likely due to the added iron oxide, which has a higher atomic mass compared to other key components like silicon and aluminum.

Similarly, for series X2 (10% doping), exhibits the highest densities, with values ranging from 1.796 g/cm³ (FOS-X2) to 2.069 g/cm³ (ABK-X2). This further

increase in density is consistent with the additional iron oxide incorporated into the clay, resulting in a more compact structure. Interestingly, the increase in density from X1 to X2 series is less pronounced than from X0 to X1, indicating that the effect of doping may be approaching saturation. Conversely, there is significant improvement of density from X0 series to X2 series

With respect to elemental contributions to density, it is noted that Silicon (Si) is a critical component of clay minerals, contributing to the formation of a silica (SiO_2) framework that provides structural integrity to the material. The silicon content generally decreases slightly from the X0 series to the X2 series. However, silicon's direct contribution to density is less pronounced compared to heavier elements like iron because of its lower atomic mass (Grim 1968). This is illustrated in the graphs showing the relationship between density and Si concentration. On the other hand, aluminum (Al), in the form of aluminum oxide (Al_2O_3), helps to harden the clay material, contributing to its overall strength. The concentration of aluminum remains fairly constant across all series. Aluminum's role in increasing density comes from its ability to reduce porosity and enhance the cohesion of clay particles, which in turn adds to the material's weight (Rahaman, 2003)). In this study, it was observed that the FOS series (X0, X1 and X2) samples which were Kaolin clays were the richest in aluminum, however they were the least dense potential due to the grain size distribution. Furthermore, correlation curves show a negative gradient between the plot of aluminum concentration and clay density. Additionally, according to Bronick & Lal (2005)., some elements like potassium (K) generally, lowers the bulk density of clay soils by improving aggregation and reducing dispersion of clay particles. This trend is noted in FOS-X0 with the

highest K content of 5673mg/kg and the lowest density of the clays in this study. The overall effect on density depends on a combination of factors like potassium concentration, clay type, and soil moisture content. In well-managed soils with adequate potassium, there is a balance between soil structure, compaction resistance, and density (Bronick & Lal (2005)).

From the results obtained, all other parameters remaining constant, iron oxide (Fe_2O_3) is the key factor contributing to the increase in density with doping. Iron has a significantly higher atomic mass (55.845 g/mol) than silicon and aluminum, and its presence in the form of iron-rich oxides directly increases the weight of the material such as mortar or fired clay (Masdeu, et al., 2021). The increase in iron content correlates well with the increase in density observed in the X1 and X2 series samples as found in other studies. At the X0 series as can be seen in Fig. 4.3.2b the correlation between iron and aluminum ratio and density is moderate, however, it is observed that as the concentration of dopant increases the correlation becoming stronger as seen in 4.3.6b indicating that there is a minimum threshold beyond which the impact of the iron can be felt significantly all other things remain constant.

Silva, et al., (2021), contend that titanium's effect on the density of fired clay is minimal, as titanium oxide (TiO) contributes more to the thermal stability and strength of the material under high-temperature conditions rather than directly affecting the overall density. Titanium's atomic mass (47.867 g/mol) is lower than that of iron, and it plays a more subtle role in the densification process compared to iron (Silva, et al., 2021). The results in this study however show that even though concentration of titanium is low and may not significantly contribute to density, a curve fitting between Ti and density show a strong R^2 value offering

insight into a first order approximation predictive model as seen in Fig 4.3.1d, Fig 4.3.3d, and Fig 4.3.5d.

With the exception of Al, it is noted that Ti, Si, and Fe, tend to have a positive correlation relationship with respect to their impact on clay density, It is therefore important to view their impact jointly through a ratio between them and Al. The Si/Al, Fe/Al, and Ti/Al graphs with density reveal a positive trend with varying degrees of agreement giving insights as to how they can be used to predict density values to varying extents.

Beyond elemental composition, there are some other factors that influence density like porosity, tiring temperature and duration and particle sizes (García, et al., 2016.; Gu & Ling (2024).; Eissa et al., (2024); Rahaman, (2003).

The doping of fired clay with iron oxide increases the density of the material, with the highest densities observed in the X2 series (10% doping). Iron oxide is likely to be the primary contributor to this increase due to its high atomic mass. While silicon, aluminum, and titanium also contribute to the structural integrity of the material, they have a less pronounced effect on density. The doping process reduces porosity and enhances the material's cohesion, leading to an overall increase in density. This makes the doped clay samples more suitable for applications in construction and ceramics where enhanced radiation shielding, strength, thermal stability, and aesthetic properties are required.

4.1.2.1 Elemental constituents and density relationship for clays undoped (X0 series)

4.1.3.1.1 Relationship between elemental concentration and density for selected elements

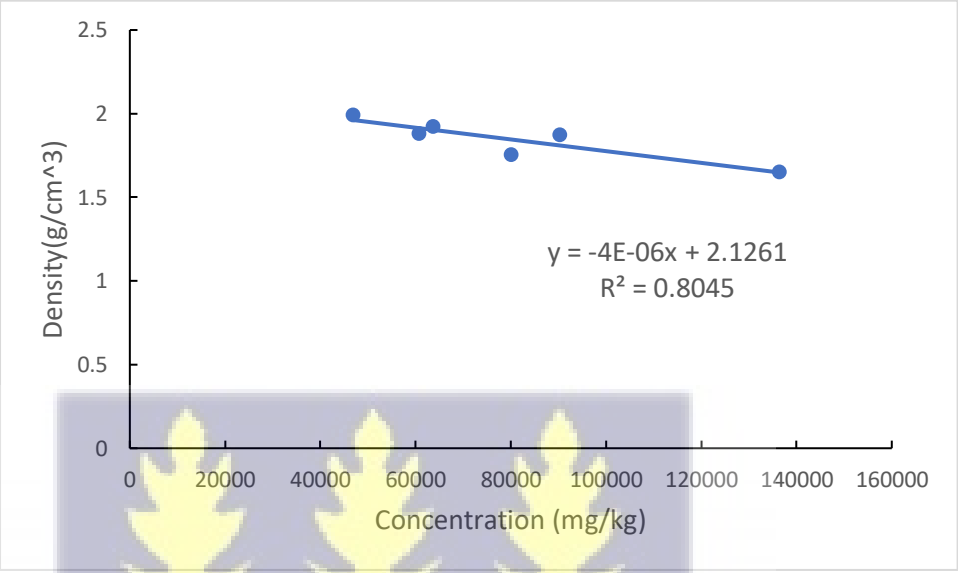

Figure 4.3.1a: A graph showing the relationship between Al concentration and density of undoped clay

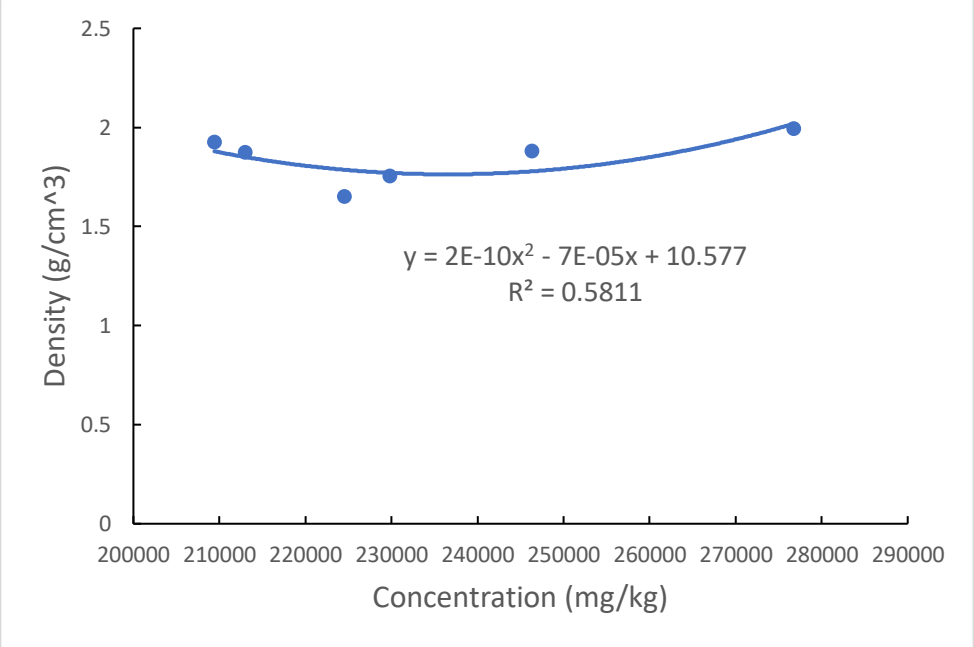

Figure 4.3.1b: A graph showing the relationship between Si concentration and density of undoped clay.

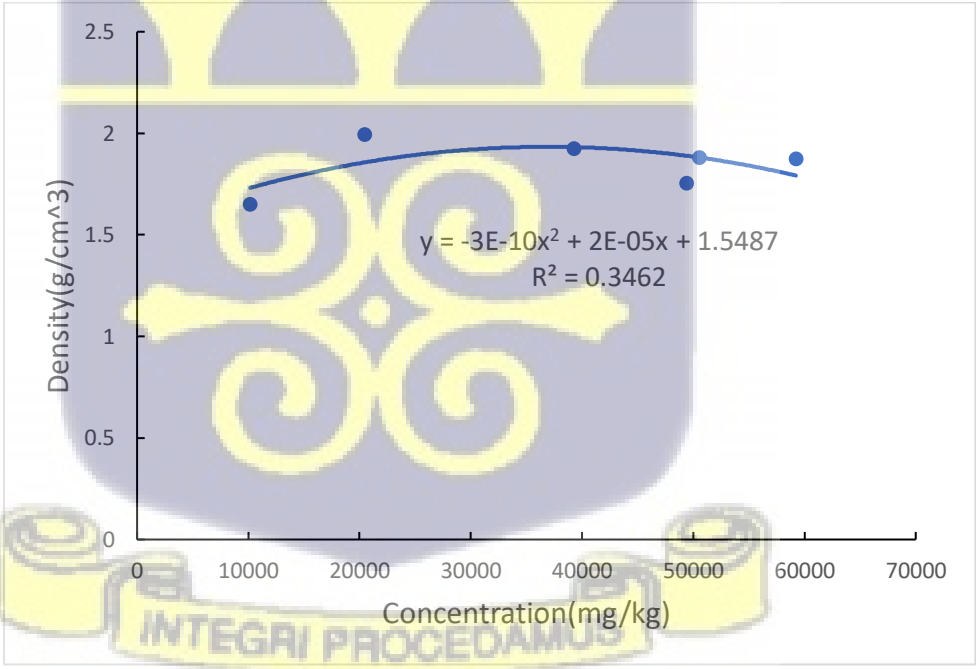

Figure 4.3.1c: A graph showing the relationship between Fe concentration and density of undoped clay

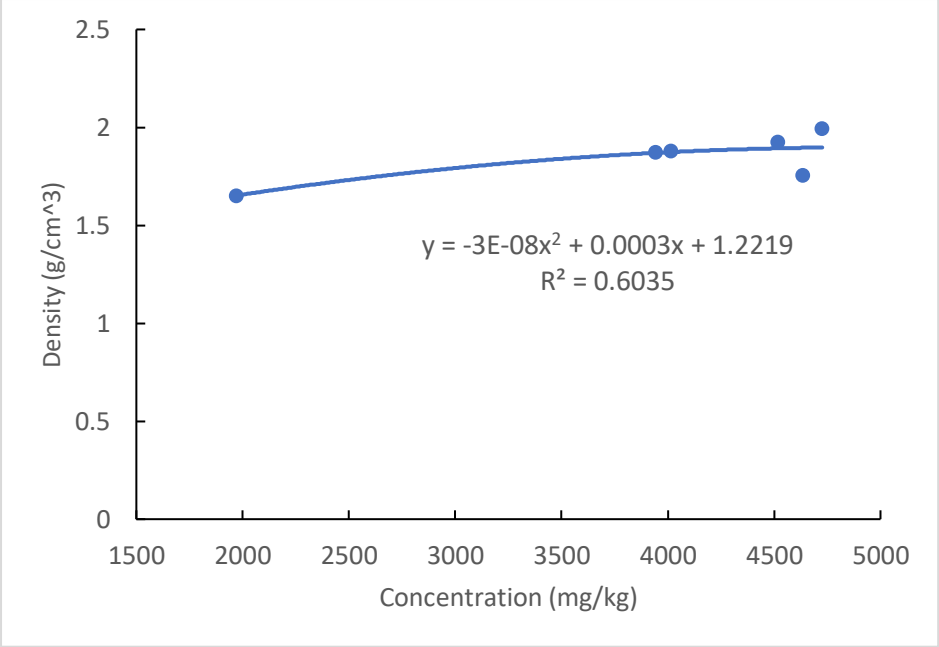

Figure 4.3.1d: A graph showing the relationship between Ti concentration and density of undoped clay.

4.1.3.1.2 Relationship between elemental concentration ratio with Al and density of undoped clay for selected elements

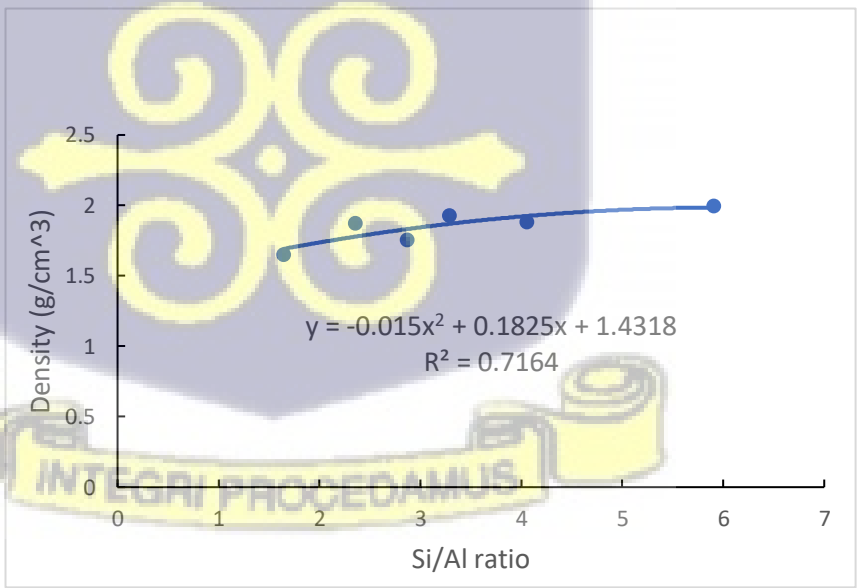

Figure 4.3.2a: A graph showing the relationship between Si/Al concentration ratio and density of undoped clay

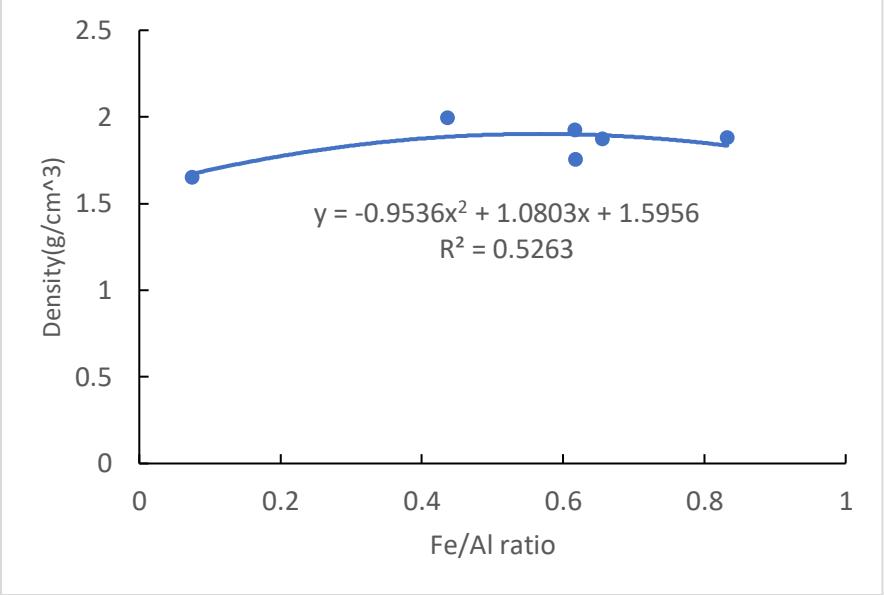

Figure 4.3.2b: A graph showing the relationship between Fe/Al concentration ratio and density of undoped clay.

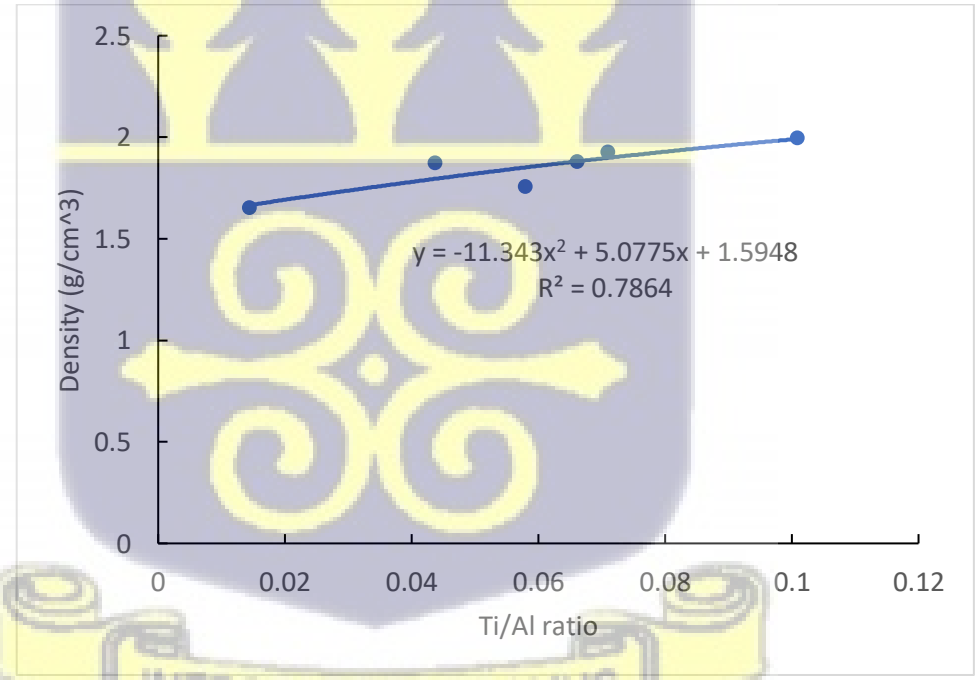

Figure 4.3.2c: A graph showing the relationship between Ti/Al concentration ratio and density of undoped clay

4.1.3.2 Elemental constituents and density relationship for clays doped at 5% by wt (X1 series)

4.1.3.2.1 Relationship between elemental concentration and density of 5% doped clay for selected elements

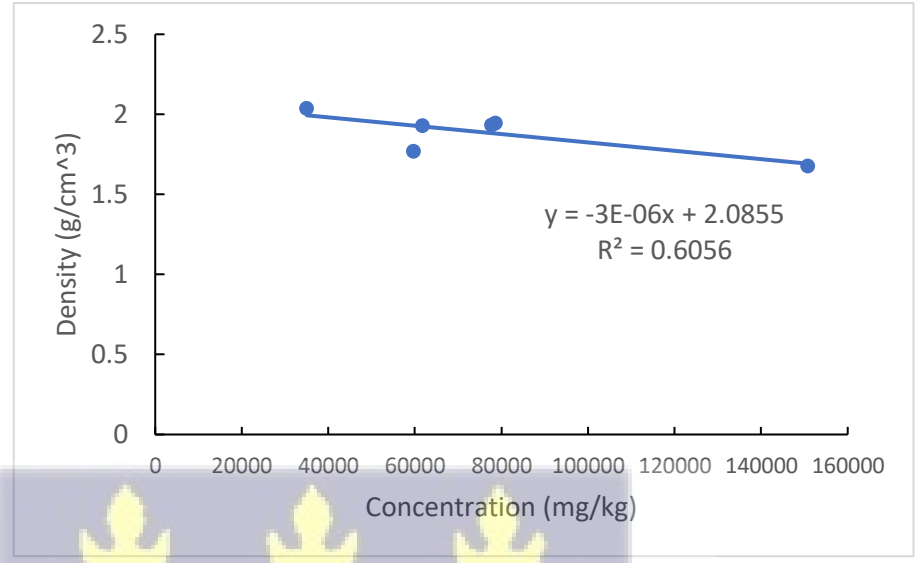

Figure 4.3.3a: A graph showing the relationship between Al concentration and density of 5% doped clay.

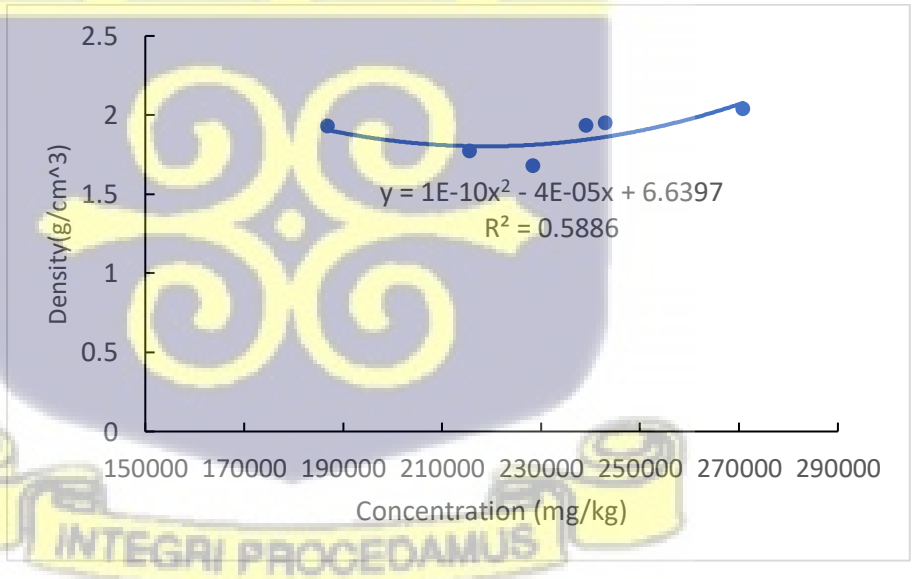

Figure 4.3.3b: A graph showing the relationship between Si concentration and density of 5% doped clay

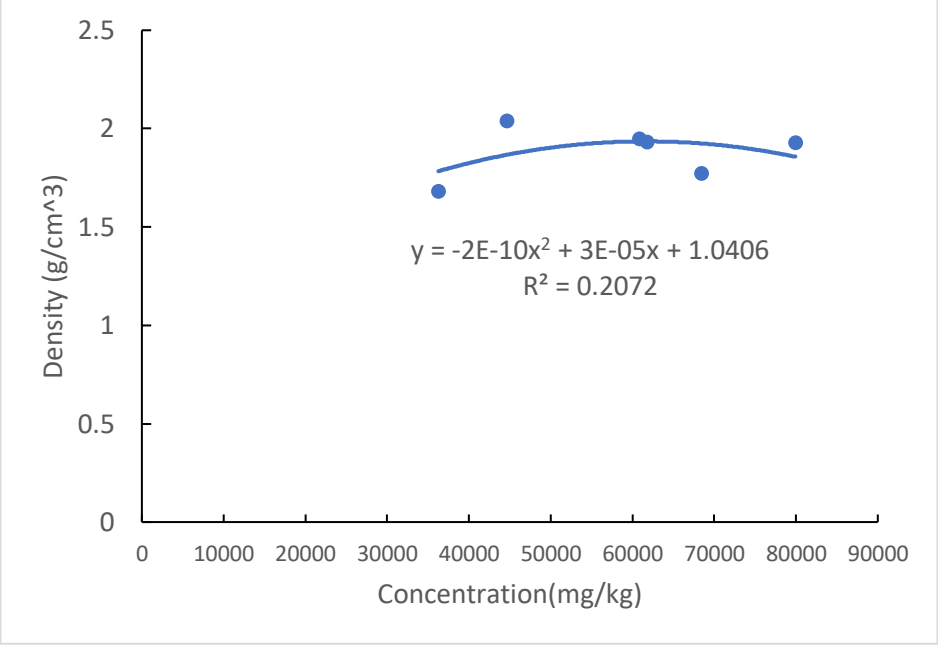

Figure 4.3.3c A graph showing the relationship between Fe concentration and density of 5% doped clay

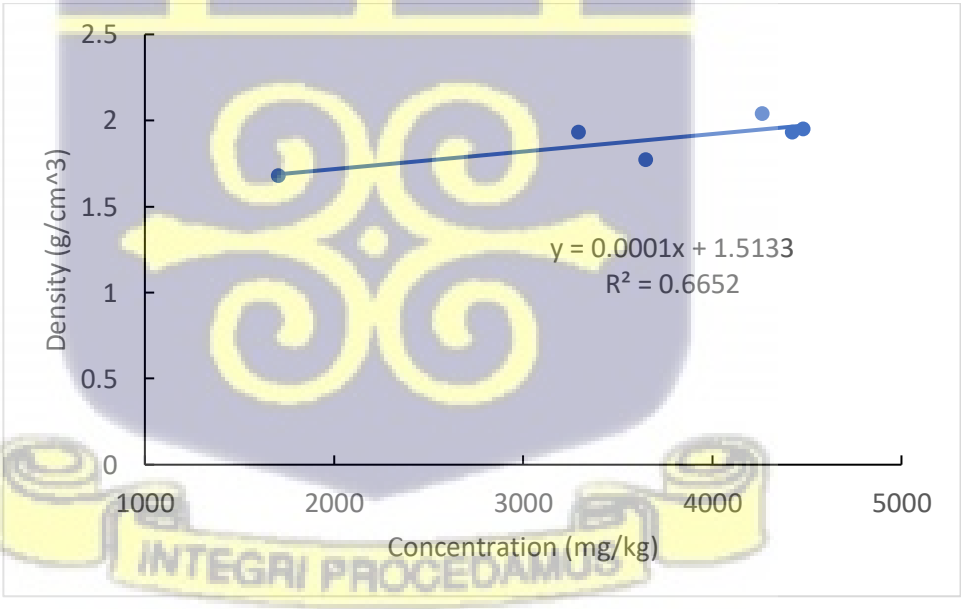

Figure 4.3.3d: A graph showing the relationship between Ti concentration and density of 5% doped clay

4.1.3.2.2 Relationship between elemental concentration ratio with Al and density of 5% doped for selected elements

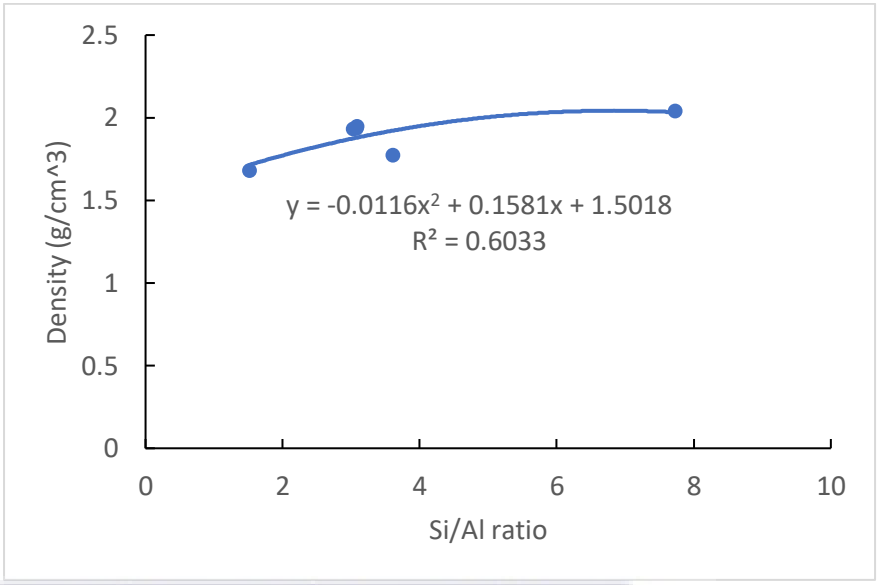

Figure 4.3.4a: A graph showing the relationship between Si/Al concentration ratio and density of 5% doped clay

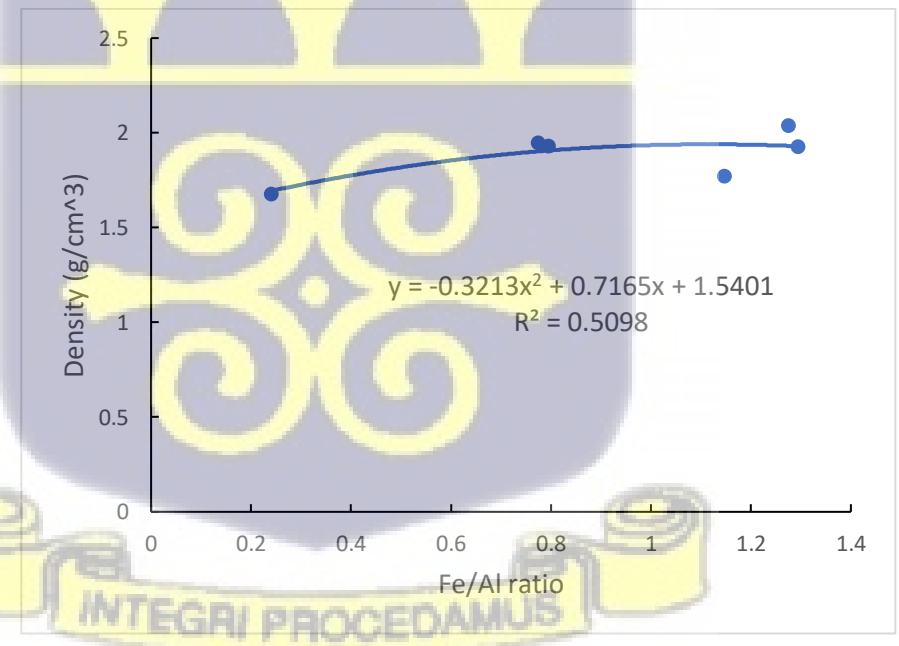

Figure 4.3.4b: A graph showing the relationship between Fe/Al concentration ratio and density of 5% doped clay

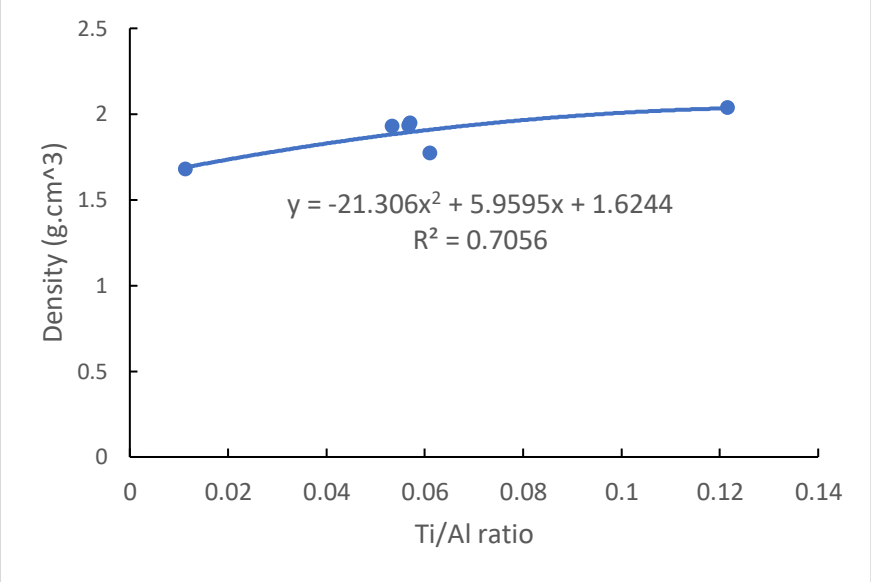

Figure 4.3.4c: A graph showing the relationship between Ti/Al concentration ratio and density of 5% doped clay

4.1.3.3 Elemental constituents and density relationship for clays doped at 10% by wt (X2 series)

4.1.3.3.1 Relationship between elemental concentration and density of 10% doped clay for selected elements

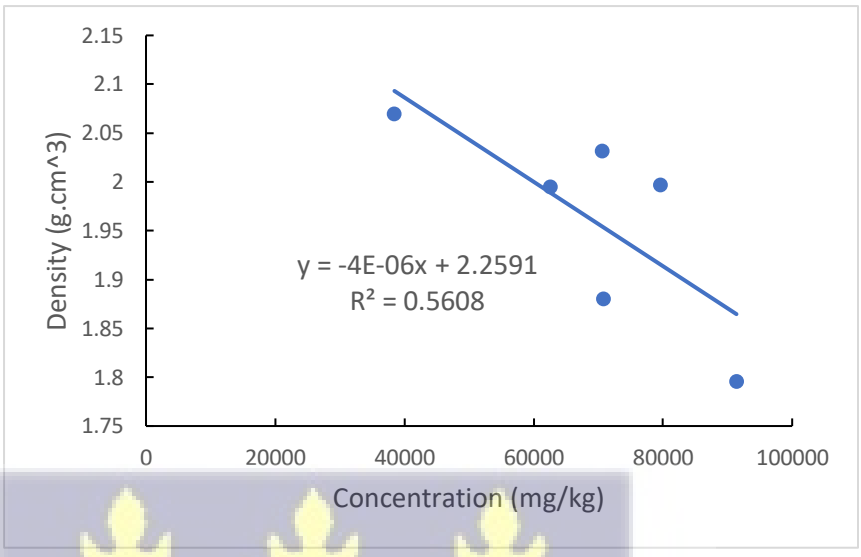

Figure 4.3.5a: A graph showing the relationship between Al concentration and density of 10% doped clay

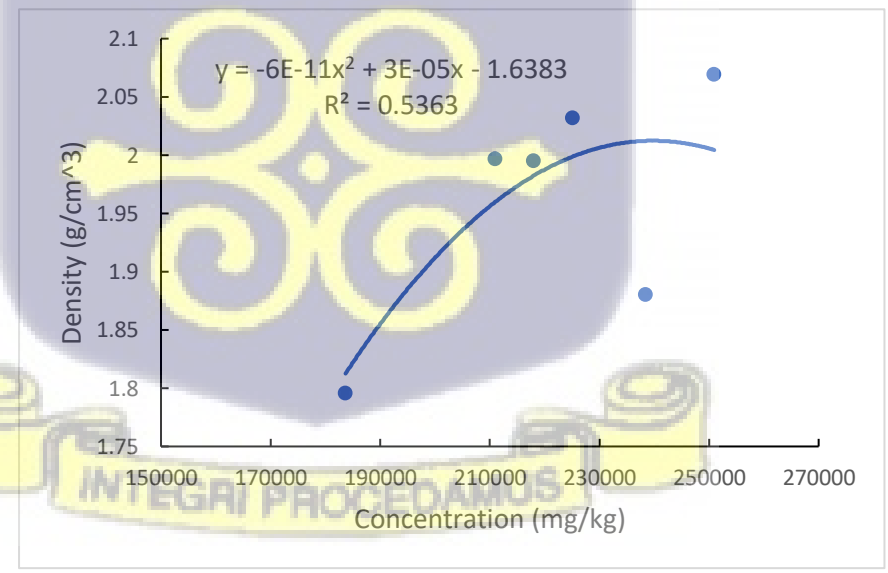

Figure 4.3.5b: A graph showing the relationship between Si concentration and density of 10% doped clay

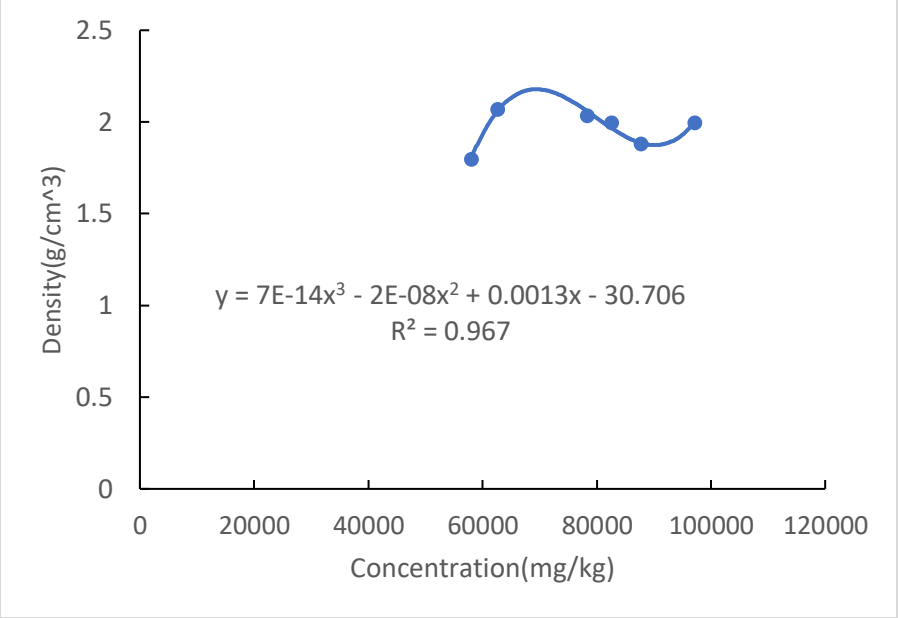

Figure 4.3.5c: A graph showing the relationship between Fe concentration and density of 10% doped clay

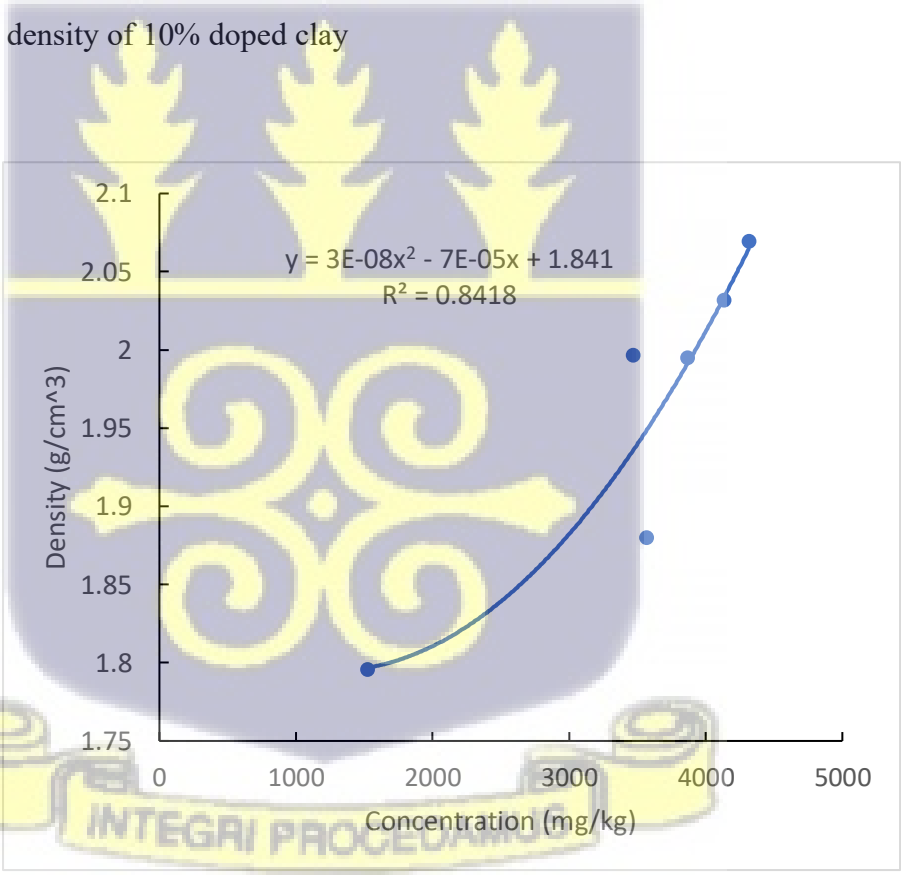

Figure 4.3.5d: A graph showing the relationship between Ti concentration and density of 10% doped clay.

4.1.3.3.2 Relationship between elemental concentration ratio with Al and density for selected elements

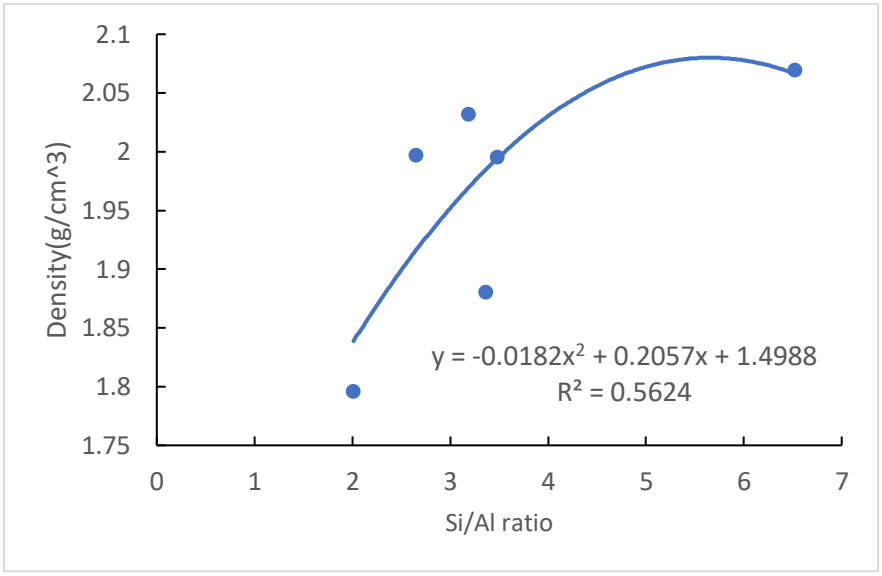

Figure 4.3.6a: A graph showing the relationship between Si/Al concentration ratio and density of 10% doped clay

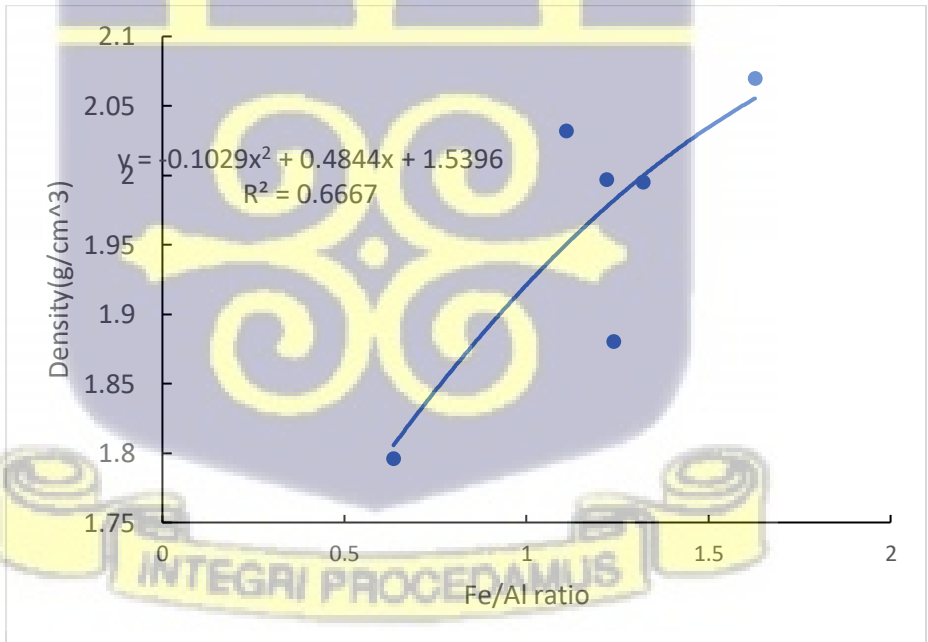

Figure 4.3.6b: A graph showing the relationship between Fe/Al concentration ratio and density of 10% doped clay

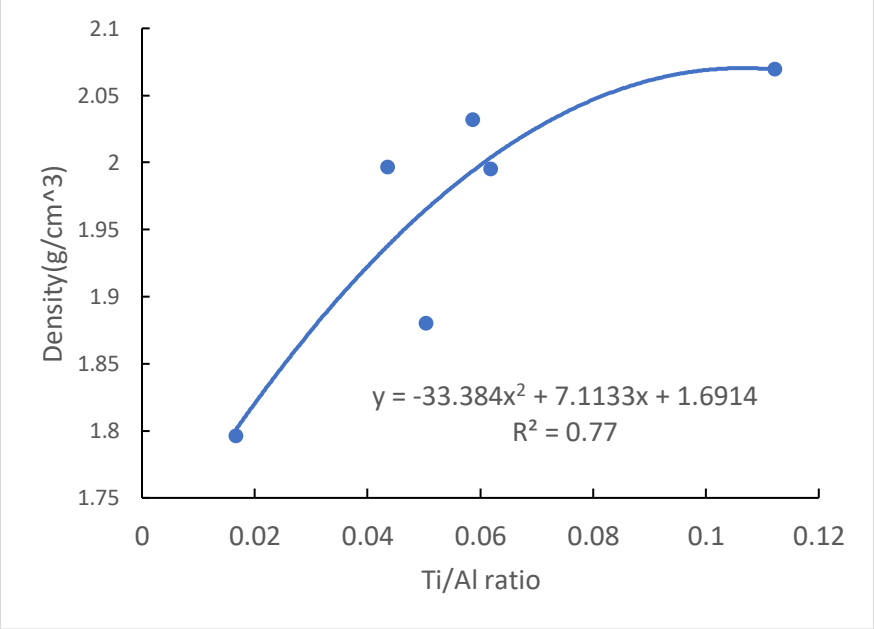

Figure 4.3.6c: A graph showing the relationship between Ti/Al concentration ratio and density of 10% doped clay

Figures 4.3.1a to 4.3.6c have provided some first-hand insights into the relationships between elements in the clays and their density. From the graphs only elemental aluminium had an inverse relationship with density as can be seen in Fig. 4.3.1a, Fig. 4.3.3a and Fig. 4.3.5a.

The negative slope of Al concentration in fired clay compared to its density which is largely described by a linear curve can be attributed to the chemical and physical transformations that occur during the firing process. Aluminum in clay is usually found in minerals such as kaolinite, illite, and smectite, which are aluminosilicates. According to Gu & Ling (2024), during firing, the clay undergoes a series of transformations due to increased temperature, which causes the decomposition of these minerals and the release of volatile components like water and carbon dioxide (Gu & Ling 2024).

Furthermore, when clay is fired, the removal of volatile substances and the densification of the material result in a reduction in porosity and an increase in density (Abubakar, et al 2020). However, this densification may lead to the loss of aluminum from the structure as it reacts with other elements, or as aluminum-containing minerals like kaolinite transform into othe mineral like mullite and feldspar, which typically have lower aluminum content (Gu & Ling 2024). This transformation leads to a decrease in aluminum concentration, while the clay becomes more compact, increasing its density.

Thus, the negative slope reflects a trade-off between aluminum concentration and the physical changes occurring during firing, which result in a denser, less porous material with lower aluminum content (Abubakar, et al 2020; Gu & Ling 2024).

On the other hand, from Figures 4.3.1a to 4.3.6c it is observed that all the other elements as seen largely expressed a positive relationship at varying degrees signifying that although an increase in elemental concentration can improve density to certain extent, it is not the only contributory factor- the relationship is complex and not necessarily linear.

The relationship between the density of fired clay and the concentrations of elements like Si, Fe, and Ti is closely tied to the mineral composition and phase transformations that occur during the firing process. As clay is heated, its mineral components undergo various transformations, which affect both its physical properties (such as density) and its chemical composition (Kingery, et al 1976).

Silicon is a key component of many clay minerals, particularly aluminosilicates, and plays a critical role in the densification process. As the clay reaches higher

temperatures, silica (SiO_2) reacts with alumina to form mullite and glassy phases, contributing to a denser microstructure (Rahaman, 2003). Similarly, iron and titanium, both of which are present in various clay minerals, influence the densification process and the overall strength of the fired clay. Fe often forms iron oxides, while Ti is commonly found in rutile or anatase forms, both of which can contribute to the clay's mechanical properties and density as they affect the sintering process (Kamseu, et al. 2007).

The relationship between the elements' concentrations and density can often be quantified by a regression analysis, producing R^2 values that indicate how well the concentration of each element predicts the density of the fired clay. Higher R^2 values demonstrate a stronger correlation between the two variables, suggesting that the elemental content is a key factor in determining the density. Studies have shown that Fe and Ti exhibit more complex relationships, often with lower R^2 values. This suggests that Fe and Ti may have secondary effects. (Kingery, et al 1976; Rahaman, 2003). Other parameters such grain size can play a role in density. Also, in order to evaluate the overall impact of an inverse relationship as in the case of Al as compared to the positively trending elements, a ratio of the major elements with Al was compared to the densities as seen in Figures 4.3.2 a- 4.3.2c, 4.3.4a – 4.3.4c and 4.3.6a – 4.3.6c. These graphs give an idea on the extent and impact of the opposing "forces",i.e. elements with positive trending impact and that of Al which has a negative trending impact on density.

4.2 Physico-Mechanical Properties

4.2.1 Grain size distribution of samples

The particle size distribution of the clay samples plays a crucial role in determining the material's physical properties, including its density, porosity, and strength. In this analysis, we are examining the percentage passing through a series of sieves for various undoped samples undoped (denoted as ABK-X0, AMK-X0, FOS-X0, KBU-X0, OFM -X0, OKY-X0). The same test analysis was done for the iron-rich oxide dopant. The particle size distribution is given for a range of sieve sizes from 0.85 mm to 0.000001 mm (representing the pan) These are presented in Fig 4.4.

Plotting the dopant % passing data on the same graph illustrates graphically its contribution to the effect of iron oxide doping on the particle size distribution. This is particularly significant because the incorporation of dopants can change the physical characteristics of the fired clay, influencing its overall performance in applications such as ceramics, construction, and other materials science areas.

The sieve sizes start from 0.85 mm (larger particles) and the setup is completed at the bottom with an impermeable pan (assumed as 0.000001 mm), with each value indicating the percentage of material that passes through the corresponding sieve. The finer the sieve, the smaller the particles that pass through, and the higher the percentage of material retained on the sieve.

At the 0.85 mm sieve, all samples have very high percentages passing through, ranging from 98.3% to 100%. This indicates that most of the material in these

samples consists of particles smaller than 0.85 mm, which is typical for clays used in construction and ceramics. The 0.71 mm sieve shows slightly lower percentages passing through, with

AMK-X0 showing a notably lower value of 95%, indicating a slightly coarser composition in this sample. At the 0.5 mm sieve, there is a greater variation, with FOS -X0 (94.5%) and KBU-X0 (83.8%) showing higher percentages passing through compared to OFM-X0 (81.6%) and OKY-X0 (77.8%). This suggests a finer particle distribution in FOS-X0, but a relatively coarser composition in KBU-X0, OFM-X0, and 0KY-X0.

It can be seen that for smaller sieve sizes like 0.3 mm, the differences between the samples become more apparent. Samples like AMK-X0 and FOS-X0 still show relatively high passing percentages (56.4% and 62%, respectively), while other samples like AFM-X0 and OKY-X0 show much lower passing percentages (31.5% and 45.7%, respectively). Upon approaching the 0.212 mm and 0.15 mm sieves, the proportion of finer material decreases significantly, with OFM-X0 and OKY-X0 showing the lowest values (7.1% and 9.6%, respectively). This indicates that these samples contain a larger proportion of coarser particles, which will have an impact on the material's porosity and density.

It is further observed that the curves of ABK-X0 and OFM-X0 have the very similar grain size distribution because their curves nearly coincide.

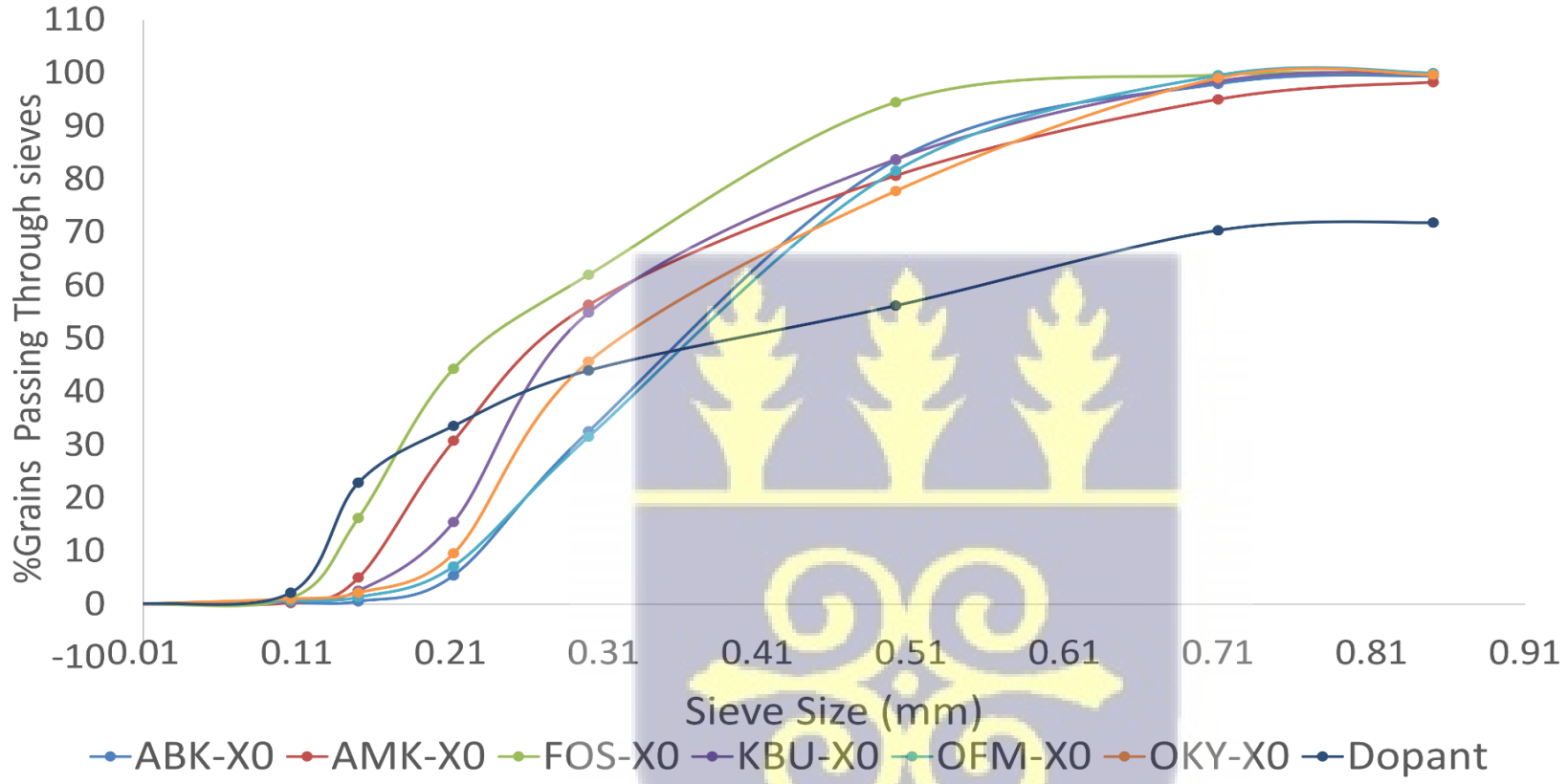

Figure 4.4: A graph showing the grain size distribution of the clay samples and dopant

Regarding the dopant, there is a marked difference in the % passing compared to the clay samples. At 71.9% passing through the 0.85 mm sieve, suggesting that the dopant has larger particles compared to the clay samples, particularly for the smaller sieve sizes, furthermore, the adhesive characteristic of the oxide powder may have also contributed to this. This implies that the addition of iron-rich oxide may affect the particle size distribution, likely increase the size of the particles or affecting the sintering and particle agglomeration behavior during firing.

The particle size distribution directly impacts the density and porosity of fired clay materials. Several key trends can be observed in the data that are crucial for understanding the effects of particle size distribution on density:

The samples that show higher percentages of coarse particles passing through the larger sieves (OFM-X0) tend to have lower densities. Coarse particles contribute to higher porosity, which reduces the overall density of the material (Gu & Ling 2024). These coarser grains create larger voids within the structure, resulting in a less compact material.

In contrast, in the lower sieve size region at roughly 0.212 mm, samples with a higher proportion of finer particles (ABK-X0, AMK-X) tend to exhibit higher densities. Fine particles fill the voids between larger grains, resulting in a more compact and denser structure (Rahaman, (2003). This trend is evident when comparing ABK-X0 and AMK -X0 with samples like OFM-X0 and OKY-X0.

The addition of iron-rich oxide, as seen in the dopant data, appears to shift the particle size distribution towards slightly larger particles. This shift in particle size distribution could result in increased porosity or, conversely, the densification of certain materials due to the effect of iron oxide on the sintering behavior (Silva, et al., 2021). This can explain why the doped material has a different distribution compared to the original samples, potentially leading to different mechanical properties and performance.

The iron oxide dopant may facilitate sintering, causing smaller particles to agglomerate and form larger particles during the firing process. This process can affect the final density by altering the way in which the particles bond together at high temperatures (García, et al., 2016).

The particle size distribution of these fired clay samples is markedly different from that of ordinary concrete. In ordinary concrete, the particle size distribution typically includes a larger proportion of coarse aggregates such as gravel and sand. The distribution is designed to maximize packing density while minimizing voids. Concrete typically has a density of 2.3 to 2.5 g/cm³, which is higher than that of the fired clay samples found in this study (Eissa et al., 2024).

The particle size distribution significantly influences the properties of fired clay, including its density, porosity, and strength. The X0 series samples, which are finer and more uniformly distributed, exhibit higher densities than the course OFM-X0 sample. The introduction of iron oxide as a dopant modifies the particle

size distribution and likely enhances the sintering behavior, resulting in a different physical structure that may affect the final properties of the material.

4.2.2 Porosity of Test Pieces from Samples

Fired clay products, such as bricks and ceramics, exhibit a wide range of porosity values depending on factors like their elemental or mineral composition presence of organic matter and other impurities as well as firing conditions. Porosity is a key property that affects the material's density, strength, and water absorption.

Countless studies have established that porosity in fired clay materials typically ranges from 10% to 40%, depending on the specific formulation and firing conditions. This porosity can be categorized into macroporosity (large voids) and microporosity (small voids), which are influenced by the clay mineral content, organic matter, and other factors (Srisuwan & Nonthaphong. 2020; Benmoussa, 2019).

Srisuwan, and Nonthaphong report that fired clay bricks show porosity values around 20% to 30%. These values vary due to the local soil composition, which may include higher amounts of sand or silt. The higher porosity of these bricks typically contributes to their insulating properties. The elemental composition, such as higher levels of aluminum and silica, influences the amount and size of the pores formed during the firing process (Srisuwan & Nonthaphong. 2020)

As well, Jock, *et al* 2013, recount that traditional pottery in Sub-Saharan Africa typically exhibits a porosity range of 20% to 40%. Studies in countries like Nigeria

have shown that clays rich in kaolinite and illite have higher porosity. (Jock, *et al* 2013).

Figure 4.5 shows the porosities of the clays studied in this work. Consistently, it can be seen that the FOS series generally had higher values of porosity - always greater than 30%. This is not surprising as it is a kaolinite and very rich in aluminum as compared to all the clays.

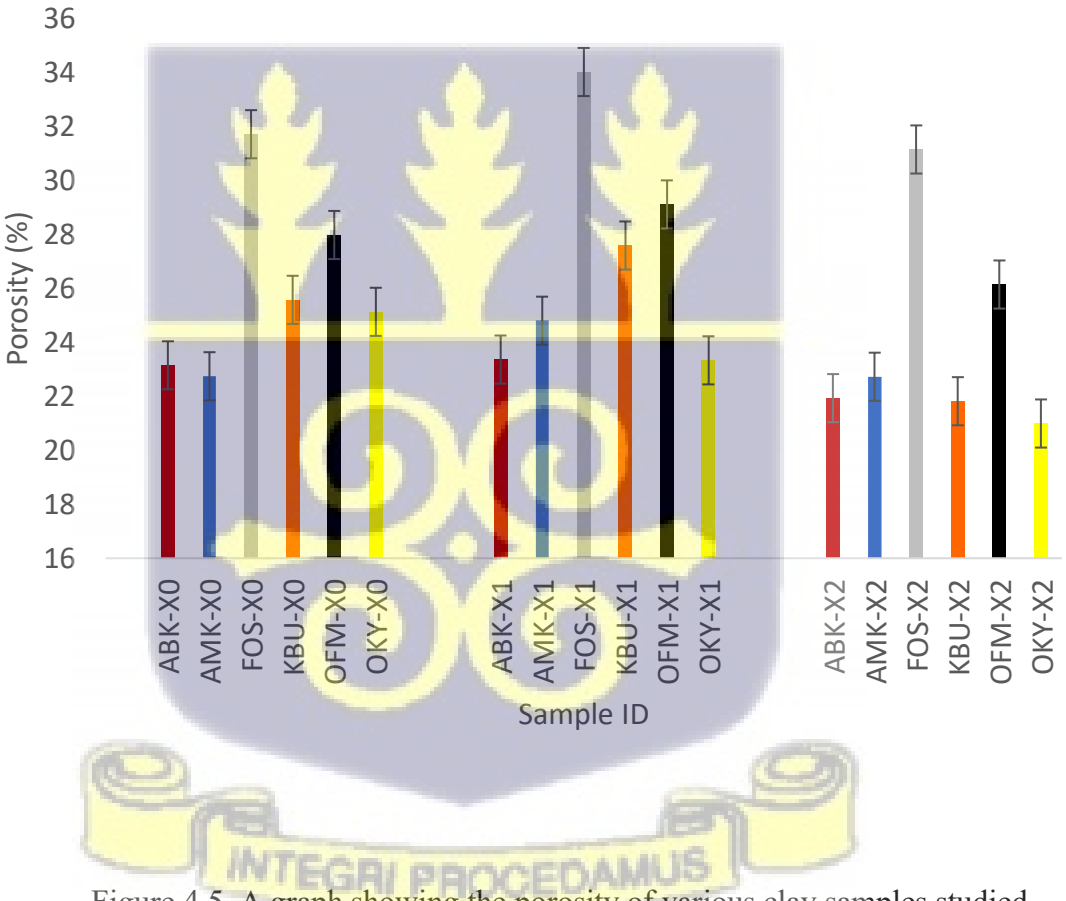

Figure 4.5. A graph showing the porosity of various clay samples studied

4.2.3 Density of Test pieces from samples

The densities of the undoped and doped fired clays have been studied as presented in Fig 4.6. It is observed that their densities increase slightly accordingly after the doping at 5% wt and also at 10% wt . Discounting the kaolinite in the study (FOS clay) since that is the one that is distinctively different form the others and focusing on the remaining five clays (ABK, AMK, KBU, OFM and OKY series), a single factor ANOVA comparing densities of X0 series to X1 series (p- value = 0.528568) reveals that even though the 5% wt doping slightly increased it did not bring about a statistically significant change. However, comparing the X0 to X2 the (p-value = 0.047785) suggests statistically different densities at 10% wt doping

This could be attributed to the addition of the Fe_2O_3-rich oxides which contributed to density enhancement in two ways – based on the density of the constituent elements of the dopant as well as the grain size distribution and how it complements the overall grain sized distribution and the associated pore structure for each clay; whether doped on undoped.

From Figure 4.1a - 4.1c it is observed that the most prominent elements in the samples are Aluminum (Al), Silicon (Si), and Iron (Fe). A simplified analysis of how these elements correlate with density Fig 4.3.1a to 4.3.6c reveal insights into the structural and compositional characteristics of the materials.

For ABK clay, the densities steadily increase from 1.995 g/cm³ (ABK-X)) to 2.070 g/cm³ (ABK-X2). Similarly, densities increase from 1.881 g/cm³ (AMK-X0) to 2.032 g/cm³ (AMK-X0). FOS densities are lower compared to the ABK and AMK samples. FSO-X0 has the lowest density at 1.651 g/cm³, and the density increases

to 1.796 g/cm³ in FOS-X2. There is a moderate increase in density of KBU samples from 1.874 g/cm³ (KBU-X0) to 1.997 g/cm³ (KBU-X2). In the case of OFM Samples the densities varied slightly within the group, from 1.755 g/cm³ (OFM-X0) to 1.880 g/cm³ (OFM-X2). OKY samples show nearly consistent densities around 1.92 to 1.95 g/cm³, with a slight increase from OYK-X0 (1.925 g/cm³) to OKY-X2 (1.995 g/cm³).

It can be gleaned from the results that the densities of the ABK and AMK samples consistently increase across the three measurements. These increases in density are likely due to the accumulation of denser minerals or elements, such as iron (Fe), which is known for its high atomic weight and impact on density. Iron-rich clays and materials typically show increased density as compared to silicon-dominated clays.

The FOS group exhibits the lowest densities. The relatively lower density in these samples may be due to their higher content of Aluminium (Al) and increased porosity. Instructively, KBU, OKY and OKY show moderate densities. These values suggest moderate mineralization, with neither particularly high iron nor silicon content. The consistency in density across these samples' hints at the presence of a balanced elemental composition.

Some studies have reported similar trends in the relationship between density and elemental composition of materials, particularly focusing on clays and mineral-rich earth materials. Jock, *et al* (2013) analyzed the mineralogical and physical properties of Nigerian clays, reporting densities ranging from 1.70 g/cm³ to 2.10

g/cm³, with clay samples rich in aluminum (Al) and iron (Fe) tending to have higher densities, similar to the ABK and AMK groups in this study. These findings align with the idea that iron significantly contributes to the higher densities observed in these samples (Jock, et al 2013).

Furthermore, Sütçü, et al., (2015) and García, et al (2016). investigated the effects of elemental composition on the properties of some fired clays , noting that clays rich in iron oxides exhibited higher densities, while silicon-rich clays, particularly those with significant kaolinite, showed lower densities (Sütçü, et al., 2015; García, et al (2016).). Their results mirror the trends observed in the ABK and AMK samples versus the FOS group in this study.

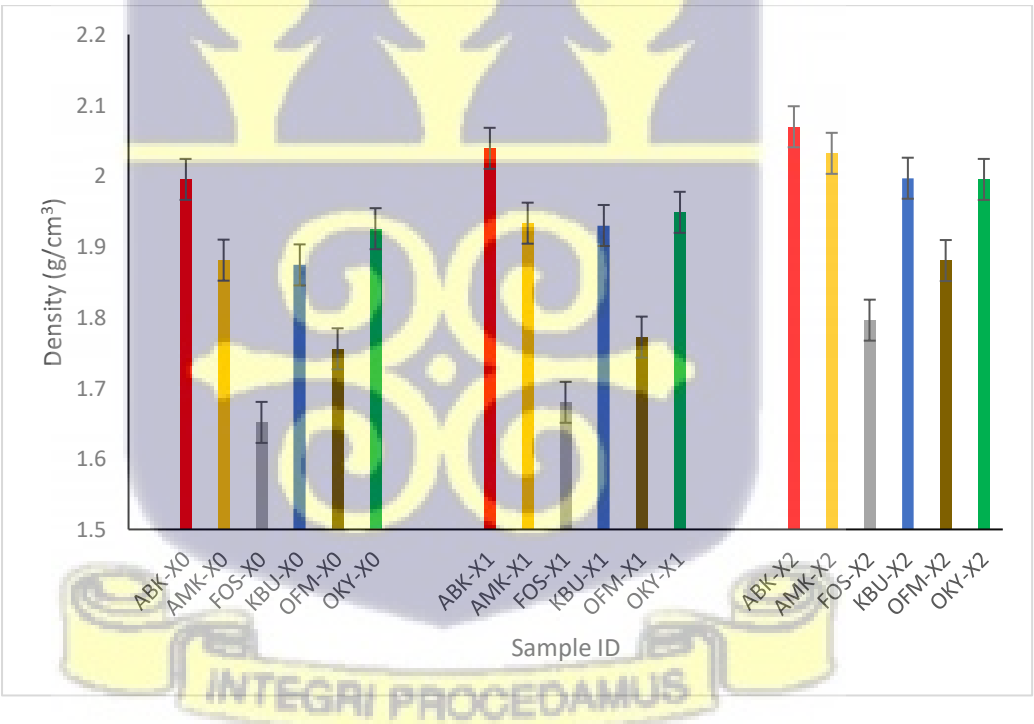

Figure 4.6 A graph showing the comparison of the densities of clay samples studied.

Considering that density is a critical parameter when assessing the suitability of materials for shielding some types of radiation it is important to ascertain the impact and dynamics of density. Higher density materials are typically more effective at attenuating gamma radiation due to their increased mass, which leads to a greater likelihood of photon interactions.

For example, ABK clay which has the highest density in all the series (1.995 g/cm³, 2.039 g/cm³, 2.069 g/cm³ for X0, X1 and X2 series respectively) are expected to offer better shielding for gamma radiation compared to lighter materials like the FOS series. The ABK may be more effective in industrial and medical applications where high radiation exposure is common.

Conversely, FOS-X0, with the lowest density of 1.651 g/cm³, may not be as effective at shielding against gamma radiation. However, it may still be useful in low-energy gamma radiation environments or where other factors like cost and material availability are important (Mori, et al., 2020).

These findings align with the general understanding in the literature, where materials with higher density, such as concrete or lead, tend to perform better in photon shielding applications. However, the clays in this study may provide a more cost-effective and locally sourced alternative.

Importantly also, other factors influence density. These include Porosity, which inversely affects the density of a material. In general, the higher the porosity, the lower the density, as more air pockets are trapped within the material. In the case

of the doped samples, the increase in iron oxide likely reduces porosity by filling the voids between particles, leading to higher density. The reduction in porosity contributes significantly to the density increase observed in the X1 and X2 series samples (Rahaman, 2003). Figures 4.7a-4.7c illustrate the negative gradient and strong correlation coefficient of the curves of density and porosity for all the clays studied across the various series confirming the inverse relationship between these two parameters.

Additionally, during the firing process, the firing temperature and duration of firing plays an important role in determining the final density of fired clay. Higher temperatures promote the sintering process, which causes the clay particles to bond more tightly, resulting in a denser material (Gu & Ling 2024). In this study, one temperature 1000 °C was used to fire the clay into bricks, it is however expected that firing the clay at higher temperatures, e.g. 1050°C or 1100°C will contribute to further increasing the density and strength of the material.

Furthermore, the particle size distribution of raw clay is another important factor influencing its density. Finer particles generally lead to a denser material because they can bond more effectively during the firing process. Coarser particles, on the other hand, may result in a more porous structure. The particle size distribution in the raw materials used for doping could therefore have affected the final density of the fired clay.

Ordinary concrete typically has a density in the range of 2.3 to 2.5 g/cm³ (Eissa et al., (2024). This is higher than the density of the fired clay samples, especially

those in the X0 series, which range from 1.651 to 1.995 g/cm³. However, it is important to note that concrete's higher density is due to the incorporation of heavy aggregates like sand, gravel, and crushed stone. These aggregates are much denser than the clay materials used in this study.

Fired clay, on the other hand, is used in applications where lower density, thermal insulation, and aesthetic properties are desired. The increase in density observed in the X1 and X2 series makes these doped clay samples more suitable for applications that require enhanced strength or thermal properties, such as construction bricks, tiles, and ceramics (Silva, et al., 2021).

The findings from this analysis have several practical applications, particularly in the fields of radiation protection. The materials studied, particularly those with high iron and silicon content, could serve as cost-effective alternatives to conventional shielding materials like lead or concrete, particularly in developing countries where cost and material availability are significant factors (Tyagi, et al (2020). By utilizing naturally abundant materials, these clay materials could reduce the need for resource-intensive commercial materials, making them more sustainable and environmentally friendly.

This is especially important in areas with limited access to imported shielding materials (El-Samrah, et al., 2023). These materials could find application in medical facilities for X- ray and radiation therapy shielding, as well as in nuclear facilities for protection against radiation leaks. Their use in radiation therapy centers in developing countries could help reduce costs while still maintaining adequate safety standards (Mori, et al., 2020).

4.2.4 Relationship between Porosity and Density of Test pieces

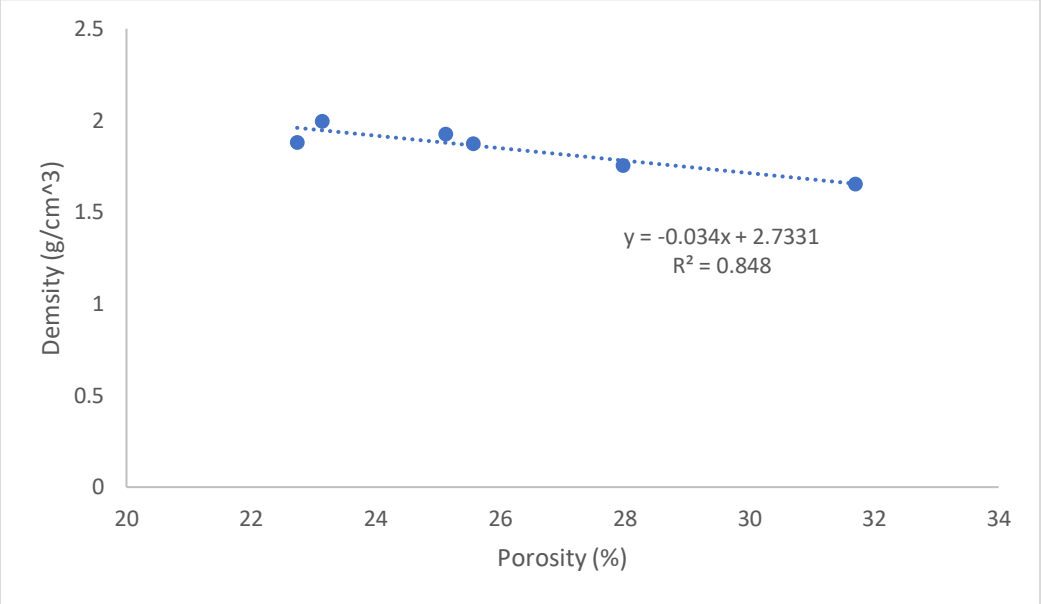

Figure 4.7a: A graph showing the relationship between density and porosity of undoped clay

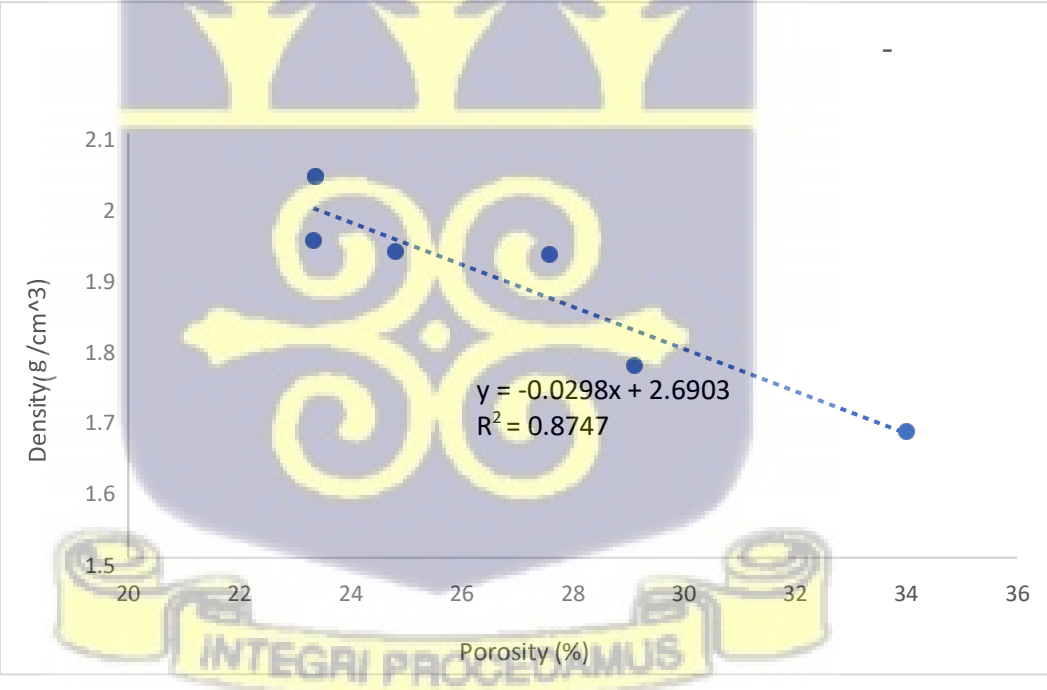

Figure 4.7b A graph showing the relationship between density and porosity of clay doped at 5% wt

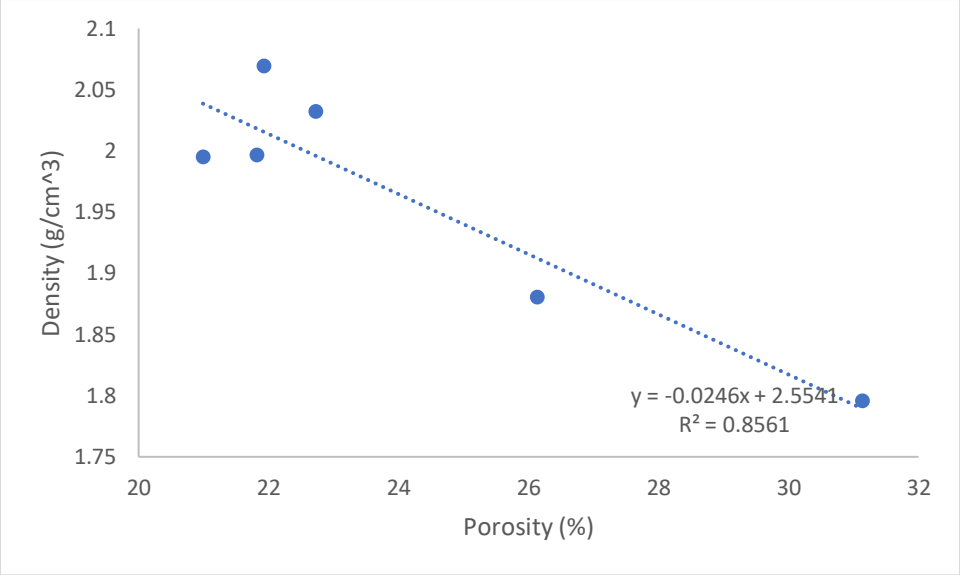

Figure 4.7c A graph showing the relationship between density and porosity of clay doped at 10% wt.

4.3 Radiation Shielding Properties

4.3.1 Evaluation from Laboratory Experiments

Gamma radiation shielding is a critical aspect in the protection of sensitive environments such as nuclear reactors, medical facilities, and space equipment. The effectiveness of materials used to shield gamma radiation is generally quantified using parameters such as the linear attenuation coefficient (LAC), mass attenuation coefficient (MAC), half-value layer (HVL), tenth-value layer (TVL), and mean free path (mfp). These parameters provide insights into the ability of materials to absorb or scatter gamma rays, thus reducing the radiation dose.

In practical terms, the LAC represents the material's ability to attenuate gamma radiation in terms of distance or shield thickness. This means that higher LAC values suggest better attenuation. The MAC on the other hand measures the material's effectiveness in attenuating gamma rays relative to its mass it is a more useful parameter when comparing two materials as against using LAC. Figures 4.8a through to 4.10f which are radiation transmission curves illustrate the LAC results obtained in their work while 4.12 and 4.13 compare the LAC and MAC of the studied materials. Fig. 4.11 also show the transmission curves through 4mm aluminum composite panels (Alucobond)

Additionally, evaluating how much thickness of a shield is adequate is reliant upon two concepts first the HVL which is the thickness of the material needed to reduce the gamma ray intensity by half, and the TVL which is the thickness required to reduce the gamma ray intensity by 90%. For both HVL and TVL a smaller value indicates that the material has better shielding capacity. Finally, the mfp describes

the average distance gamma photons travel through the material before being attenuated. A shorter mfp indicates higher attenuation.

For each of the of clay-based materials studied these parameters have been obtained and compared with Polyethylene, Ordinary Concrete, Aluminum, and Lead to give context. The HVL, TVL and mfp results are presented in Fig 4.14a, 4.14b, and 4.14c.

From the results obtained, a comparison of density and linear attenuation coefficients (LACs) for several clay-based materials undoped and doped with iron-rich oxides (denoted as ABK, AMK, FOS, KBU, OFM, and OKY), alongside traditional shielding materials such as Polyethylene, Ordinary Concrete, Iron, Lead, Aluminum, and Alucobond. The LAC values are provided for Am-241 (59.5 keV), Cs-137 (662 keV), and Co-60 (average 1.25 MeV) gamma rays are presented.

Gamma shielding effectiveness is determined by both the density and atomic composition of a material. A higher density generally indicates better gamma shielding because it increases the likelihood of photon interactions. The LAC represents the material's ability to attenuate gamma radiation at specific energy levels, with a higher LAC indicating better shielding performance.

The clay-based materials show a range of densities from 1.651 g/cm³ FOS-X0 to 2.069 g/cm³ (ABK-X0, which are significantly lower than materials like Lead (11.35 g/cm³) and Iron (7.874 g/cm³). This lower density suggests that the clay-based materials have reduced gamma shielding efficiency compared to heavier,

denser materials. However, with extra treatment to optimize their density, they can be at par with ordinary concrete in terms of linear attenuation coefficient.

The LAC values for the clay-based samples at Am-241 which represent the low energy range is from 0.372 cm ^{1} for FOS-X0 to 0.596 cm $^{-1}$ for ABK-X2. These values are notably higher than Polyethylene (0.1832 cm^{-1}) and Alucobond (0.295 cm^{-1}), suggesting that the clay-based materials may offer better attenuation than these materials. However, they are still far less effective than Lead (56.988 cm^{-1}), which is the most efficient shielding material for low-energy gamma radiation.

With regard to the LAC values for the clay-based materials at Cs-137 representing intermediate energy, it ranged from 0.116 cm ^{1} FOS-X0 to 0.145 cm ^{1} ABK-X2. These values are lower than Lead (1.2419 cm ^{1}) and Iron (0.5821 cm ^{1}), indicating that the clay-based materials provide less shielding for this energy range. However, Ordinary Concrete (0.1822 cm ^{1}) is comparable to the higher-density clay samples, particularly ABK-X2.

For higher-energy gamma rays like Co-60, the LAC values for the clay-based materials range from 0.08 cm ^{1} (FOS-X0) to 0.107 cm ^{1} (ABK-X2). These values are relatively low, reflecting the lower shielding efficiency of these materials for high-energy gamma radiation. In comparison, materials like Lead with density 11.35 cm ^{1} and an LAC for Co-60 of 0.6669 cm ^{1} and Iron (7.874 cm ^{1}) are much more effective in attenuating high-energy gamma rays.

By far, Lead is the most efficient material for gamma shielding, especially for low-energy gamma rays such as Am-241. It very high density and LAC values make it ideal for applications requiring high radiation protection. Its ability to attenuate Co-60 gamma rays with an LAC of 0.6669 cm^{-1} is also significant, making it the most preferred choice currently in both medical and industrial applications where high- energy gamma radiation is prevalent. However, its toxicity and potentially low melting point when int interacts with very high temperatures calls for alternative if possible. Ordinary Concrete with a density: 2.3 g/cm^3 and an LAC for Am-241 being 0.6118 cm^{-1}, 0.1822 cm^{-1} for Cs-137 and 0.1336 cm^{-1} for Co-60 makes ordinary concrete a good substitute shielding material due to its affordable cost and moderate density. While not as effective as Lead in attenuating Co-60, concrete is known to provide good protection at intermediate and low energies such as Cs-137 and for Am-241 as well as medical level X-rays. As can be observed from Fig 4.12 its LAC values are close to the best-performing clay-based materials, particularly ABK-X2, signifying promise for clay in gamma radiation shielding.

Polyethylene, with its low density (0.93 g/cm^3), performs poorly as a gamma shield, particularly at higher energies. Its LAC values for all gamma energies are much lower than those of the clay-based materials, making it ineffective as a primary shielding material in environments with significant gamma radiation.

Aluminum has a moderate density (2.699 g/cm^3) and performs better than Polyethylene in terms of attenuation of gamma radiation. Its LAC for Am-241 and Cs-137 is notably higher than that of the clay-based materials, making it an

effective option for shielding at lower and intermediate energies. However, it does not provide the high level of shielding necessary for high-energy gamma rays like Co-60.

Numerous studies have focused on the gamma shielding properties of various materials, including clay-based composites, and have compared them to traditional materials like Lead and Concrete. Elsafi, et al. (2021) found that clay-based composites, particularly those doped with elements like bismuth, cadmium, barium or tungsten, can significantly improve shielding properties, though they still fall short of Lead in terms of attenuation at high gamma- ray energies (Elsafi, et al. 2021). Additionally, Eisa, et al (2024). demonstrated that ordinary concrete and clay composites with various additives perform similarly for medium-energy gamma rays such as Cs-137 (Eisa, et al., 2024).

Furthermore, Olukotun, et al (2021). compared clay-based materials with Polyethylene and Iron, concluding that clay composites with higher density elements showed superior shielding at low gamma energies but could not match the high-energy shielding performance of Lead (Olukotun, et al 2021).

The gamma shielding performance of clay-based materials is moderate across the energy spectrum, with their best performance is observed at low energies like Am-241. However, at higher gamma-ray energies (e.g., Cs-137 and Co-60), their shielding effectiveness falls behind traditional materials like lead and iron.

4.3.1.1 Radiation Transmission in undoped clay series

For all clay types and for all energies the impact of the iron-rich dopant is most felt in the X2 series which were doped at 10% by wt. This improvement in attenuation capacity was most obvious in X2 series for Am-241. This demonstrates that for lower photon energies 50keV to about 200 keV clay whose density has been improved performs equally and even better when MAC is considered showing its suitability to be applied as shielding material for medical X-ray room shielding. Figures 4.8a to 4.8f show the transmission of the selected radiation in the undoped clays.

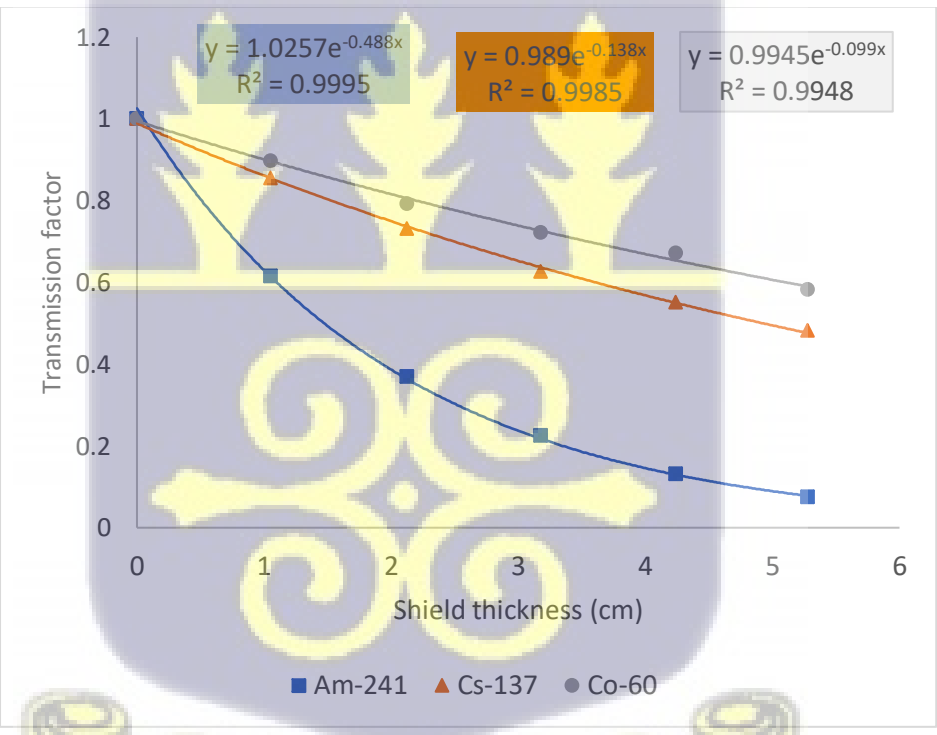

Figure 4.8a: A graph showing photon transmission through ABK-X0 clay

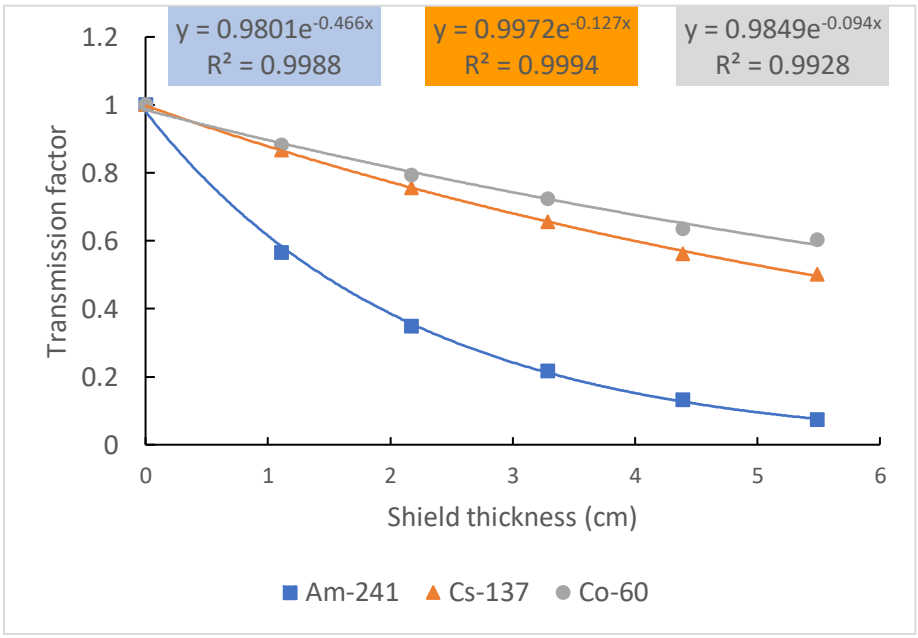

Figure 4.8b: A graph showing photon transmission through AMK-X0 clay

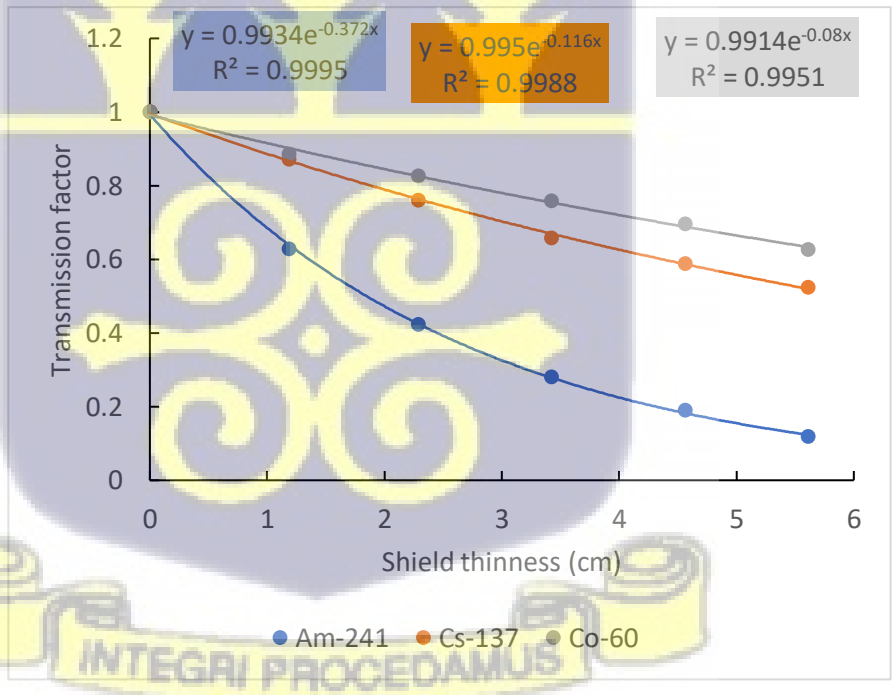

Figure 4.8c: A graph showing photon transmission through FOS-X0 clay

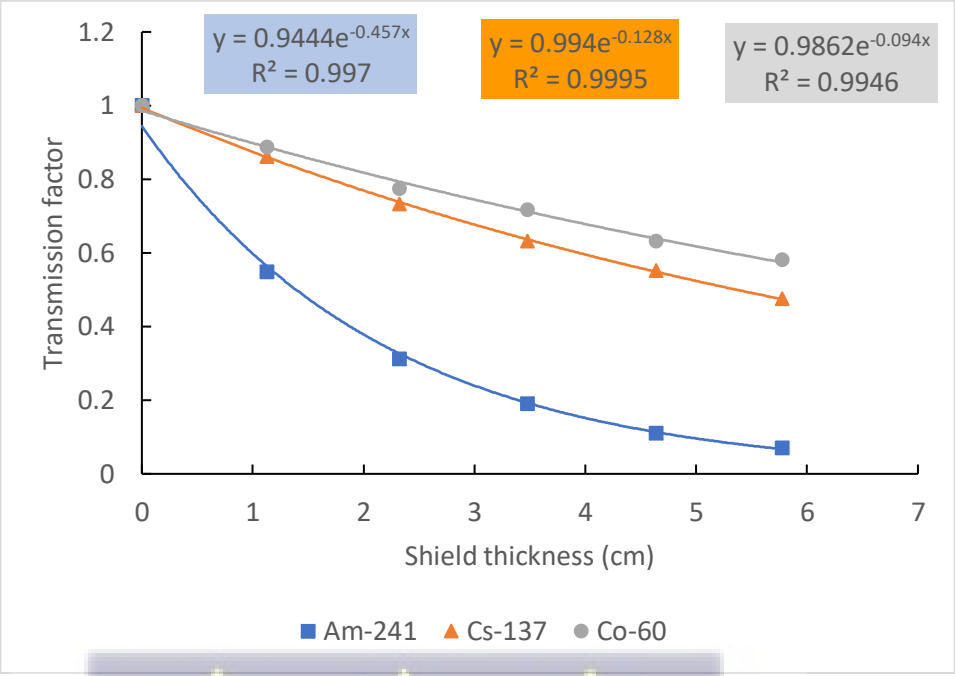

Figure 4.8d: A graph showing photon transmission through KBU-X0 clay

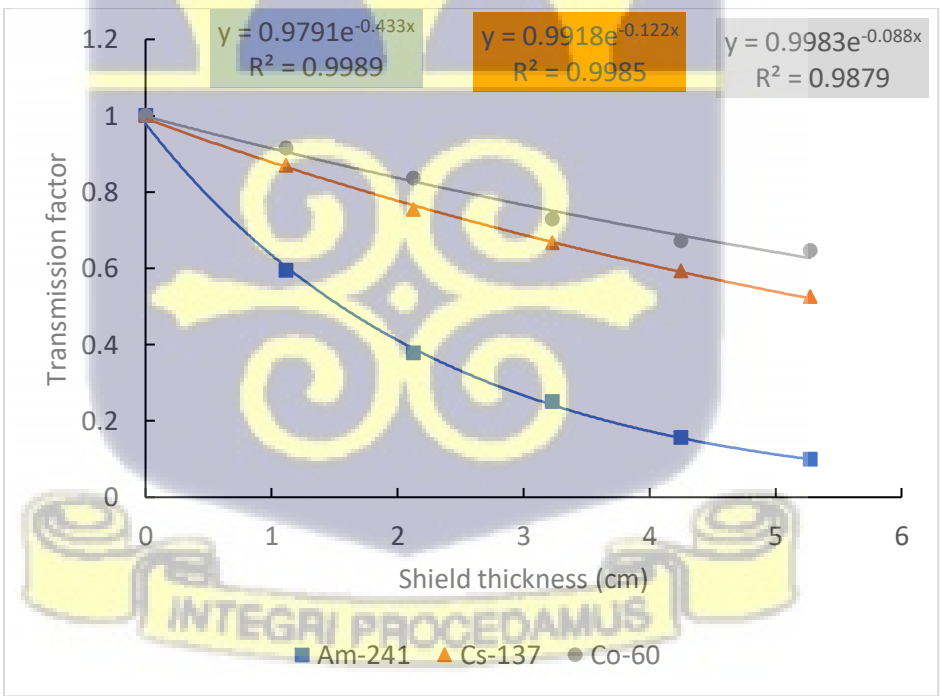

Figure. 4.8e: A graph showing photon transmission through OFM-X0 clay

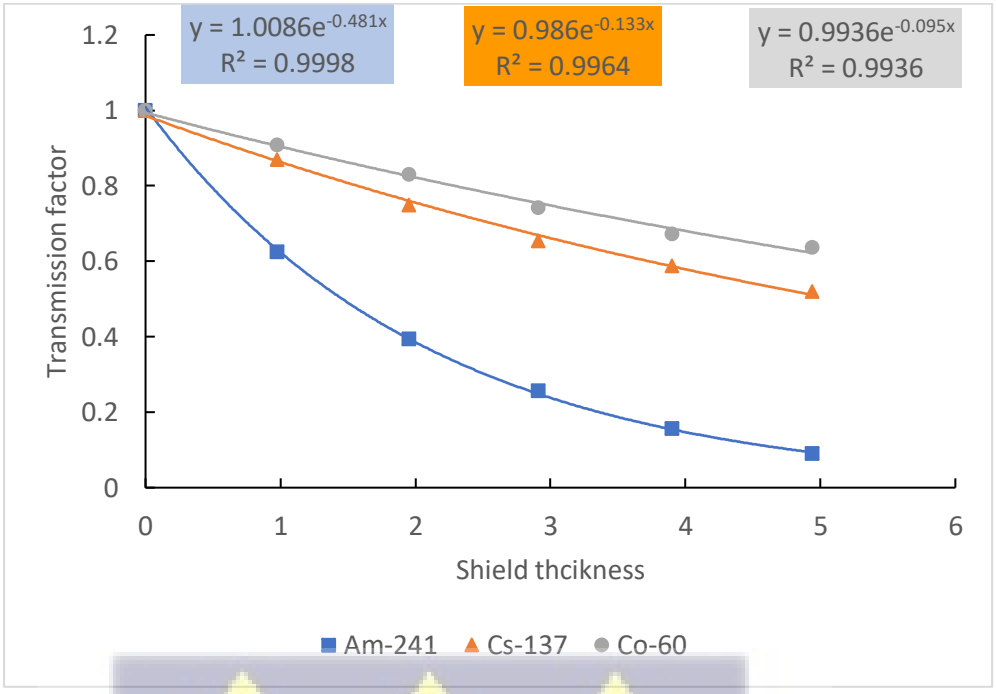

Figure. 4.8f: A graph showing photon transmission through OKY-X0 clay

4.3.1.2 Radiation Transmission in doped clay (5% by wt) series

Figures 4.9a to 4.9f show the transmission of the selected radiation in the clays doped at 5% by wt.

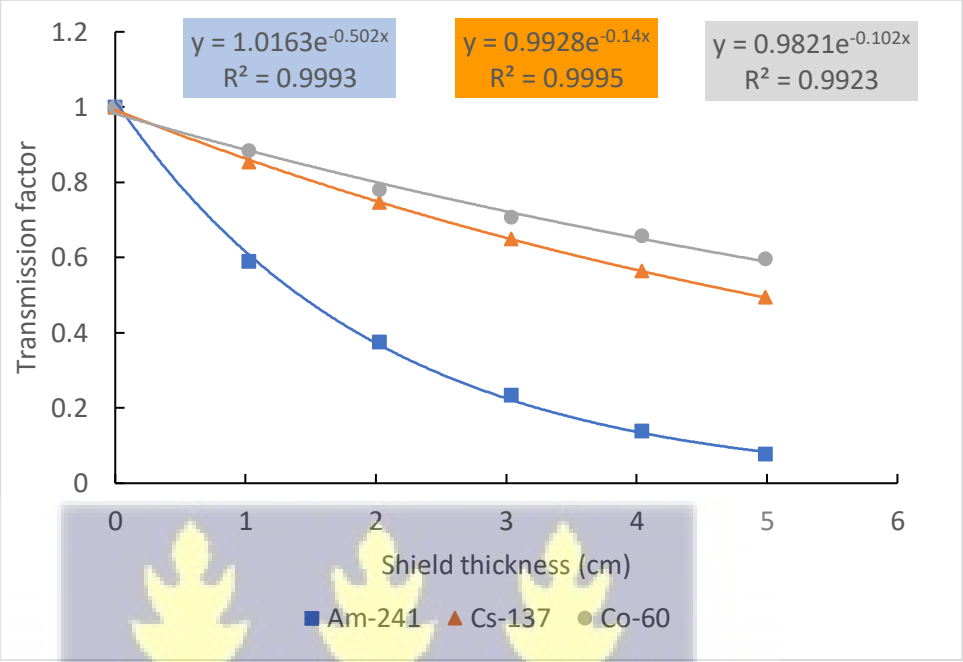

Figure. 4.9a: A graph showing photon transmission through ABK-X1 clay

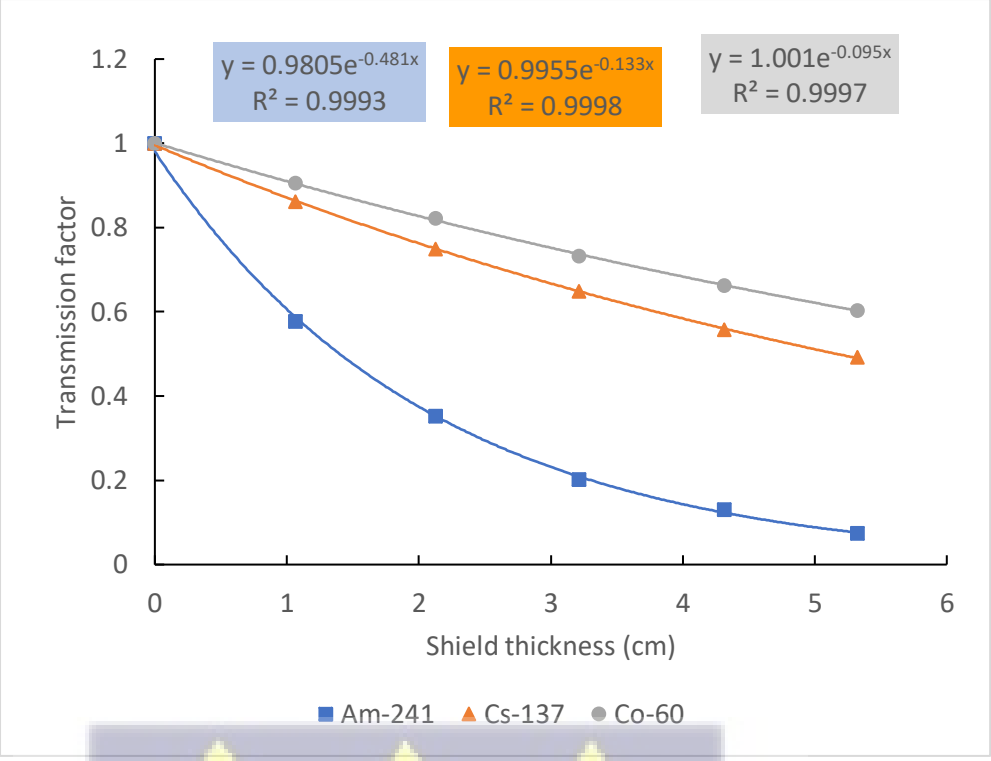

Figure. 4.9b: A graph showing photon transmission through AMK-X1 clay

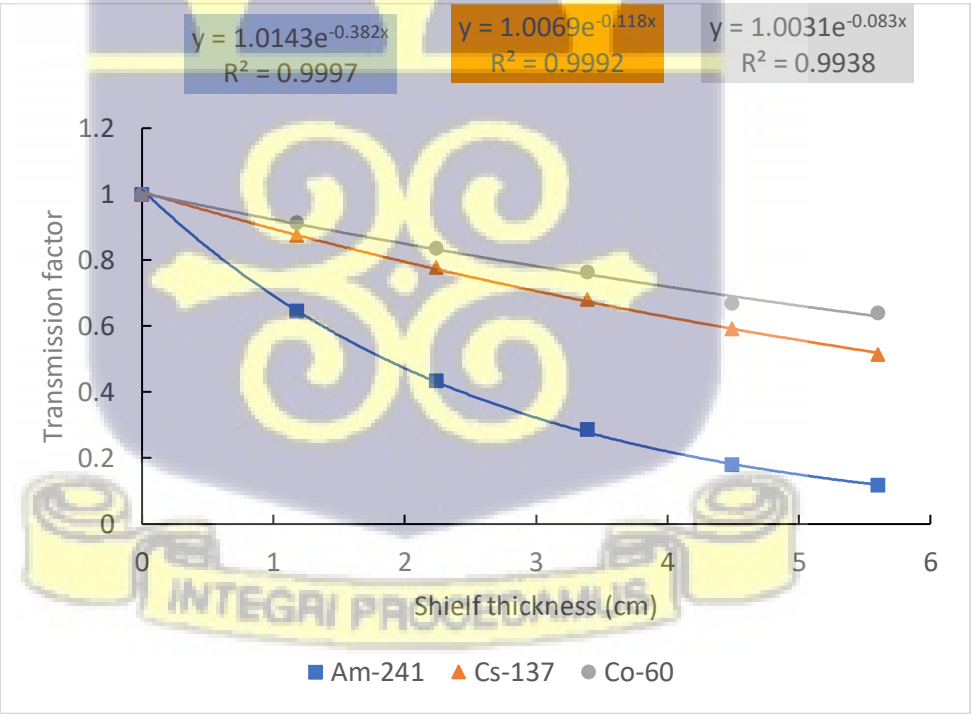

Figure. 4.9c: A graph showing photon transmission through FOS-X1 clay

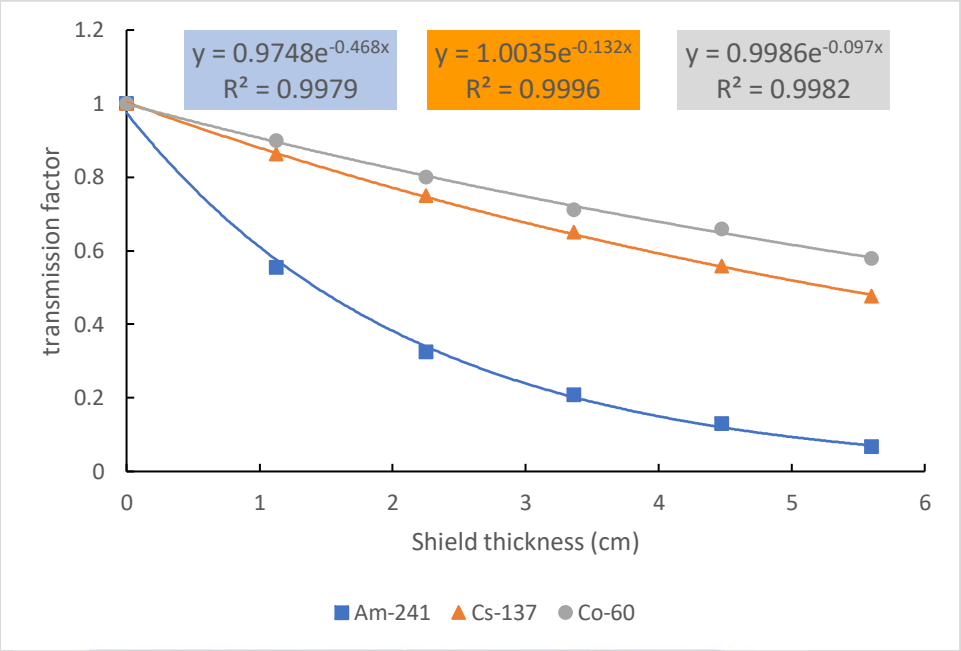

Figure. 4.9d: A graph showing photon transmission through KBU-X1 clay

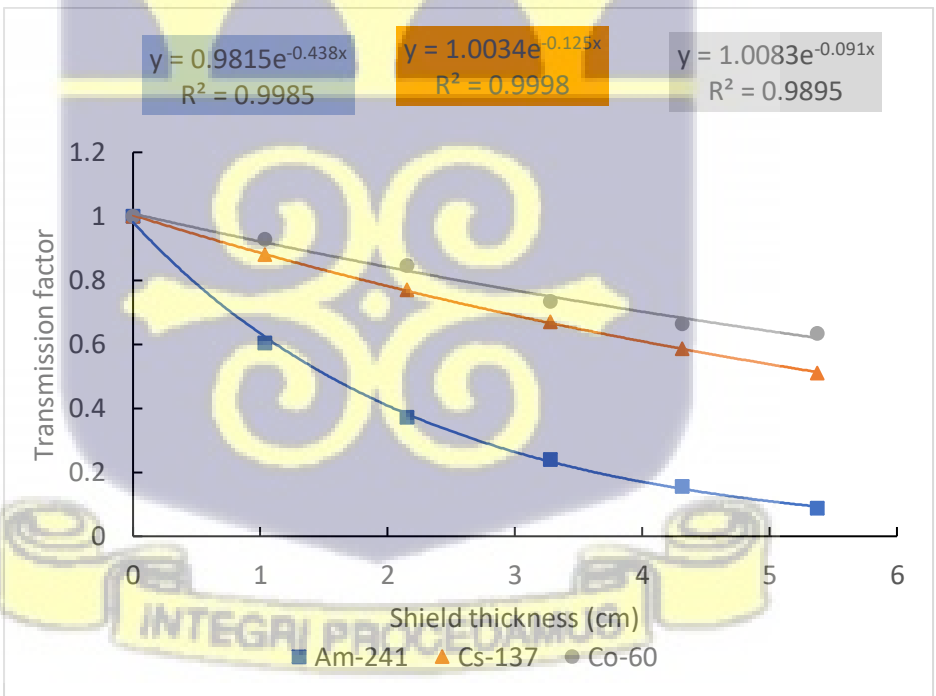

Figure. 4.9e: A graph showing photon transmission through OFM-X1 clay

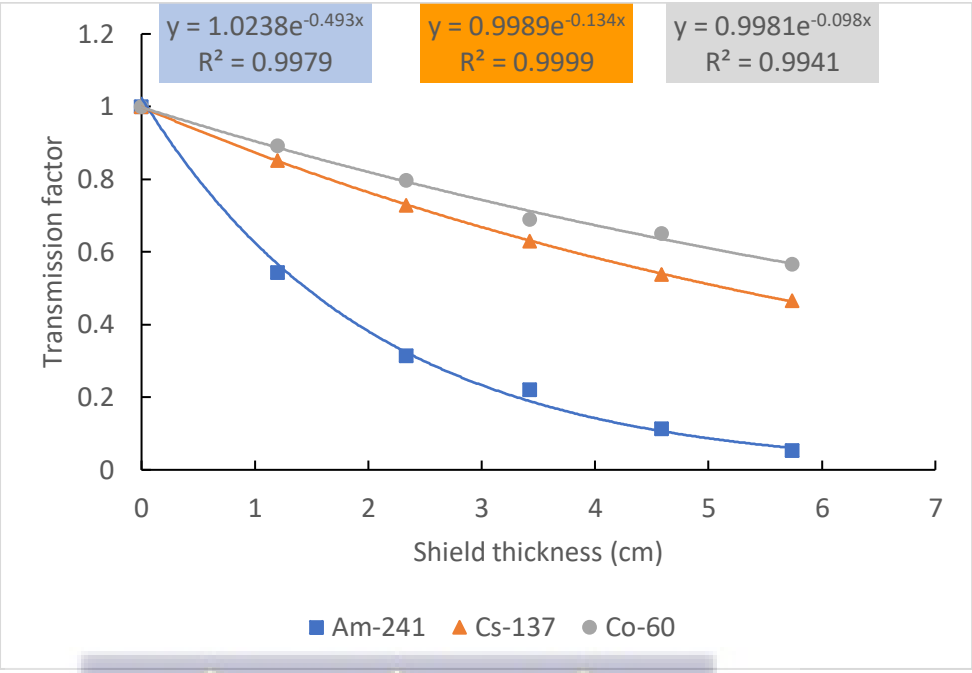

Figure. 4.9f: A graph showing photon transmission through OKY-X1 clay

4.3.1.3 Radiation Transmission in doped clay (10% by wt) series

Figures 4.10a to 4.10f show the transmission of the selected radiation in the clays doped at 10% by wt.

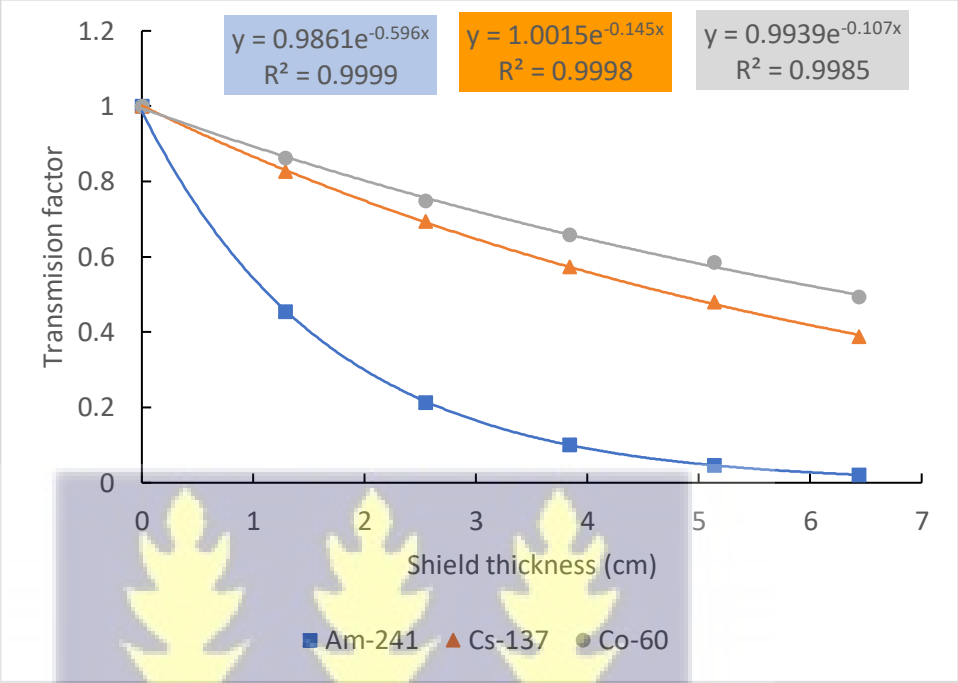

Figure. 4.10a: A graph showing photon transmission through ABK-X2 clay

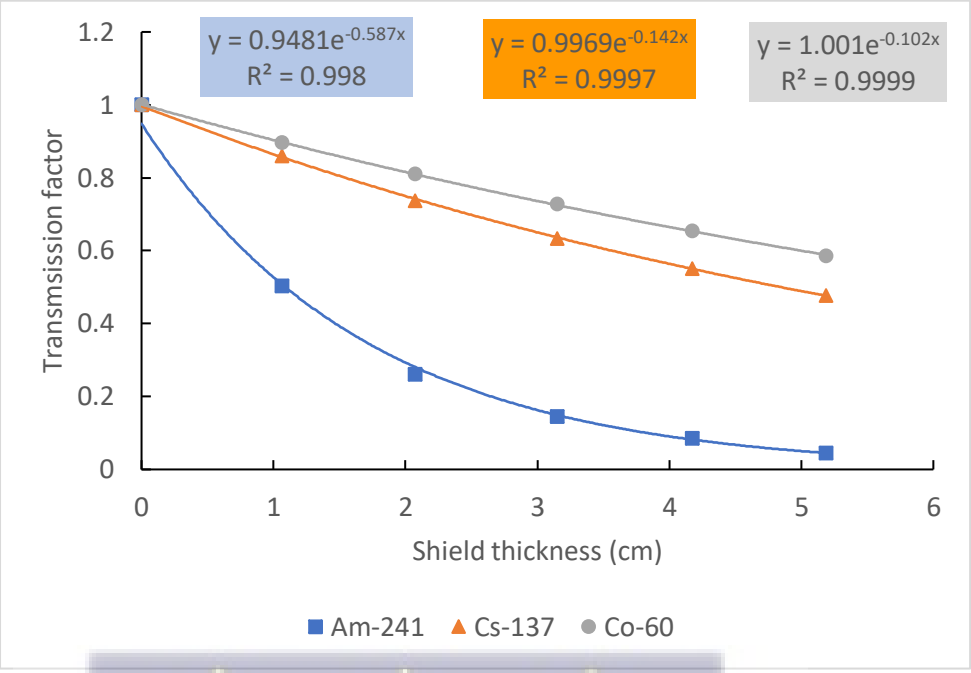

Figure. 4.10b: A graph showing photon transmission through AMK-X2 clay

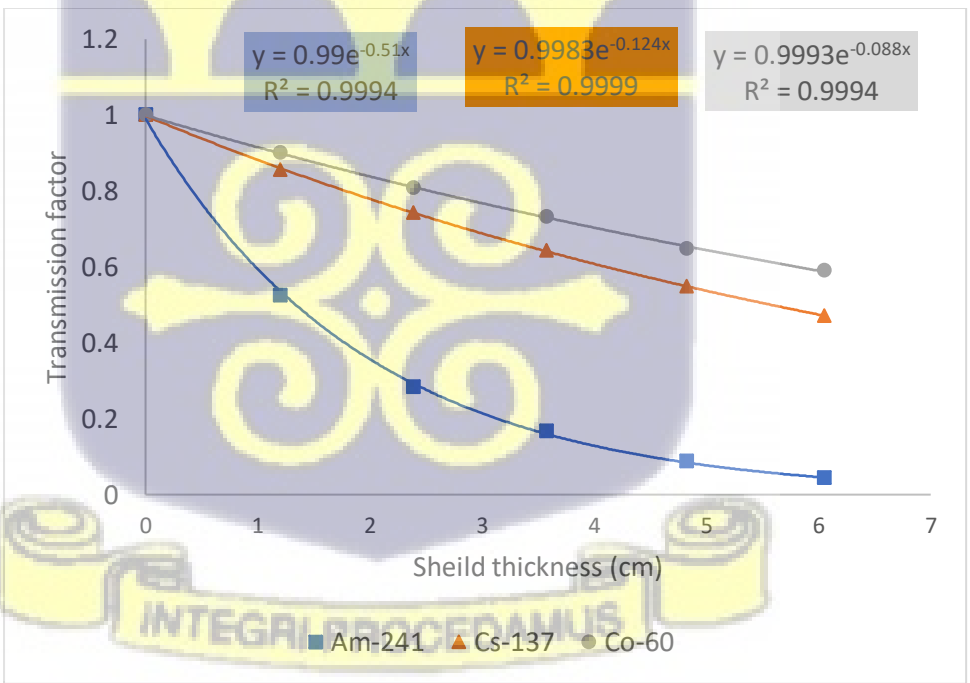

Figure. 4.10c: A graph showing photon transmission through FOS-X2 clay

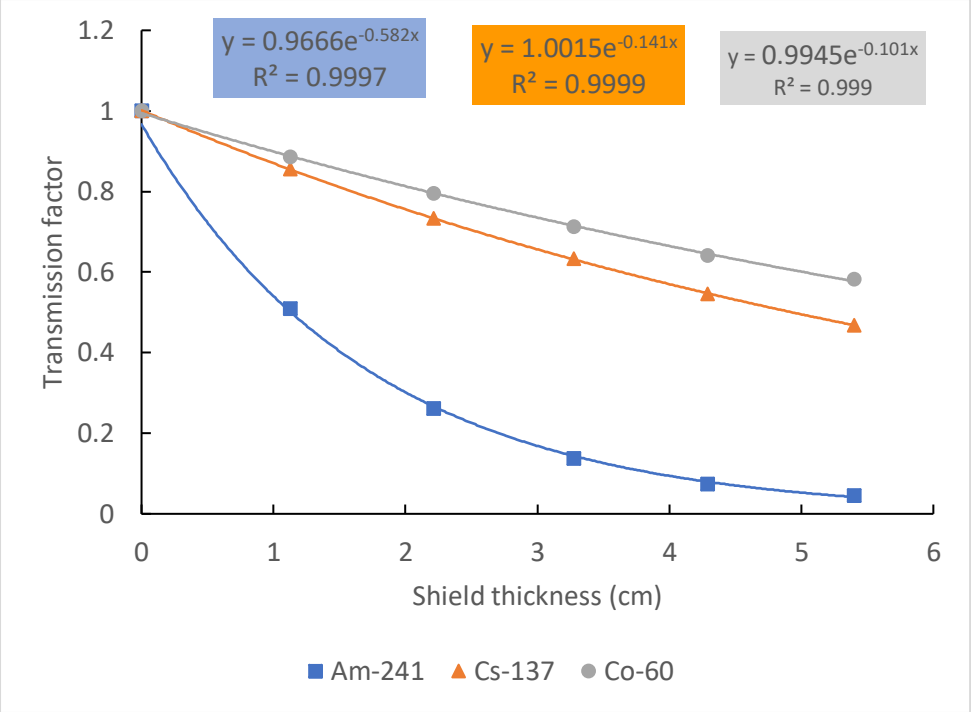

Figure. 4.10d: A graph showing photon transmission through KBU-X2 clay

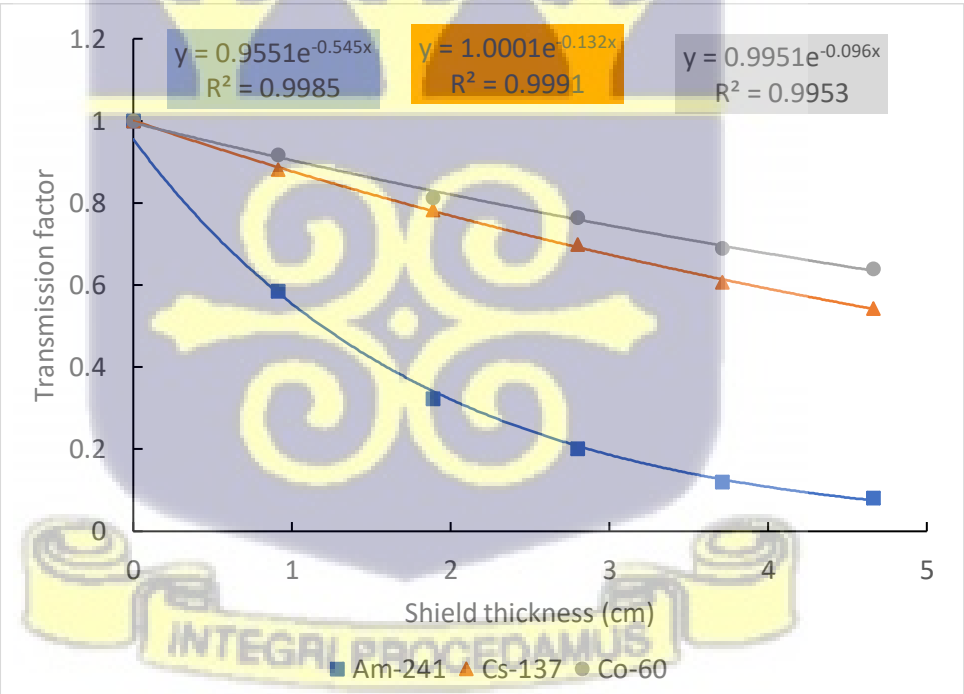

Figure. 4.10e: A graph showing photon transmission through OFM-X2 clay

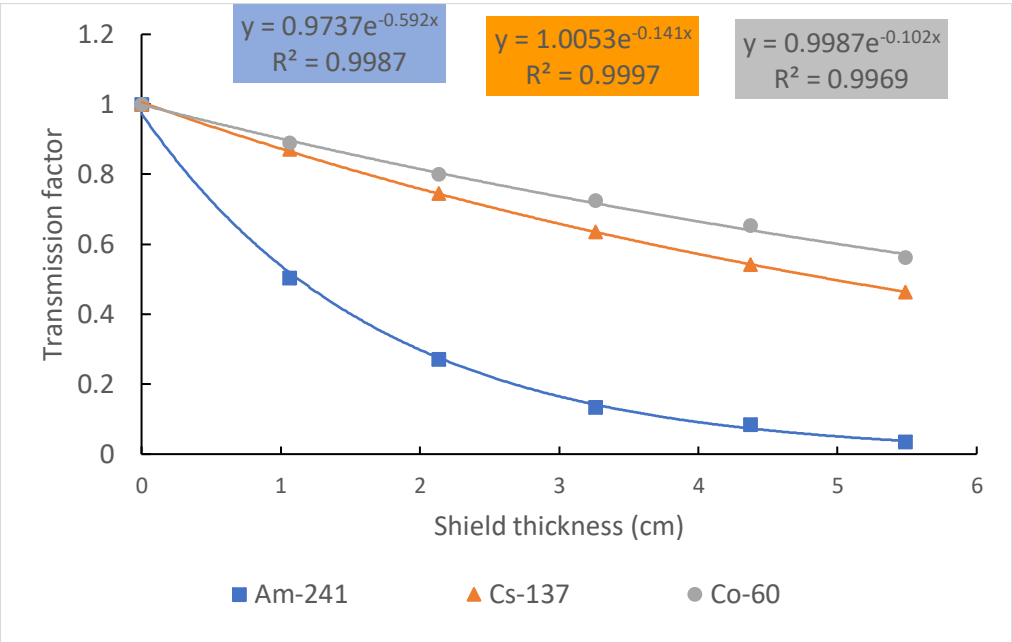

Figure. 4.10f: A graph showing photon transmission through OKY-X2 clay

4.3.1.4 Radiation Transmission in 4mm Alucobond panel

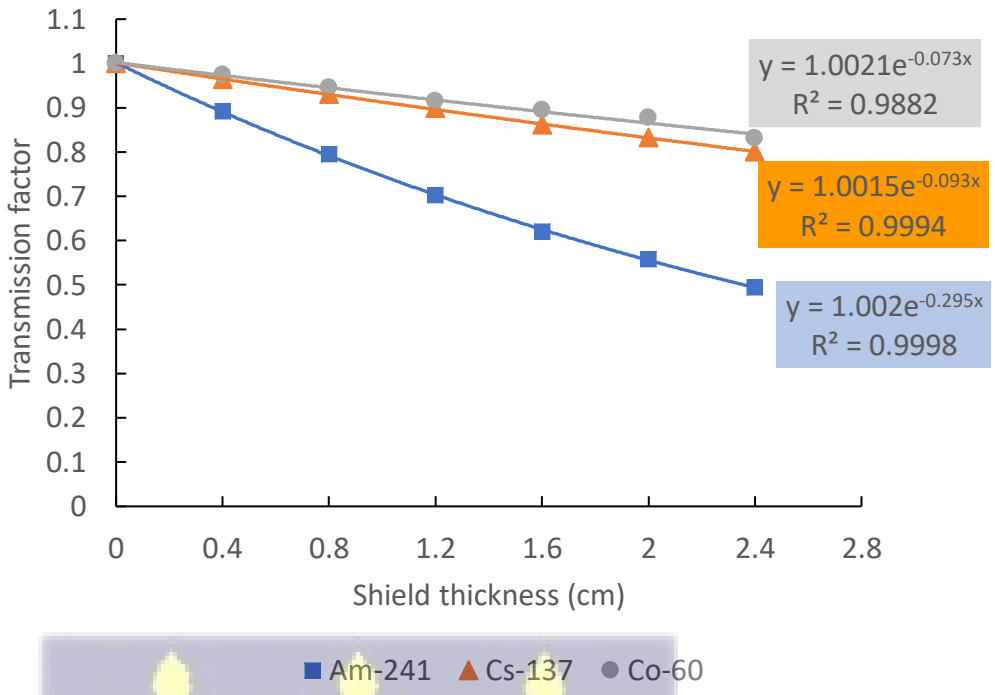

Figure. 4.11: A graph showing photon transmission through 4mm Alucobond panels

4.3.1.5 Comparisons of the Linear Attenuation Coefficient (LAC) and Mass Attenuation (MAC)

At this relatively low energy, Am-241 emits gamma radiation that is particularly attenuated by materials with a higher atomic number. The LAC values for the ABK and AMK samples (ranging from 0.466 cm^{-1} to 0.596 cm^{-1}) show that these materials perform well in shielding against low-energy gamma radiation. Specifically, ABK-X2 (2.069 g/cm^3) exhibits the highest LAC value of 0.596 cm^{-1}, followed by AMK-X2 (2.031 g/cm^3) at 0.587 cm^{-1}. These values are significantly higher than those observed for Polyethylene (0.1832 cm^{-1}), which is typically not effective at shielding low-energy gamma rays.

The HVL values for clay-based materials range from 1.42 cm (ABK-X0) to 1.86 cm (OS-A). This is far superior to the Polyethylene HVL of 3.78 cm, indicating that clay- based materials offer better attenuation of Am-241 than Polyethylene. Likewise, the TVL for clay-based materials is notably small, ranging from 4.7 cm (ABK-X0) to 6.2 cm (FOS-X0), suggesting that these materials are efficient in attenuating low-energy gamma rays.

Several studies report higher LAC values for similar clay composites, reinforcing the suitability of these materials for shielding low-energy gamma rays. For comparison, polyethylene offers significantly weaker shielding, with an HVL of 3.78 cm, whereas Ordinary Concrete provides better attenuation with an HVL of 1.13 cm.

At Cs-137 energy levels, the attenuation properties of materials become more dependent on both atomic number and density. Higher density materials generally show better attenuation properties for medium-energy gamma rays.

It is observed that the LAC values for clay-based materials range from 0.116 cm^{-1} (FOS -X0) to 0.145 cm^{-1} (ABK-X2. These are significantly higher than Polyethylene (0.0823 cm^{-1}) and indicate a better performance at Cs-137 energies.

The LAC is largely dependent on the density and composition of the fired clay. Elsafi, et al (2021) and Adjei (2012) also investigated the attenuation of gamma radiation in different fired clay. They reported similar values for the LAC in the range of 0.123 to 0.160 cm^{-1} for materials like fired clay under exposure to Cs-137 radiation (Elsafi, et al (2021); Adjei (2012).

For the HVL for clay-based materials in this study, they lie between 5.02 cm (ABK-X0) and 5.98 cm (FOS-X0), which is substantially better than Polyethylene (8.42 cm), but still much less efficient than Lead (0.558 cm).

Also, with regard to the TVL for clay-based materials they range from 16.7 cm (ABK- X0) to 19.8 cm (FOS-X0). These values indicate that comparatively, clay-based materials offer decent shielding against medium-energy gamma rays.

Combining the results and literature values, it is seen that Ordinary Concrete offers better shielding with an HVL of 3.80 cm, closer to the values for clay-based materials, however, Lead remains the most effective shielding material, with an HVL of 0.558 cm, providing exceptional attenuation for medium-energy gamma rays.

For high-energy gamma rays like those emitted by Co-60, the shielding efficiency of most materials, including clay-based materials, begins to decrease due to the nature of photon interaction at these energies. In this study, the LAC for clay-based materials ranges from 0.08 cm^{-1} (FOS-X0) to 0.107 cm^{-1} (ABK-X2), which is relatively low compared to Lead (0.6669 cm^{-1}). The HVL for these materials ranges from 7.0 cm (ABK-X2) to 8.66 cm (FOS-X2), showing that these materials are less effective for high-energy gamma rays compared to low-energy ones. Adjei, 2012, studied clay materials in Ghana and reported LAC for clay for some photon energies including Co- 60 and found that linear attenuation coefficient, μ, for Co-60 ranged from 0.0918±0.0017cm^{-1} for the least dense clay to 0.1255±0.0031cm^{-1} for the densest clay. These largely agree to the results in this work. (Adjei, 2012).

Furthermore, Elsafi, et al., (2021) found similar results, with LAC for Co-60 in fired clay of about 0.11 cm^{-1} (Elsafi, et al, (2021) These values suggest that the gamma-ray attenuation of Co-60 in fired clay is moderate, as expected for materials with relatively low atomic numbers compared to metals or high-density elements.

Similarly, the TVL for clay-based materials at Co-60 energies is between 23.2 cm (ABK-X0) and 28.8 cm (FOS-X0), demonstrating their relatively poor shielding performance for high-energy gamma radiation.

The HVL for Polyethylene is 11.48 cm, and for Ordinary Concrete, it is 5.19 cm, both of which are less efficient than Lead but provide slightly better shielding than

the clay -based materials. Lead remains the most effective material for Co-60, with an HVL of 1.04 cm, significantly outperforming other materials.

The study highlights the potential of clay-based materials as gamma radiation shields, particularly in environments where cost and availability are key concerns. However, for high-energy applications or environments where maximum attenuation is critical, Lead continues to be the material of choice. Further research, especially on the enhancement of clay composites, could help improve the gamma shielding properties of these materials, making them more viable in commercial and industrial applications.

Martin, (2006) referenced Hubbell &, Seltzer (1995) in the extensive tables of LAC and MAC for various materials interacting with different energies. In this study, the figures of density, LAC and MAC used in the discussion for comparing the radiation shielding properties of common building materials like polyethylene, ordinary concrete and aluminum with that of the investigated clays that were used in the graphs were taken from Martin (2006) (Martin (2006); Hubbell, & Seltzer, (1995))

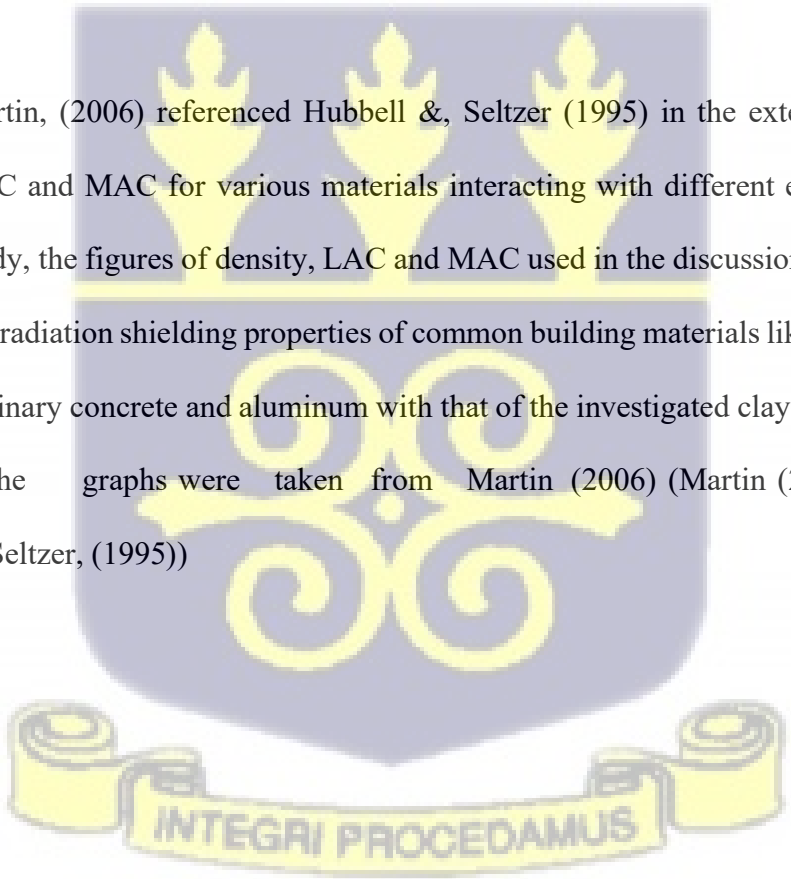

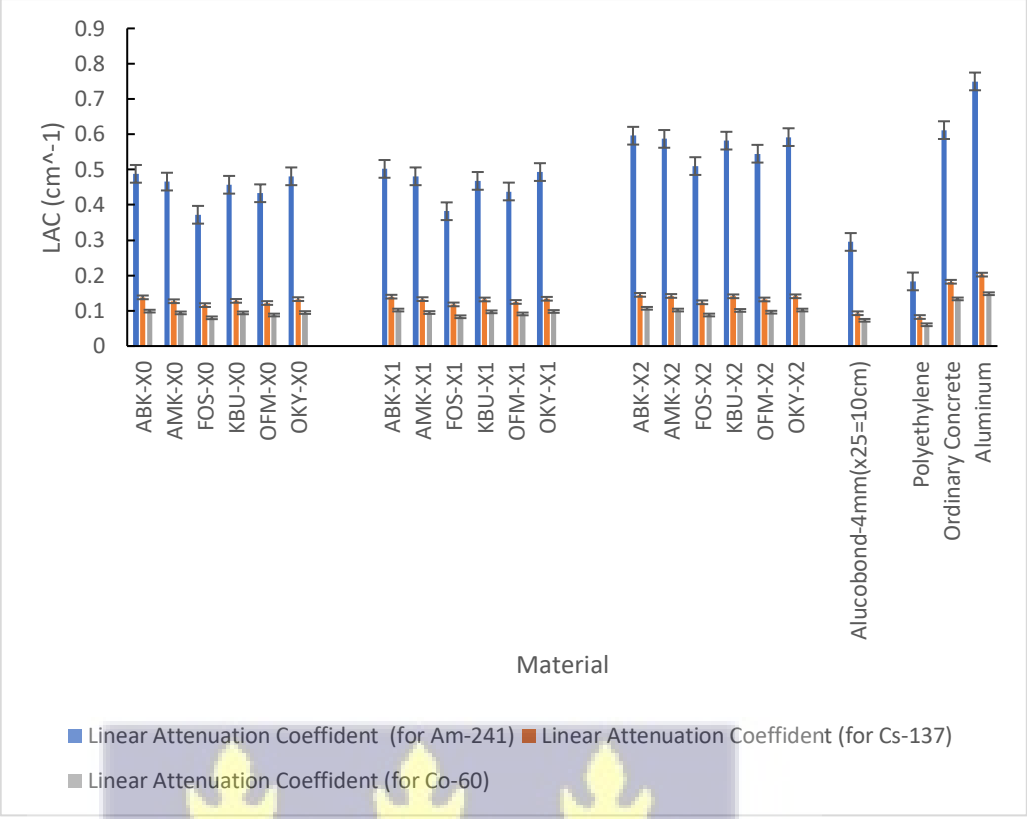

Figure. 4.12: A graph showing the Linear Attenuation Coefficient (LAC) of the studied clays at different doping rates and the LAC for some common shielding materials

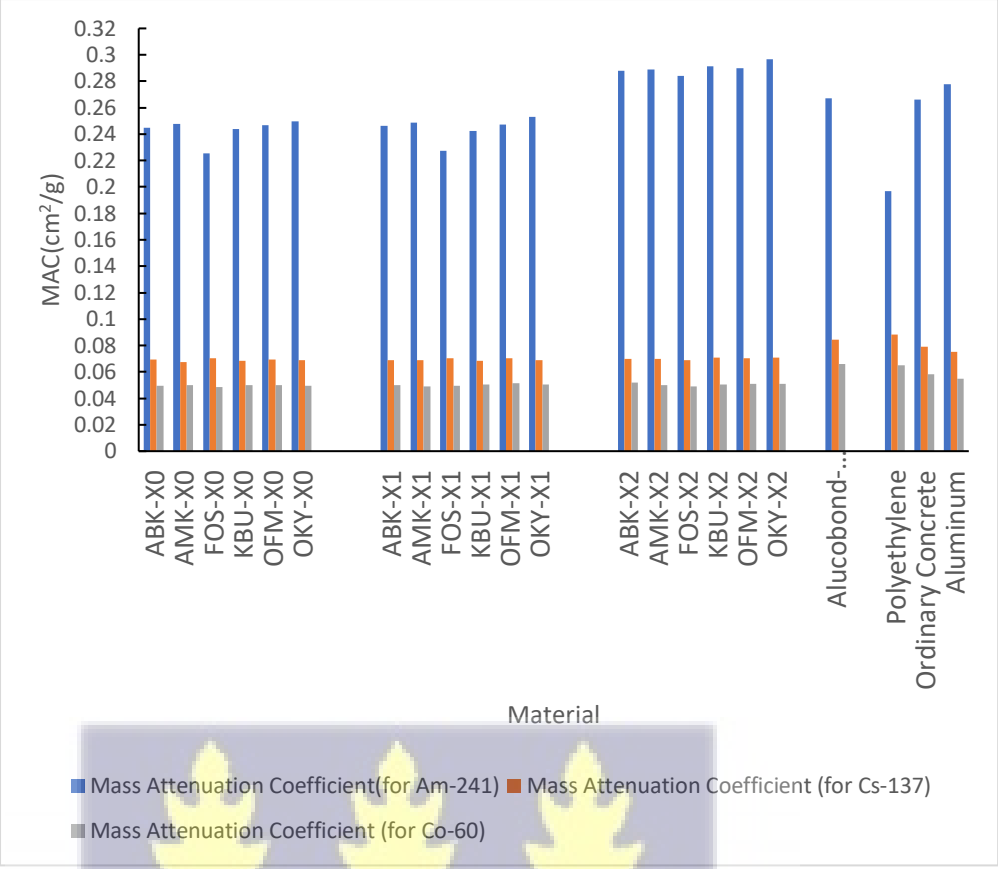

Figure. 4.13: A graph showing the Mass Attenuation Coefficient (MAC) of the studied clays at different doping rates and the MAC for some common shielding materials

4.3.1.6 Comparisons of the HVL, TVL and mfp of studied clay samples

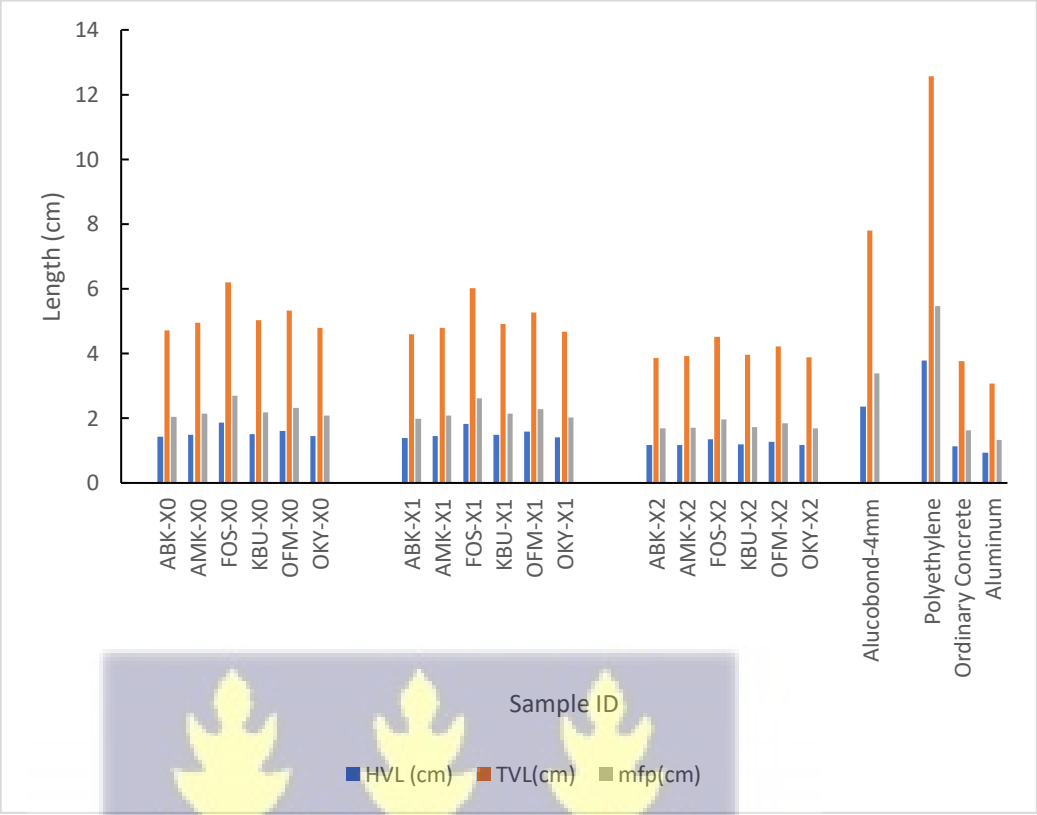

Figure 4.14a: A graph showing the HVL, TVL and mfp for Am-241 for the clays studied and that of other materials

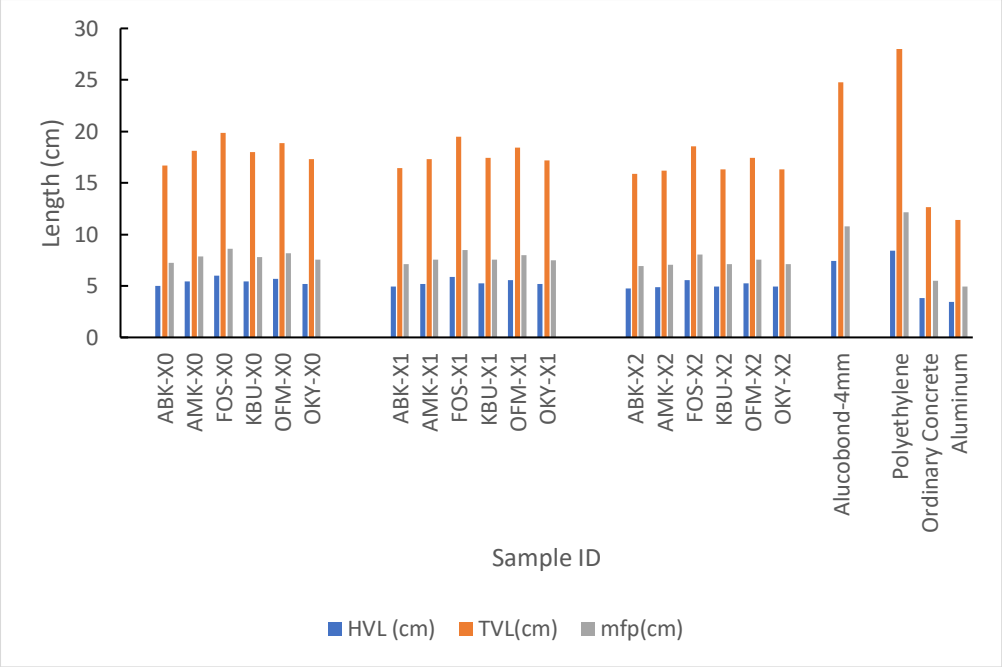

Figure. 4.14b: A graph showing the HVL, TVL and mfp for Cs-137 for the clays studied and that of other materials

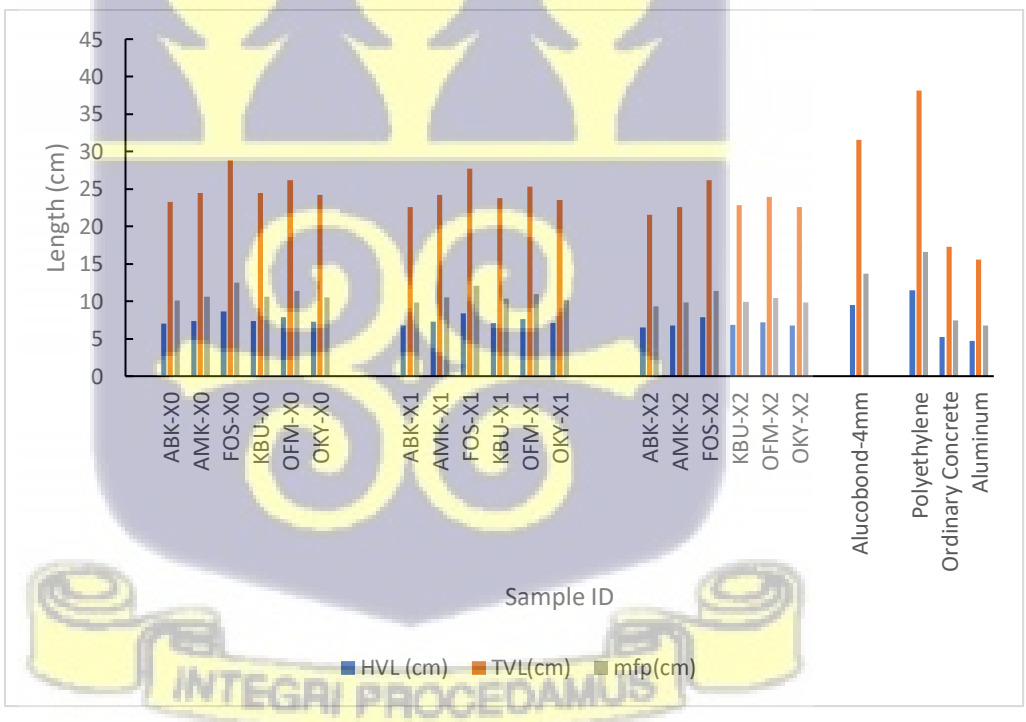

Figure. 4.14c: A graph showing the HVL, TVL and mfp for Co-60 for the clays studied and that of other materials

4.3.1.7 Relationship between fired clay density and mfp

For all the radionuclides and their energies studied, as density increased the mean free path reduced. This is because the more compact a material is, the more likely a photon will interact with that material at an increased rate thereby making it lose it energy sooner leading to a short travel path. Figures 4.15a to Fig. 4.15c illustrate this point clearly.

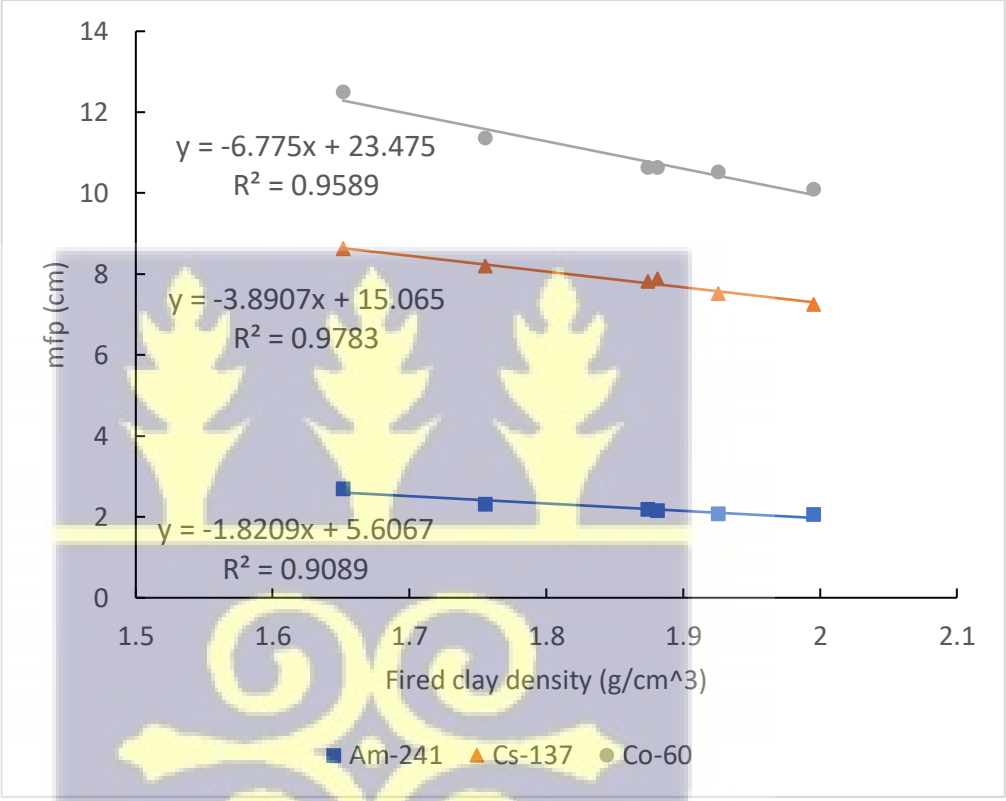

Figure. 4.15a: A graph showing the relationship between the density of fired clay and the mfp of Am-241, Cs-137 and Co-60 gamma rays for undoped clay

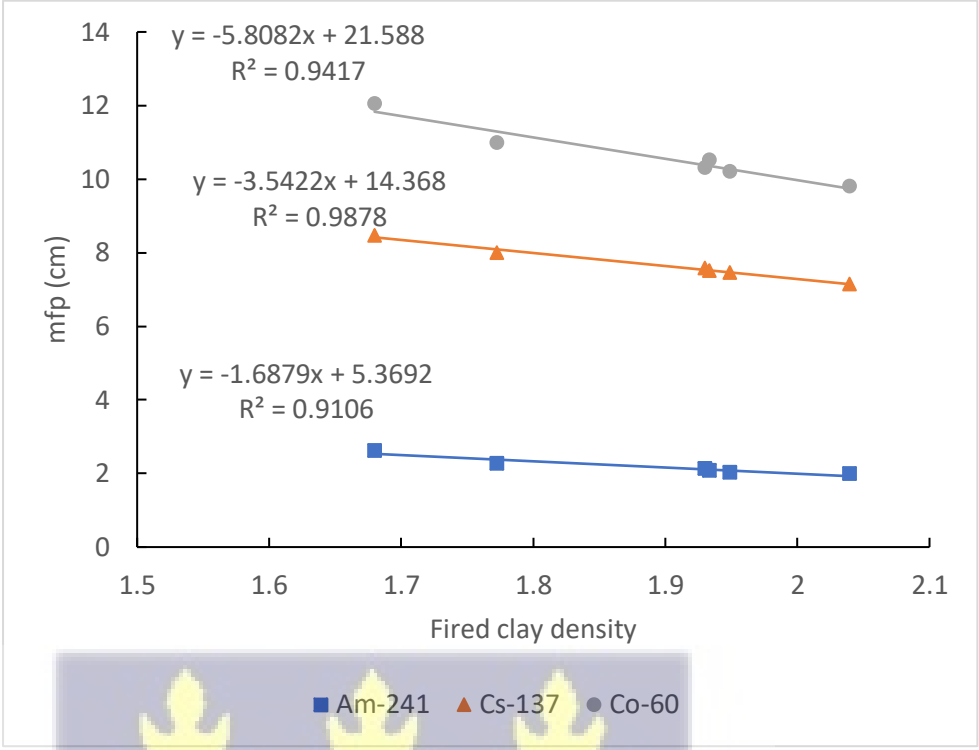

Figure. 4.15b: A graph showing the relationship between the density of fired clay and the mfp of Am-241, Cs-137 and Co-60 gamma rays for clays doped at 5% wt.

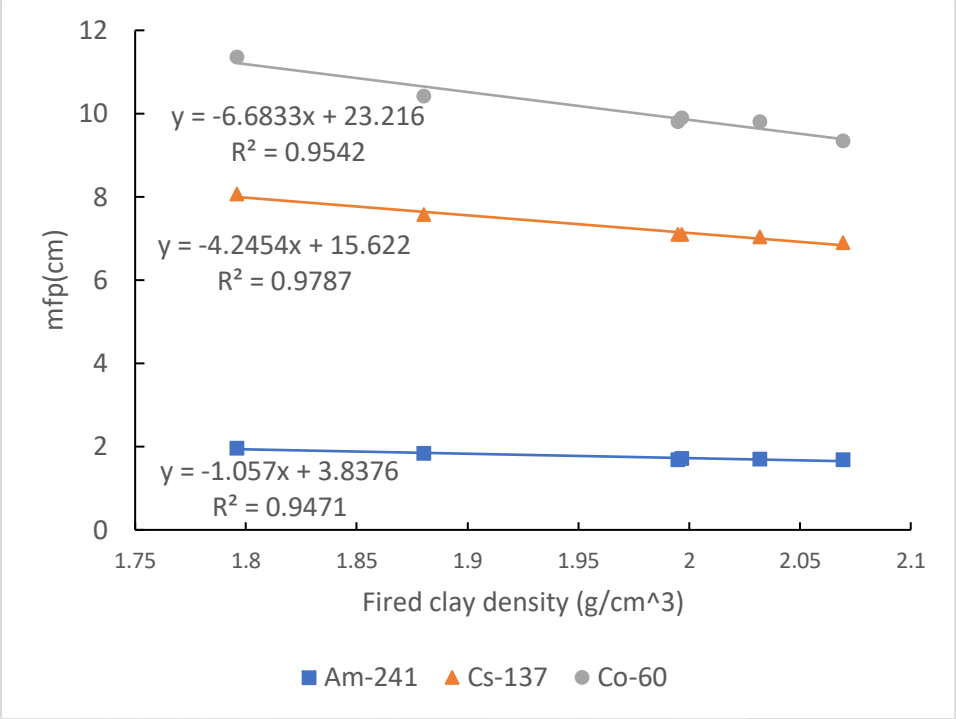

Figure. 4.15c: A graph showing the relationship between the density of fired clay and the mfp of Am-241, Cs-137 and Co-60 gamma rays for clays doped at 10% wt.

4.3.1.8 Buildup factors from Experimental work

Buildup factors in gamma shielding are used to account for the increase in the intensity of gamma radiation as it travels through a material, due to secondary scattering and secondary radiation produced within the material. The buildup factor quantifies the cumulative effect of scattered radiation, which increases the overall exposure beyond what would be expected from attenuation process that obey a simple exponential mathematical equation.

Buildup factors depend on several variables including the energy of the incident gamma radiation, the thickness and composition of the shielding material, and the material's atomic number. The buildup factor is usually expressed as a ratio of the total radiation intensity reaching the detector to the primary intensity of radiation that would have reached the detector in the absence of secondary scattering. (Martin, 2006) suggest that a well collimated narrow been will result in minimal scattering thereby resulting in a buildup factor value of 1, suggesting very good geometry in the experimental setup. Buildup factors shown in figure 4.16 all of which approximate 1, indicate that good geometry of the radiation source, shield and detector was employed in this study (Martin, 2006).

For gamma shielding calculations, particularly in nuclear engineering and medical applications, empirical models or Monte Carlo simulations are often employed to estimate buildup factors for specific materials and energies (Attix, 1986). These factors help ensure that shielding meets safety standards by effectively reducing gamma radiation exposure to acceptable levels.

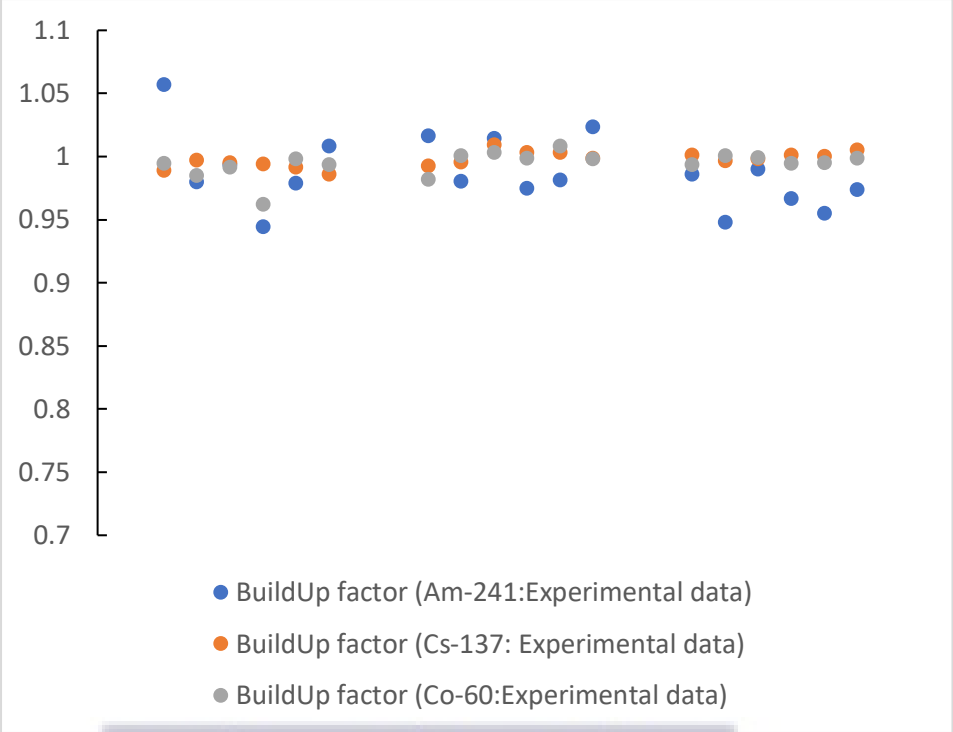

Figure. 4.16: A graph showing the average buildup factors for the three clay doping series studied for all the gamma energies studied.

4.3.1.9 Radiation transmission after incorporation of Alucobond

From the graphs 4.17a - 4.19f, shows that in all cases of clay studied for all energies, the incorporation of the Alucobond panel reduces the intensity of the radiation that is transmitted. In the case of Am-241 one layer of 4mm Alucobond on one side of a brick wall reduces the intensity of radiation that is transmitted through it by 11.1% when compared to when the Alucobond is absent. When there is an Alucobond panel on both sides, this reduction reaches nearly 21%. Similarly, one layer and two layers reduces Cs-137 intensity by 3.5% and 6.9% respectively. In the case of Co-60, it is 2.7% and 5.3%. This shows that the Alucobond has impact on the shielding and the impact is strongest for low energies, like Am-241.

When Am-241 is passed through 10cm thickness of the clays studied, it is observed from Fig 4.17a. that only about 2 % of the initial radiation is expected to be transmitted through the shields in the case of FOS-X0 and FOS-X1 clays the least dense clay type, while the others are hover around 1% transmission. For ABK-X2 the densest doped and fired clay, it transmits about 0.25% of the initial intensity while ordinary concrete transmits 0.22% which can be considered at generally being at par. When the thickness is doubled to 20cm (which is over 10 HVLs and on average about 4 TVLs for the clays investigated) as can be seen from 4.18a all the clays have nearly no transmission except for FOS-X0, and Fos-X1 which have transmission lower than 0.1% whiles FOS-X2 effectively have no transmission. When the thickness in increased to 30cm (which is over 15 HVLs and on average about 5 TVLs for the clays investigated), as can be seen in Fig 4.19a for all the clays in X0, X1and X2 series there is nearly zero (at least on the order of 10^{-3} %) transmission for the undoped clay and even lower for the doped ones.

This implies that 20cm of X2 series clays as well as 30cm of all clay's series (X0. X1. and X2) can almost completely absorb gammas from Am-241. In comparison, 30cm of ordinary concrete transmits about 1.07E-06 % of the initial gamma radiation intensity.

Similarly, as can be seen from Figure 4.17c given 10cm thickness of the clays in this study, Cs-137 would have between 23.5% to 31.2% of initial radiation as compared to 16.2% for ordinary concrete. For Co-60 between 34.1% to 44.5% will be transmitted as compared to 26.3% for ordinary concrete as seen in Fig 4.17e. Furthermore, Fig 4.19c and 4.19e, show that as the shield thickness is

increased to 30cm, between 1.3% to 3.1% of Cs-137 rays gets transmitted in comparison to 0.4% for ordinary concrete. In the case of Co-60 between 4% - 9% of the gammas get transmitted in comparison to 1.8% through ordinary concrete.

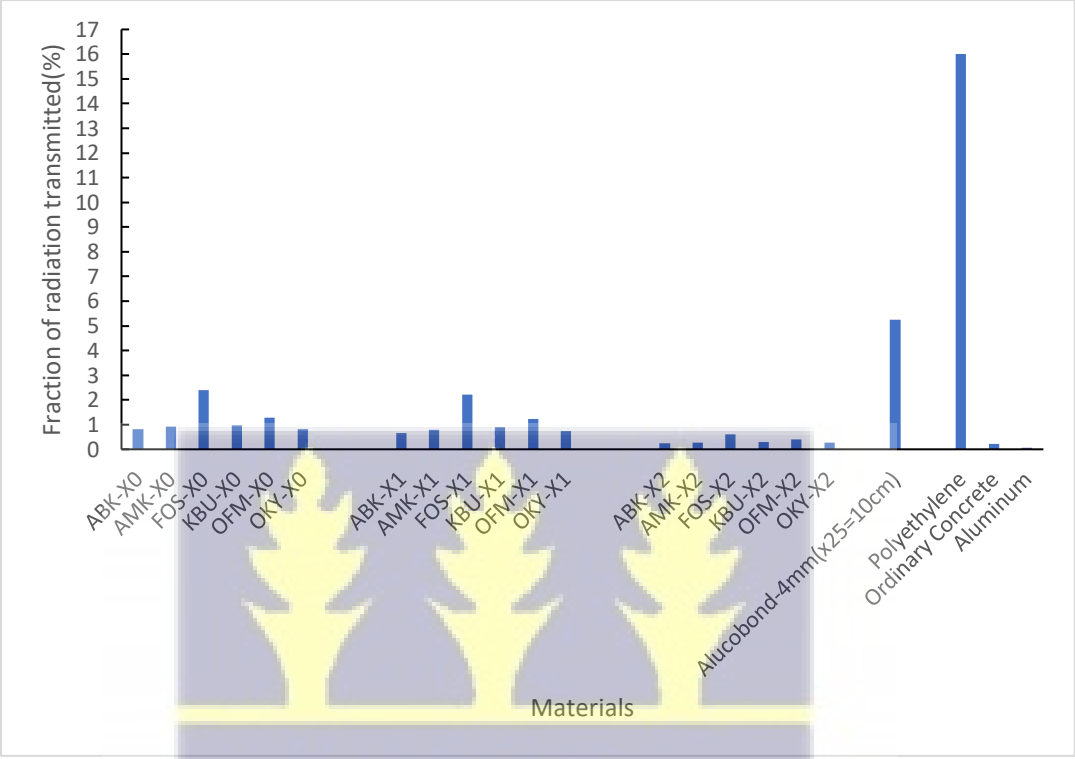

Figure. 4.17a: A graph showing the percentage of Am-241 radiation that gets transmitted through 10cm thickness of the listed materials

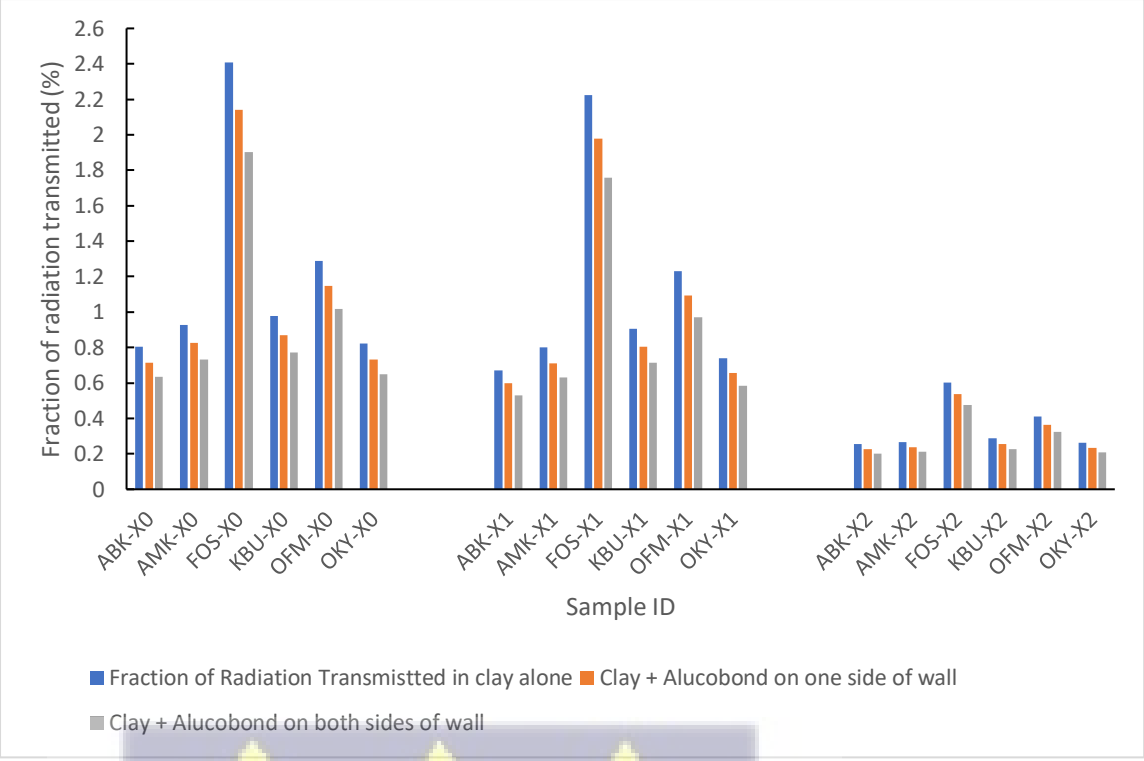

Figure. 4.17b: A graph showing a comparison of how different clay-Alucobond configurations with 10cm thick fired clay perform with respect to the percentage of Am -241 radiation they transmit

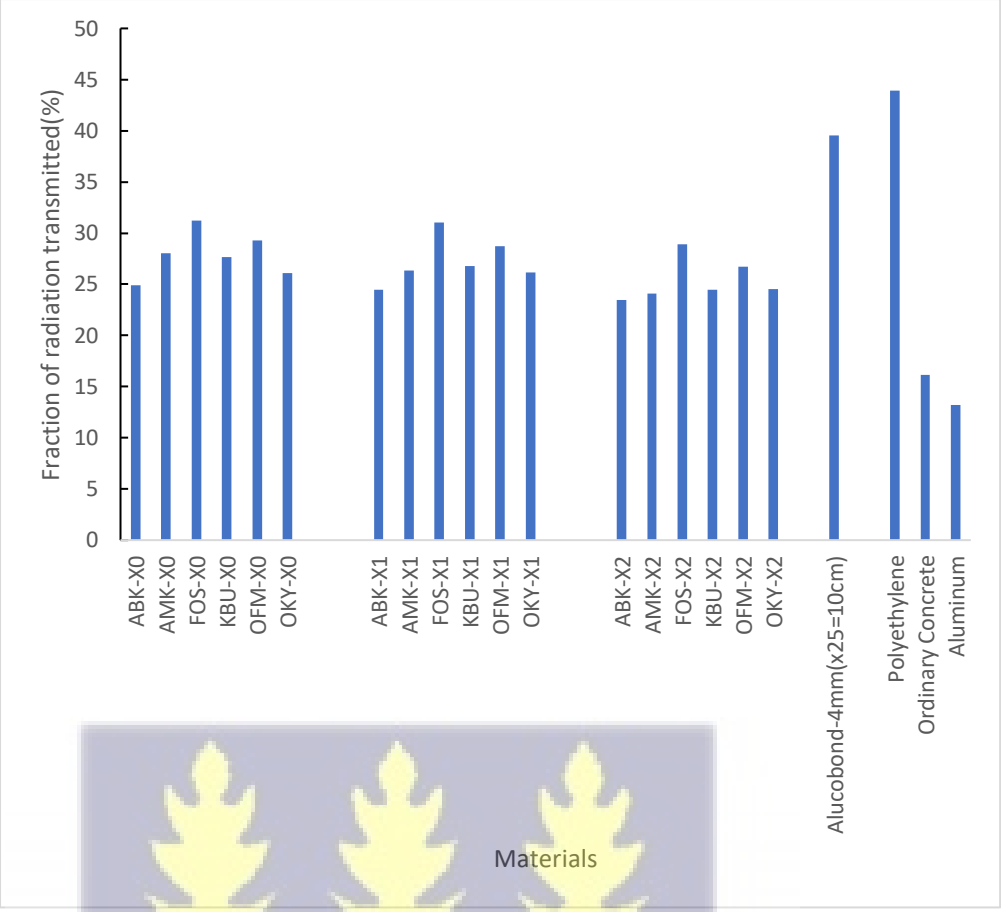

Figure. 4.17c: A graph showing the percentage of Cs-137 radiation that gets transmitted through 10cm thickness of the listed materials

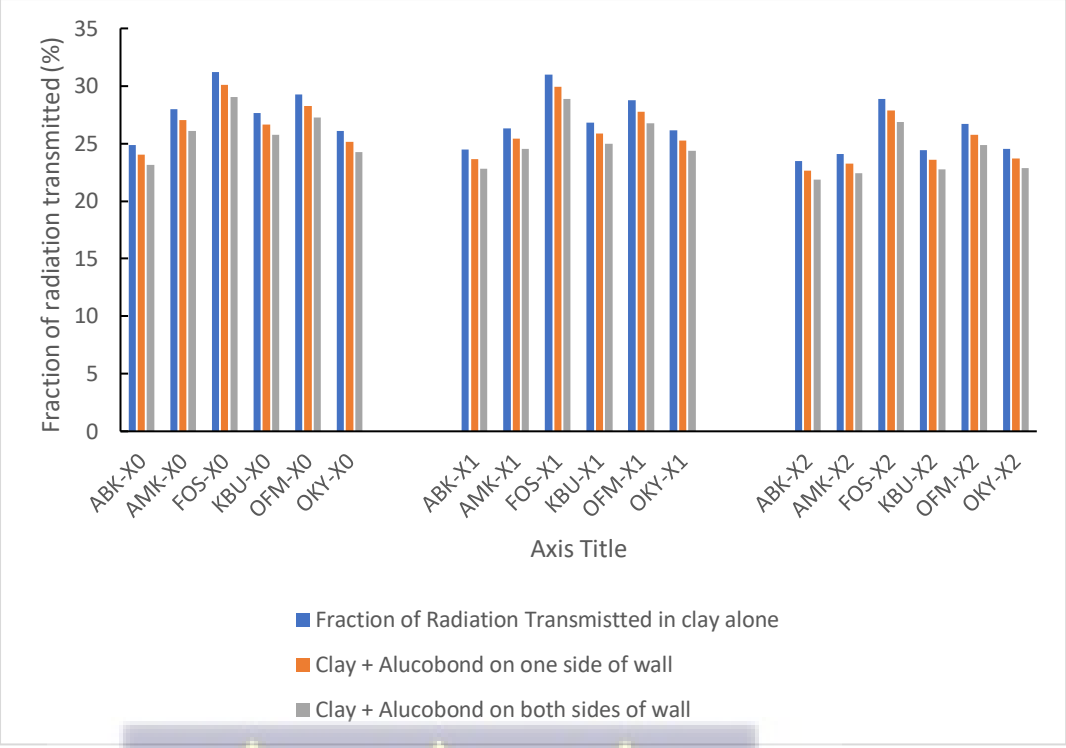

Figure. 4.17d: A graph showing a comparison of how different clay-Alucobond configurations with 10cm thick fired clay perform with respect to the percentage of Cs -137 radiation they transmit

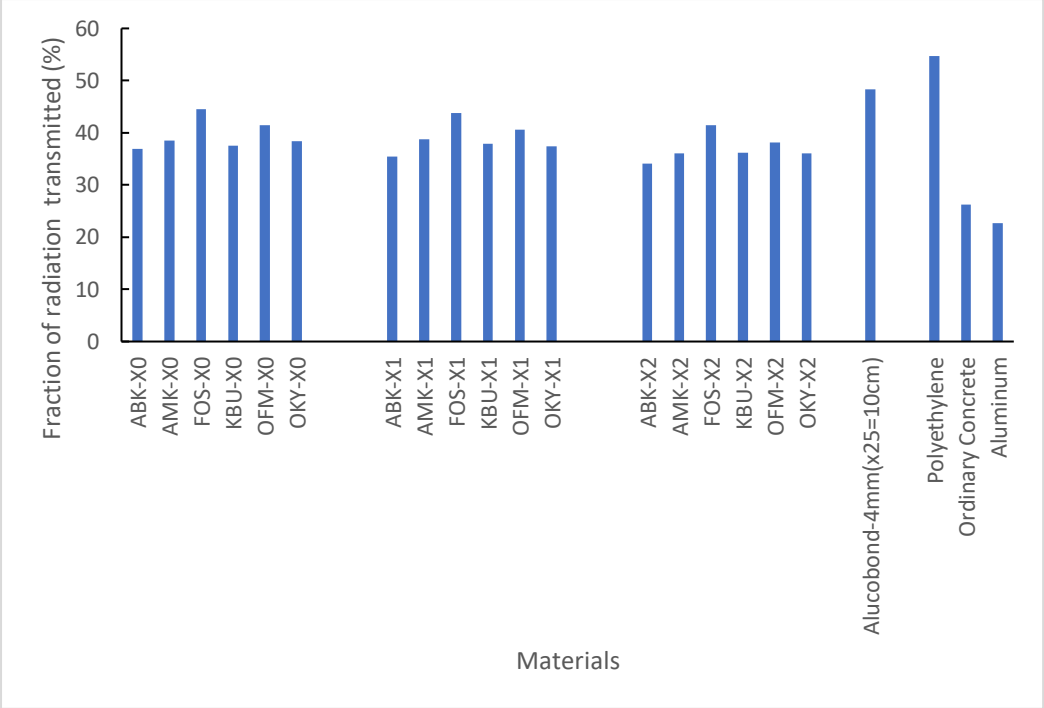

Figure. 4.17e: A graph showing the percentage of Co-60 radiation that gets transmitted through 10cm thickness of the listed materials

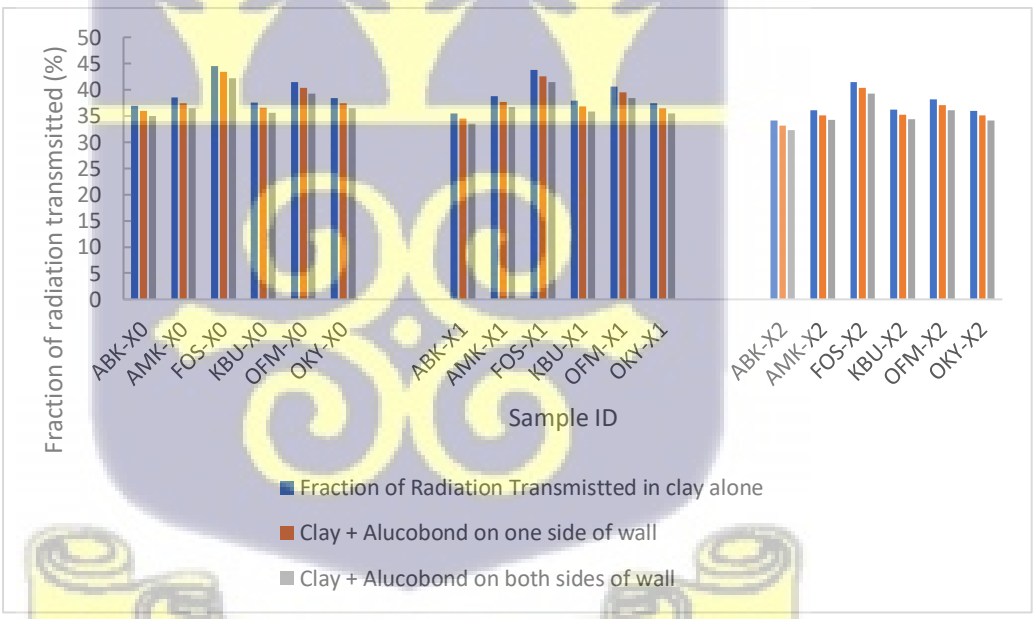

Figure. 4.17f: A graph showing a comparison of how different clay-Alucobond configurations with 10cm thick fired clay perform with respect to the percentage of Co -60 radiation they transmit.

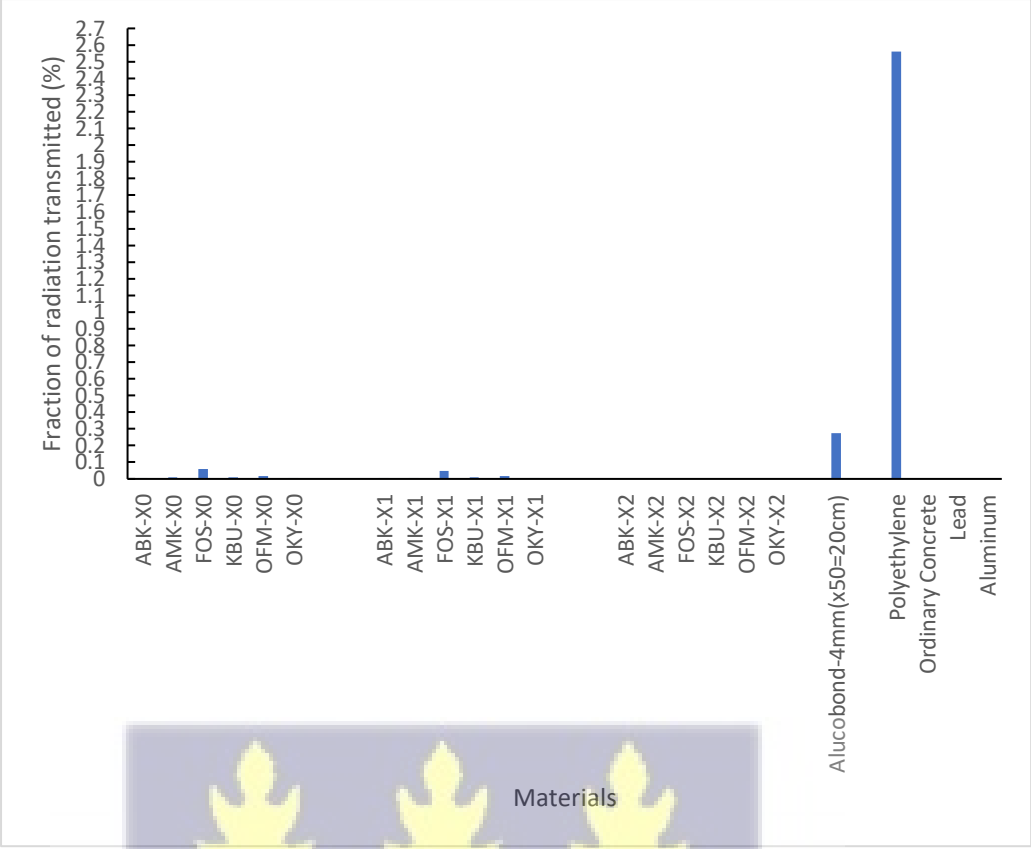

Figure 4.18a: A graph showing the percentage of Am-241 radiation that gets transmitted through 20cm thickness of the listed materials

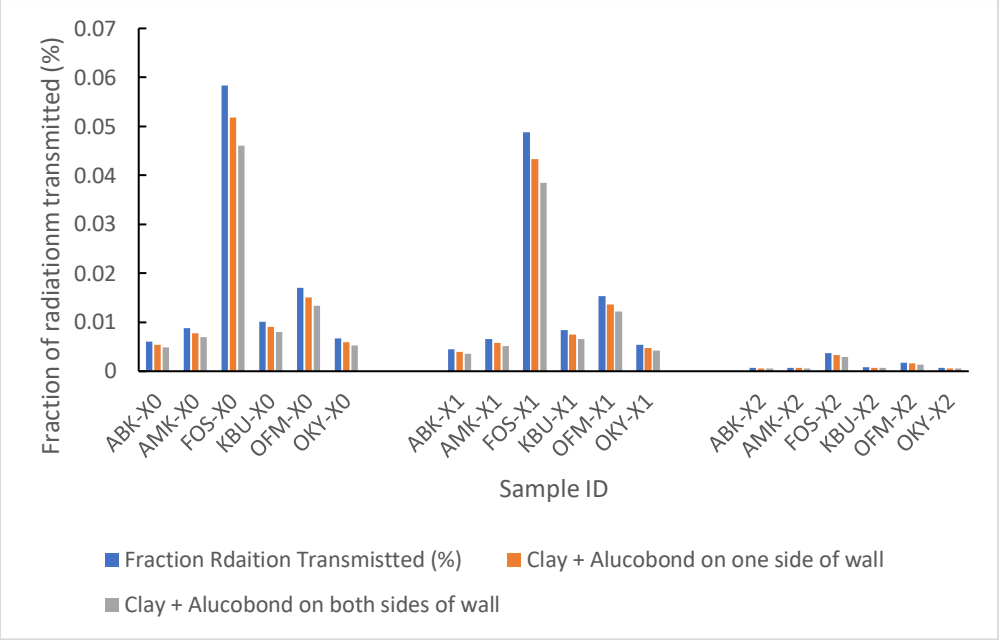

Figure. 4.18b: A graph showing a comparison of how different clay-Alucobond configurations with 20cm thick fired clay perform with respect to the percentage of Am -241 radiation they transmit

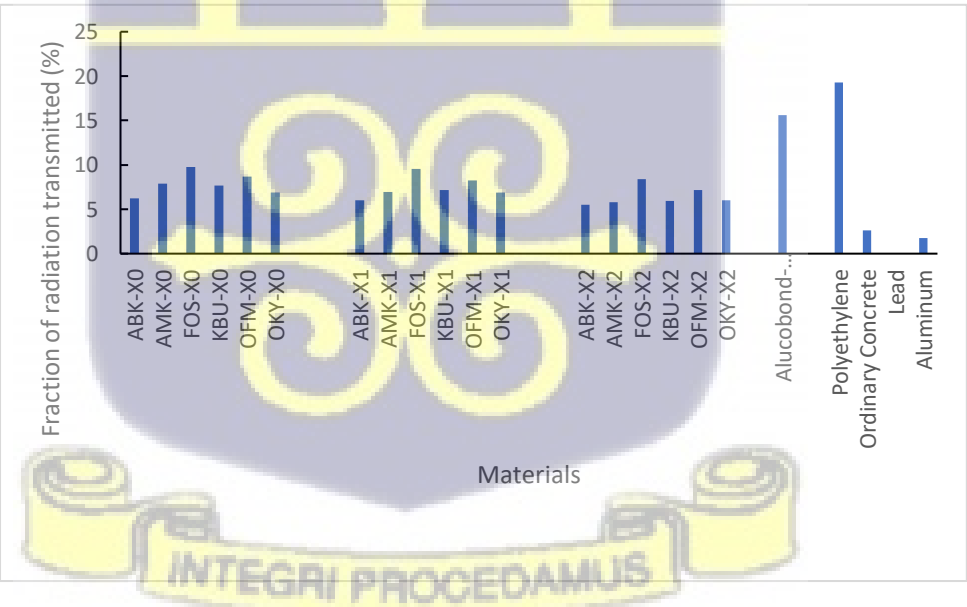

Figure. 4.18c: A graph showing the percentage of Cs-137 radiation that gets transmitted through 20cm thickness of the listed materials.

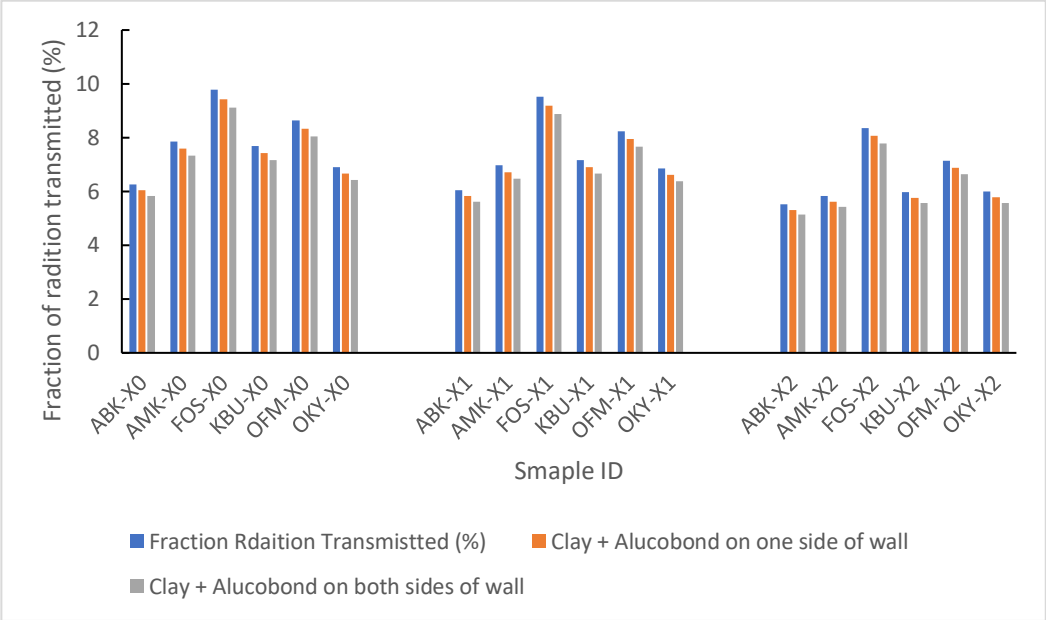

Figure 4.18d: A graph showing a comparison of how different clay-Alucobond configurations with 20cm thick fired clay perform with respect to the percentage of Cs-137 radiation they transmit

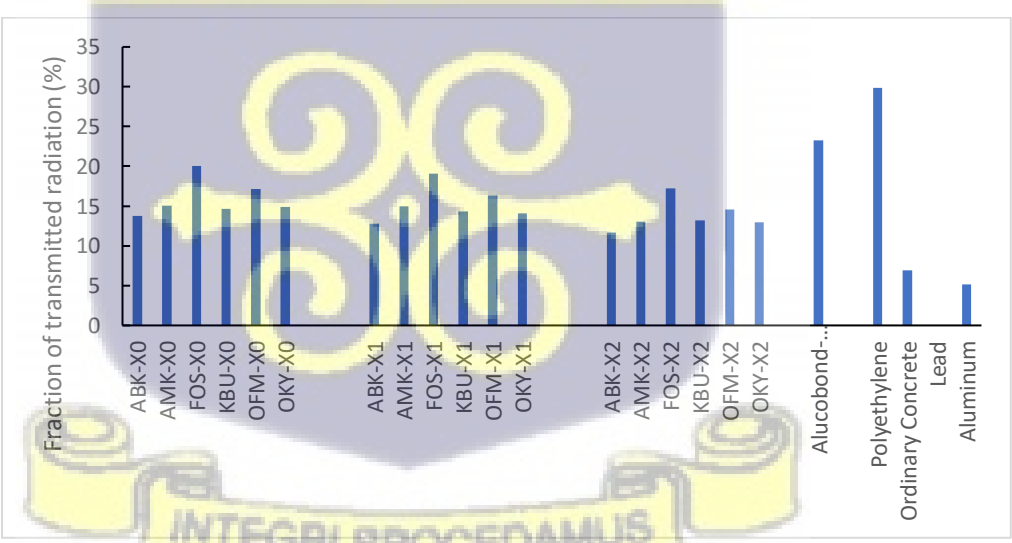

Figure. 4.18e: A graph showing the percentage of Co-60 radiation that gets transmitted through 20cm thickness of the listed materials

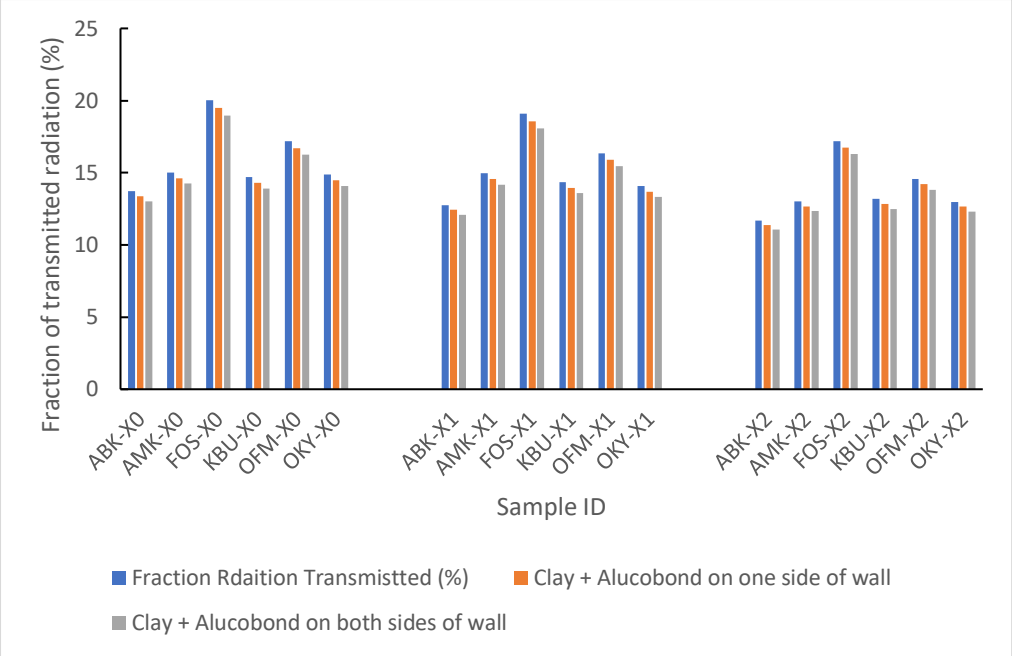

Figure. 4.18f: A graph showing a comparison of how different clay-Alucobond configurations with 20cm thick fired clay perform with respect to the percentage of Co-60 radiation they transmit

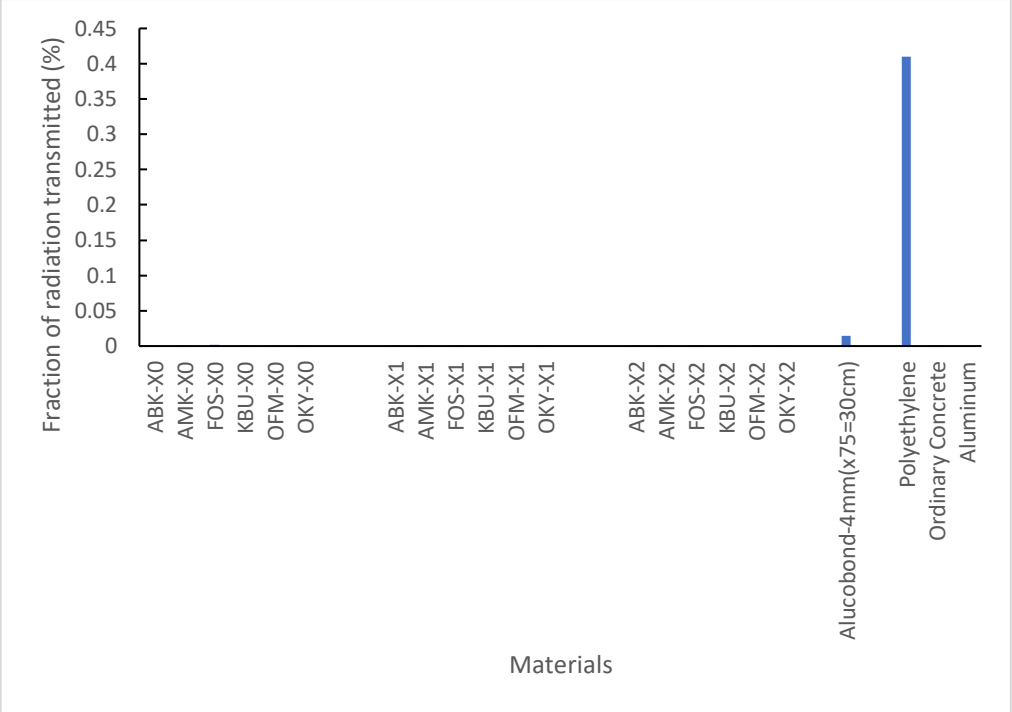

Figure. 4.19a: A graph showing the percentage of Am-241 radiation that gets transmitted through 30cm thickness of the listed materials

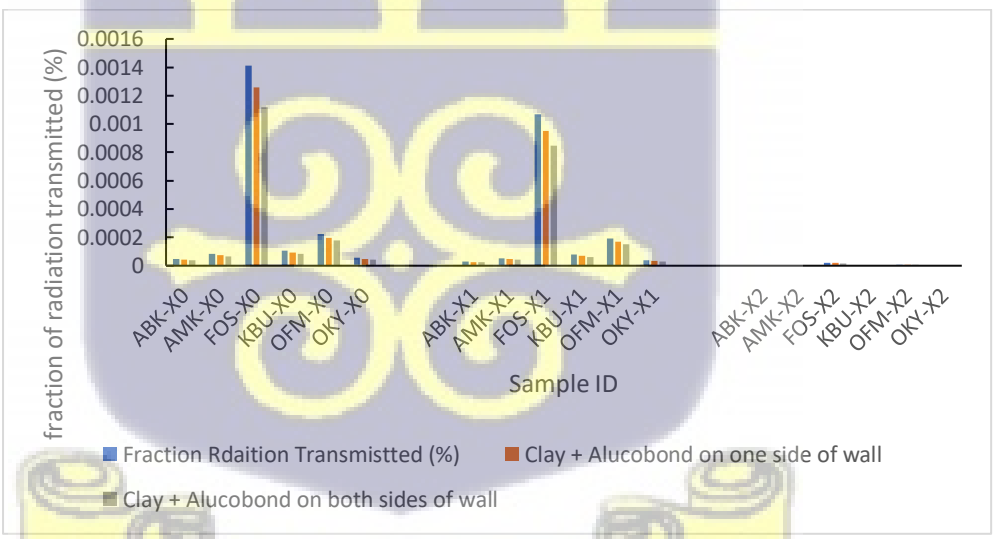

Figure 4.19b: A graph showing a comparison of how different clay-Alucobond configurations with 30cm thick fired clay perform with respect to the percentage of Am -241 radiation they transmit

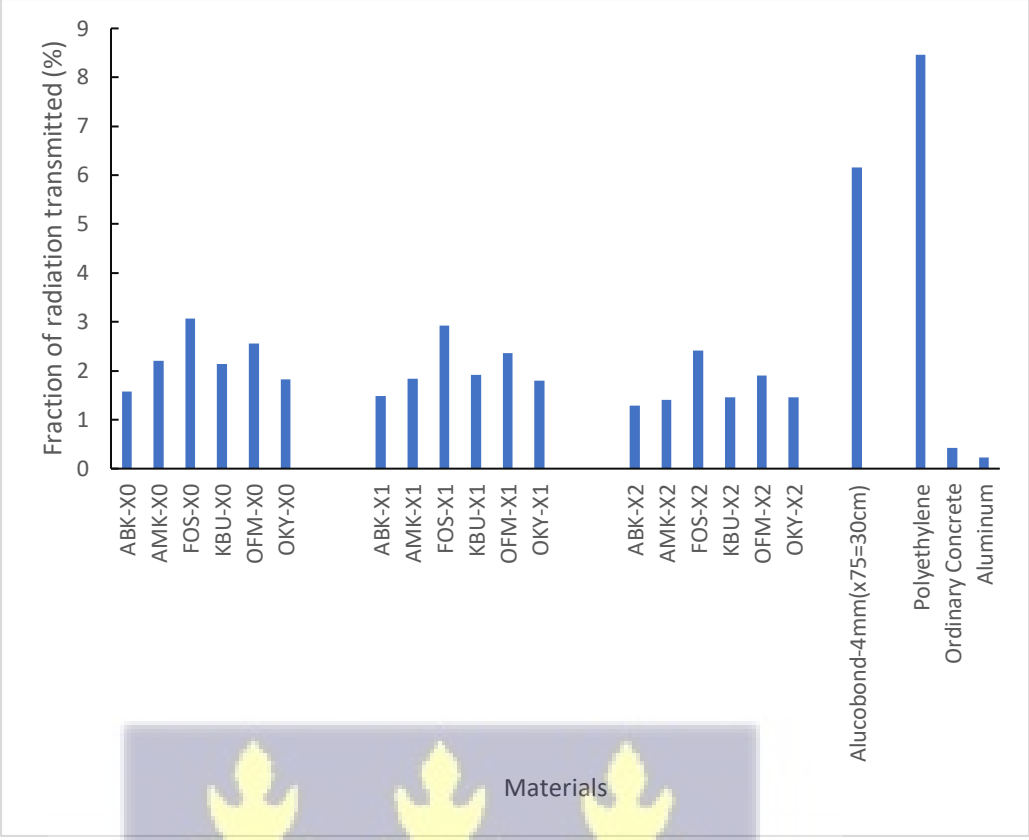

Figure. 4.19c: A graph showing the percentage of Cs-137 radiation that gets transmitted through 30cm thickness of the listed materials

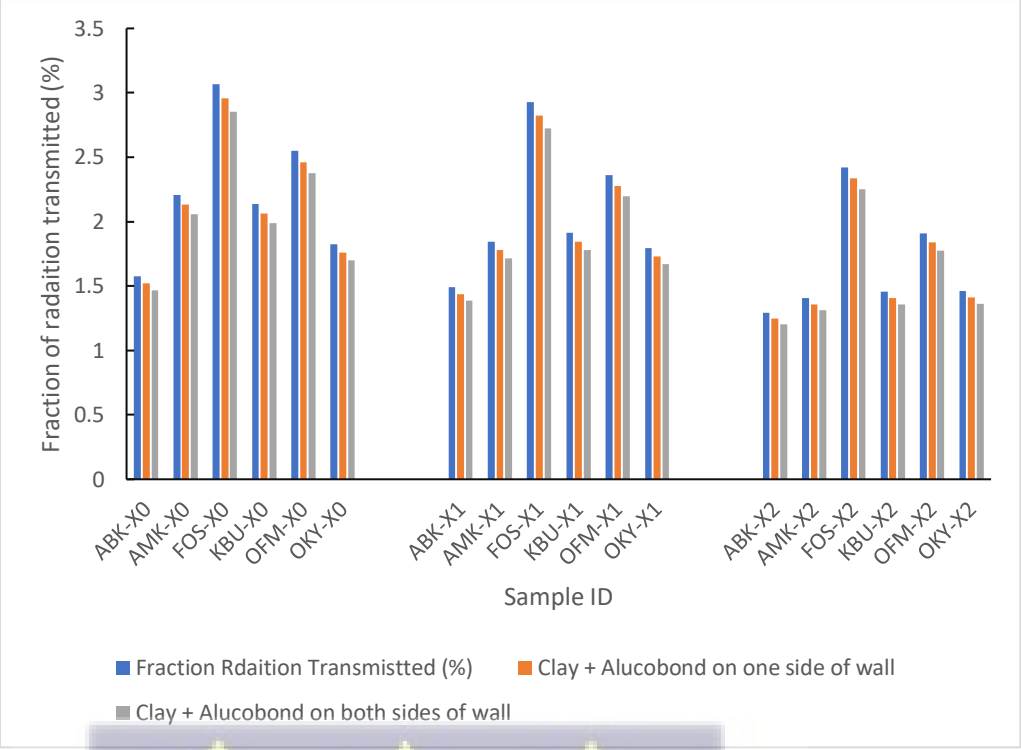

Figure. 4.19d: A graph showing a comparison of how different clay-Alucobond configurations with 30cm thick fired clay perform with respect to the percentage of Cs-137 radiation they transmit

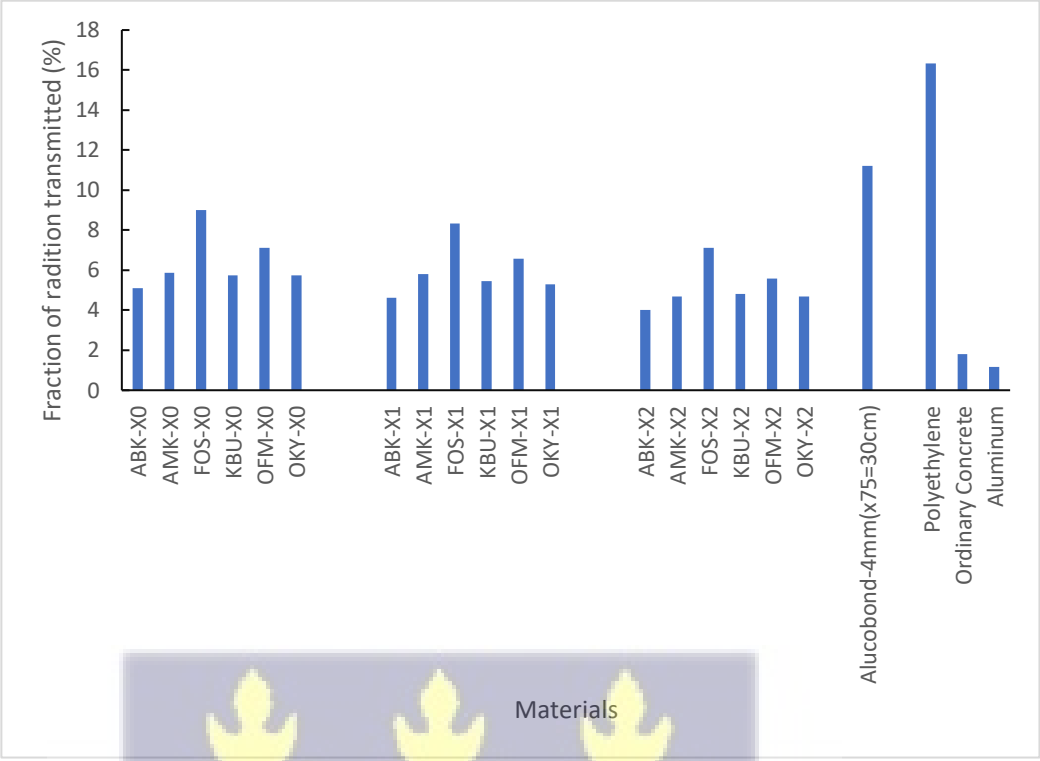

Figure. 4.19e: A graph showing the percentage of Co-60 radiation that gets transmitted through 30cm thickness of the listed materials

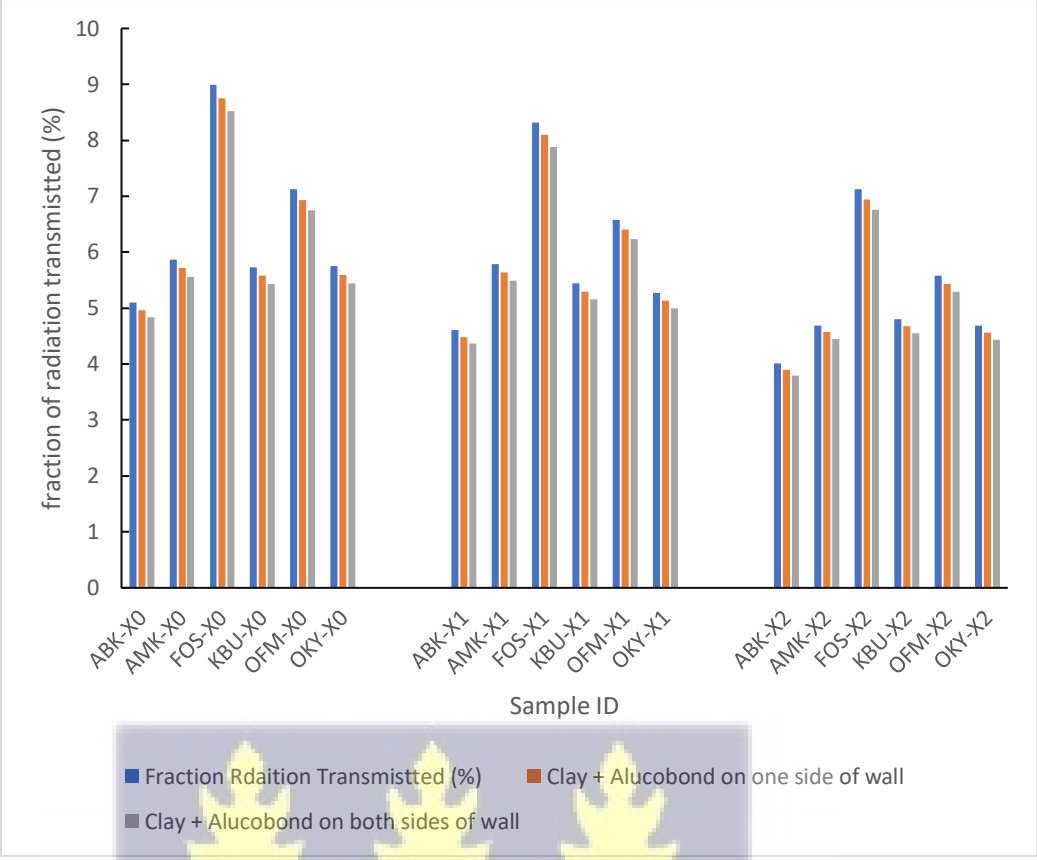

Figure. 4.19f: A graph showing a comparison of how different clay-Alucobond configurations with 30cm thick fired clay perform with respect to the percentage of Co -60 radiation they transmit.

.

4.3.1.10 Comparison of the shielding performance of selected material with respect to photon energy

Figure 4.20a below compares the photon energy dependence of linear attenuation coefficients of the best performing clay in this study ABK-X2 which is the densest and the least performing clay FOS-X0 which is undoped and the least dense, as well, the LAC for Alucobond is presented. These are assessed in the context of ordinary concrete which is a widely used photon shielding material. The plots for FOS-X0, ABK-X2 and Alucobond were done with data from this study, while that for ordinary concrete was done with data from literature from Martin (2006) quoting Hubbell. & Seltzer. (1995). The plots in Fig.20a have been generated from power equation regression curve fitting.

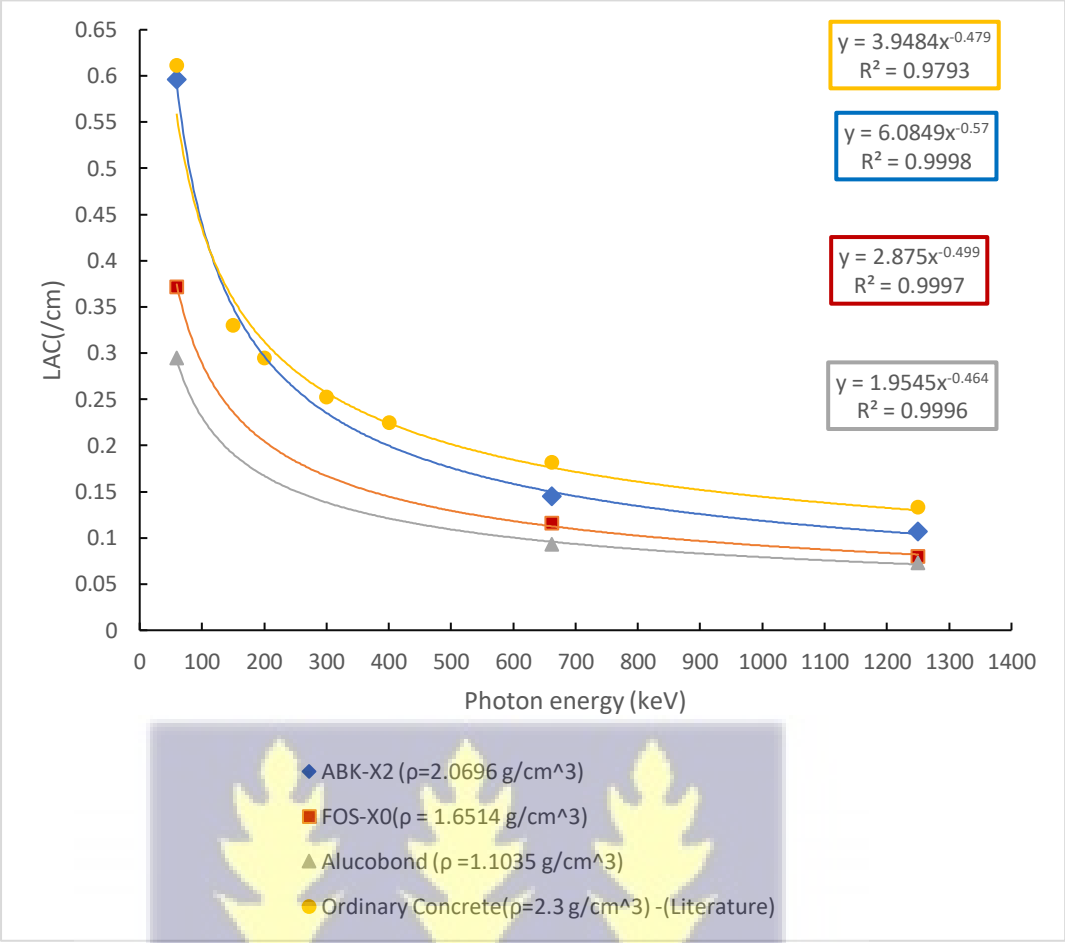

Figure. 4.20a: A graph showing the performance of the investigated clays, Alucobond and ordinary concrete.

It is observed that for all energies, the denser the material the higher the LAC. The graph shows that for lower photon energies up to about 150keV. ABK-X2 which has 10% wt doping performs practically equally to that of ordinary concrete- as can be seen, their regression curves almost coincide up to the 150 keV photon energy point. This is important because most medical x-ray applications fall below 150keV.

According to Bushberg, et al (2012), the energy range for medical X-rays generally spans from 30 keV to 150 keV, depending on the specific application and the type of diagnostic imaging being performed. For general radiography (e.g., chest X-rays), the typical X-ray energies range from 50 keV to 120 keV. In contrast, mammography typically uses lower-energy X-rays, ranging from 20 keV to 40 keV, to provide higher contrast images of breast tissue. For computed tomography (CT) scans, the X-ray tube operates at energies between 80 kV to 140 kV, which corresponds to an energy range of approximately 30 keV to 150 keV. The energy used in therapeutic X-rays, such as in radiation therapy, is higher, often ranging from 100 keV to 1 MeV to target deeper tissues (Bushberg et al 2012).

These results highlight the prospect of clay doping with Fe_2O_3 for shielding low energy photons particularly for medical applications. If Alucobond panels which as used as facades or wall finishing is added as an extra layer, the ABK-X2 clay's LAC performance will outstrip that of ordinary concrete at lower energies. Besides, when further densification techniques such as higher compression load during the clay body preparation before firing, or firing at higher temperatures, say 1100 °C, the fired clay alone would be expected to perform better than ordinary concrete at photon energies lower than 150keV.

4.3.2 Radiation Transmission Test Procedure validation

Using a set of standard absorbers of Al, Fe, Cu and Pb, the radiations transmission experiment protocol was tested for Cs-137. Figure 4.20b show transmissions curves used to determine LAC for the various absorbers. The results of the validation curve are shown in Figure 4.20c. A linear graph was obtained for the validation curve depicting strong agreement between experimental and expected (standard) results with an R^2 value of 0.99 confirming the adequacy of the experimental protocol to produce reliable results.

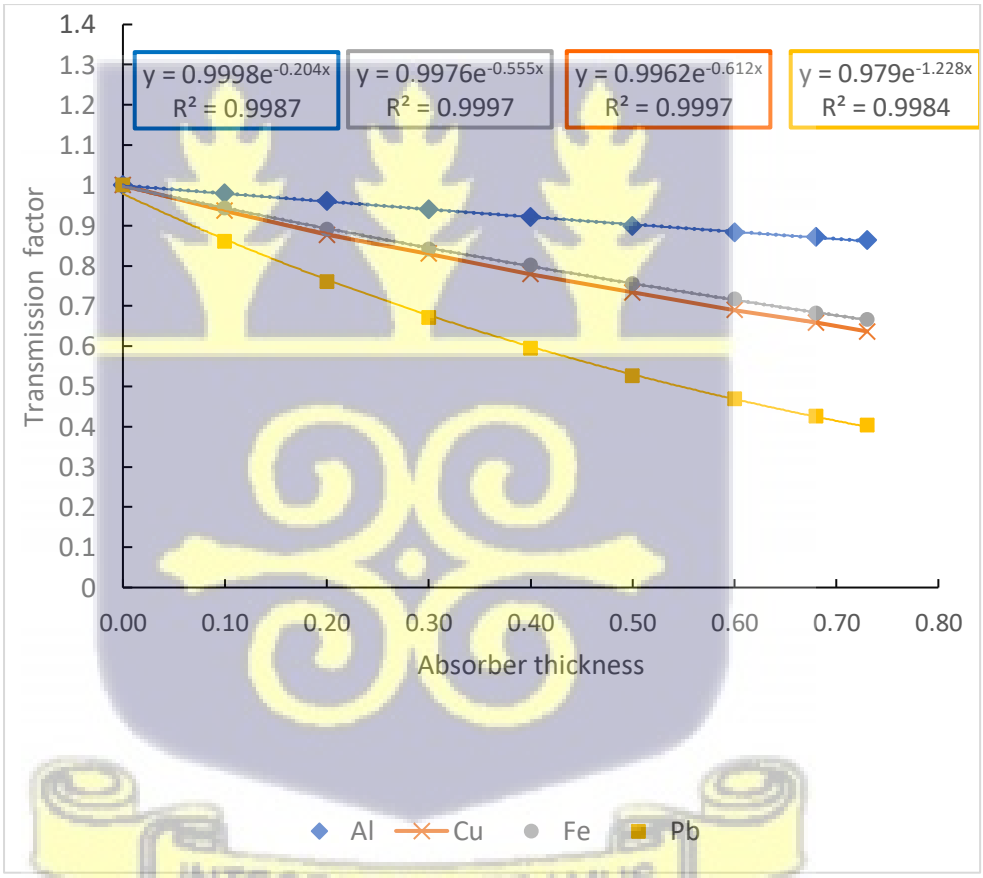

Figure. 4.20b: A graph showing transmission curves of Cs-137 radiation through standards absorbers.

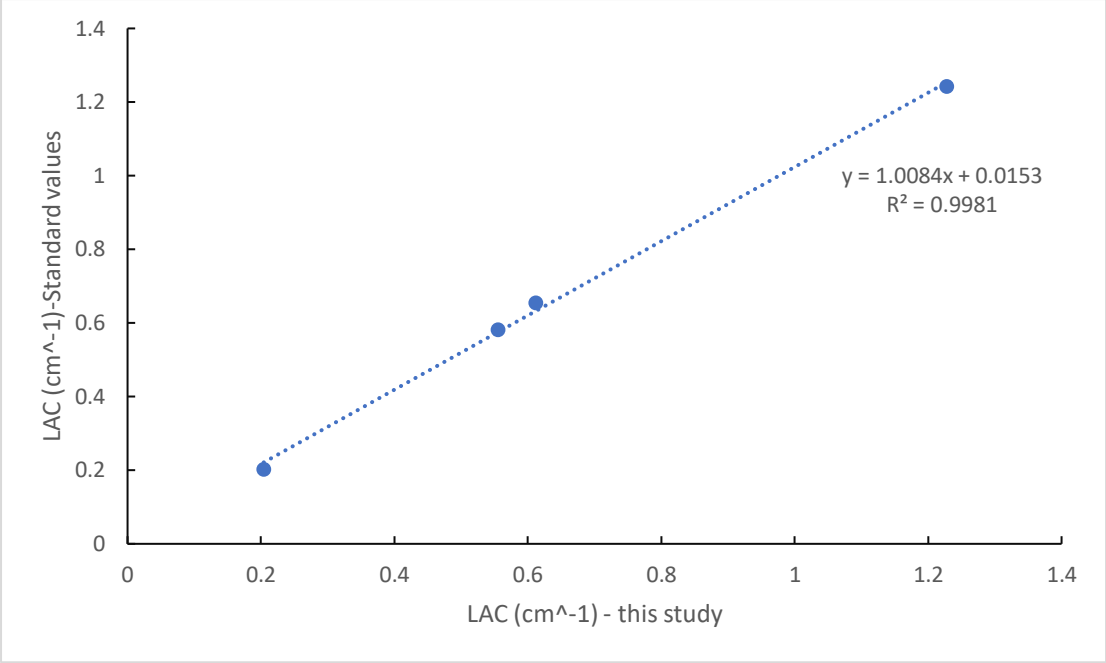

Figure. 4.20c: A graph showing a validation curve for the Cs-137 radiation through standards absorbers

4.3.3 Statistical Analysis

4.3.3.1 ANOVA test results for LAC and MAC

ANOVA (Analysis of Variance) is a statistical method used to determine if there are significant differences between the means of some independent groups. The test and analysis are done and computed usually at a significance level typically of 0.05. If the p-value from the ANOVA is less than 0.05, it calls for a rejection of the null hypothesis and a conclusion that there is a significant difference in the values between the groups. If on the other hand, the p-value is greater than 0.05, then we fail to reject the null hypothesis and conclude that there is no significant difference in the values of the parameter of interest in the groups.

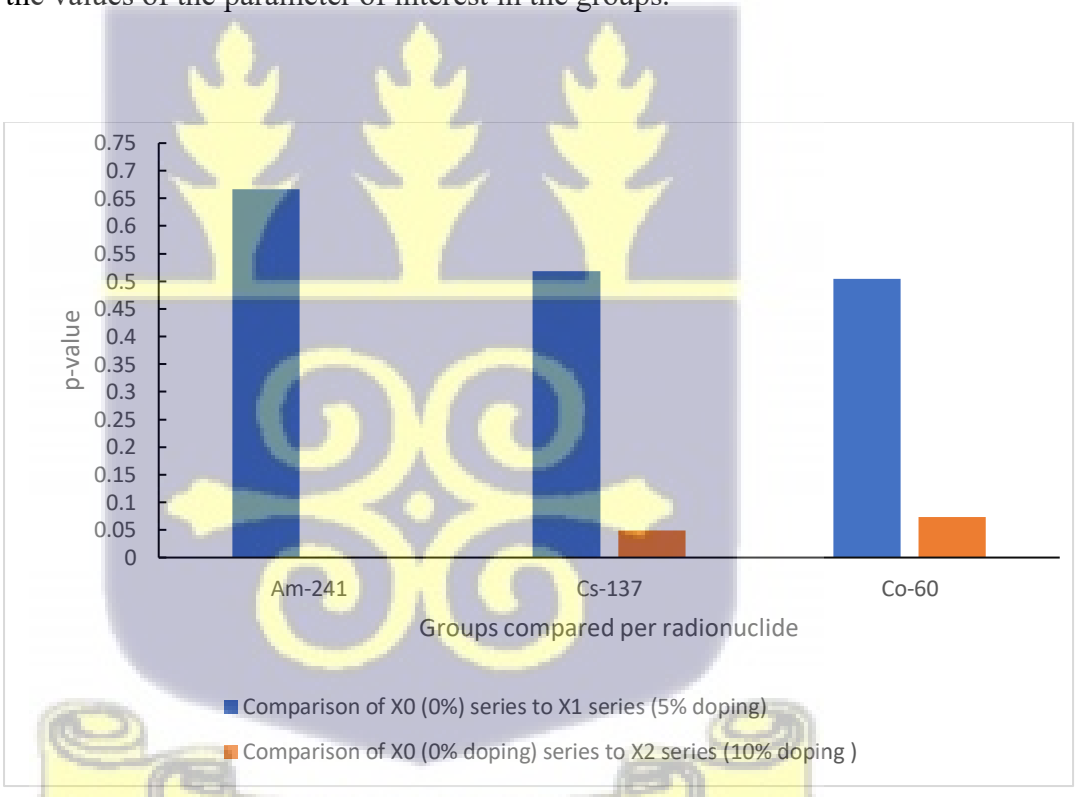

Figure. 4.21a: A graph of ANOVA p-values of LAC for the various groups of clay studied at varied energies

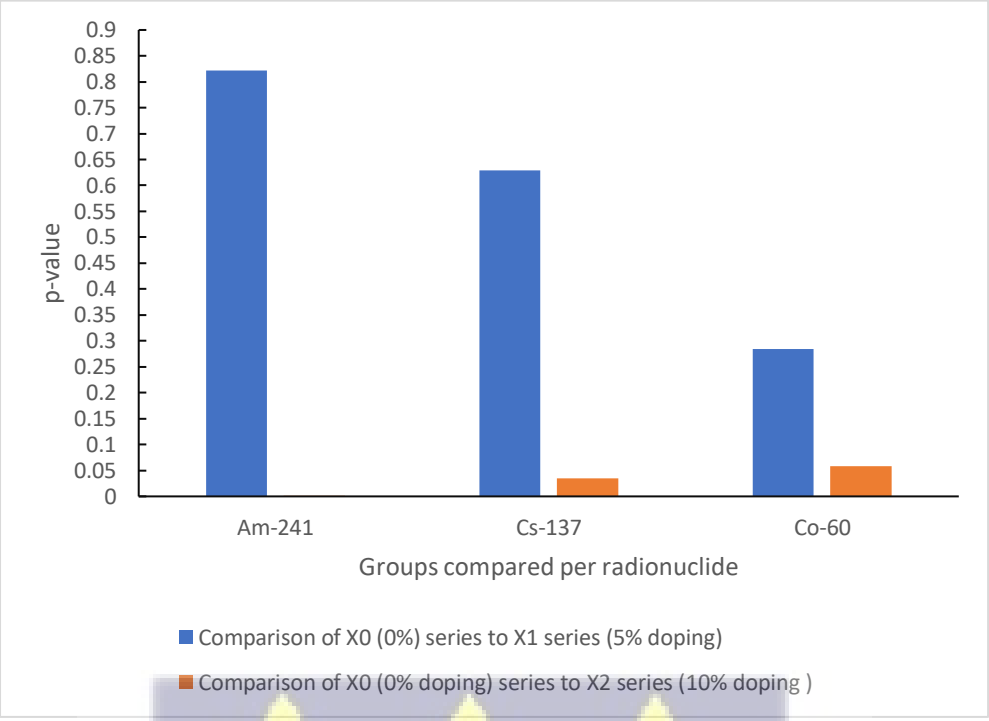

Figure. 4.21b: A graph of ANOVA p-values of MAC for the various groups of clay studied at varied energies

In fig. 4.21a and Fig. 4.21b, it is seen that for all radionuclides studied, because p-values are greater than 0.05, there is no significant difference between the LAC and MAC for X0 (undoped) series and X1(5% doping) series. Suggesting that even though there is slight improvement in density of the test pieces in the group, it does not result in statistically significant improvement in LACs and MACs. On the other hand, when the LAC and MAC of 10% wt doping are compared to undoped series, in the case of Am-241 and Cs-137 which is lower and mid-range energies respectively, the improvement in density produces a statistically significant difference in the LAC and MAC since the p-values are lower than 0.05 in those instances unlike for Co-60. But even then, considering the p-values for Co-60 which are hovering around 0.05 but only slightly higher (0.07 for LAC and 0.06 for MAC) which suggests that with extra densification

techniques such as increased pressure for clay body pressing before firing, increased firing temperature optimized grain-size distribution, there may be potential for clay even at high energy ranges of Co-60.

4.3.4 MCNP Simulation

4.3.4.1 Comparison of Experimental values of LAC to that of MCNP simulated LAC

MCNP (Monte Carlo N-Particle) code has been used to simulate the interactions of various types of photons with matter and has provided information to predict radiation transport. The data from the simulations output file has been used to calculate the linear attenuation coefficients (LAC) of some of the clays studied in this work to validate the LAC results and buildup factors from the experiment as can be seen from Figures 4.22a through to 4.24c shown below.

The following graphs show that there is strong agreement between MCNP and experimental results as shown by correlations curves Fig 4.23b to Fig. 4.23d (with $R^2 > 0.9$) It is further observed that the largest variation in the experimental and simulated is about 8% which occurs for FOS-X0 for all the radionuclides studied while the least occurs for OKY-X2 for Cs-137 at 0.3%. This variation may have statistical treatment in origins.

Considering buildup factors asl well, there is similar strong agreement between the simulation and experimental buildup figures although in all cases, the MCNP values were slightly higher than the experimental values. Both experimental and simulated buildup factors nearly approximate 1 implying and conforming the good geometry in which the experiments were conducted.

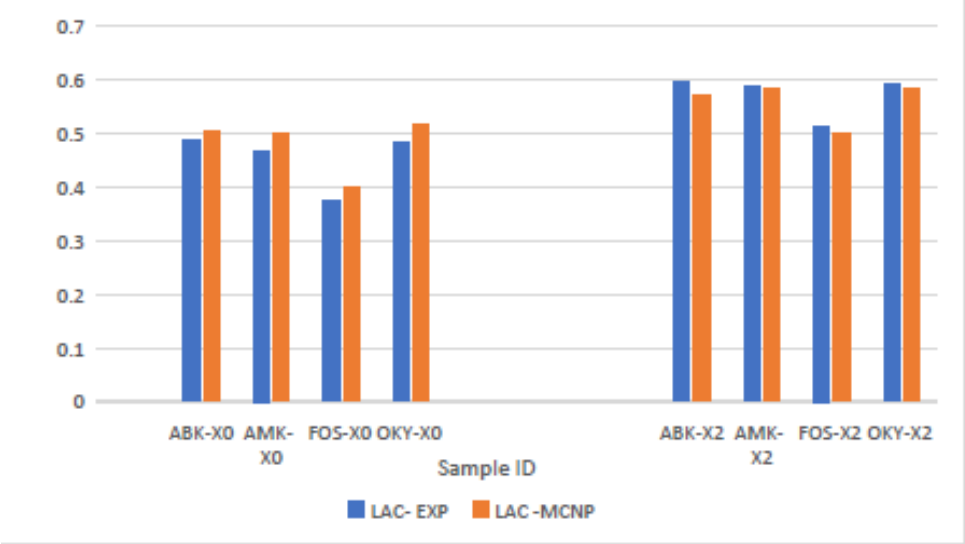

Figure. 4.22a: A graph showing the comparison of the results of experimentally determined LAC as against MCNP simulated LAC for Am-241 radiation through a selection of some the studied clay

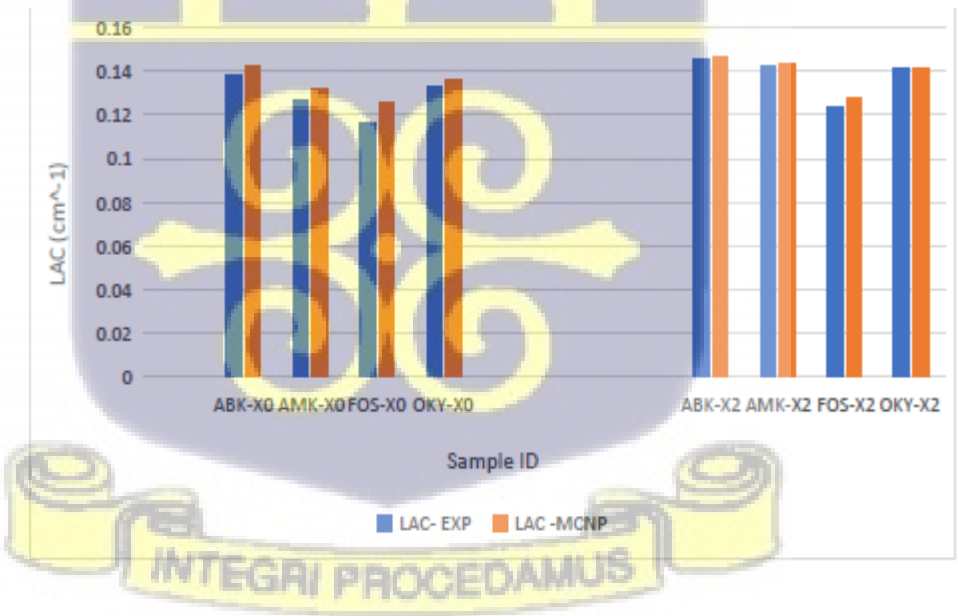

Figure. 4.22b: A graph showing the comparison of the results of experimentally determined LAC as against MCNP simulated LAC for Cs-137 radiation through a selection of some the studied clays

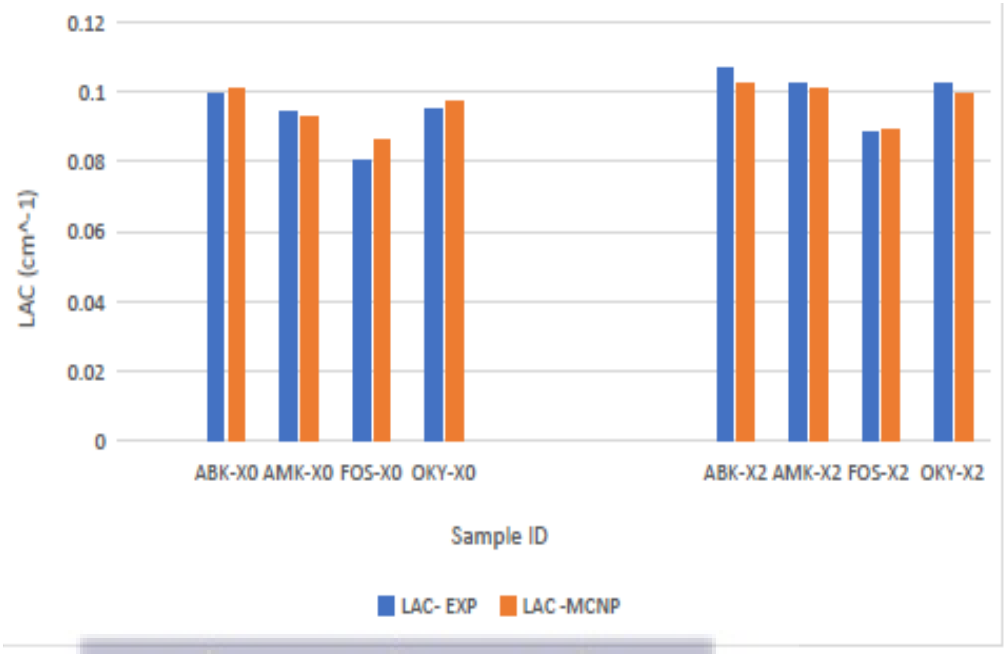

Figure. 4.22c: A graph showing the comparison of the results of experimentally determined LAC as against MCNP simulated LAC for Co-60 radiation through a selection of some the studied clays

4.3.4.2. Extent of variation between Experimental and MCNP results

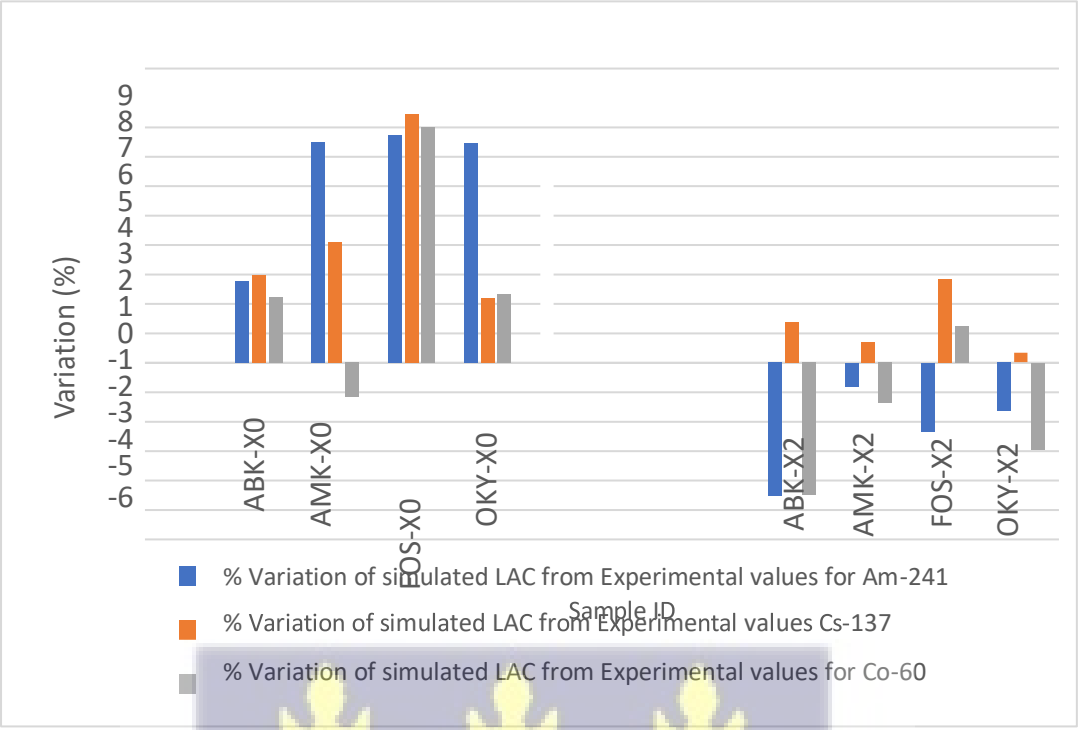

Figure 4.23a: A graph depicting the degree of variation of the simulated LAC from that of the experimental results.

4.3.4.1 Degree of agreement between experimental LAC and Simulated LAC

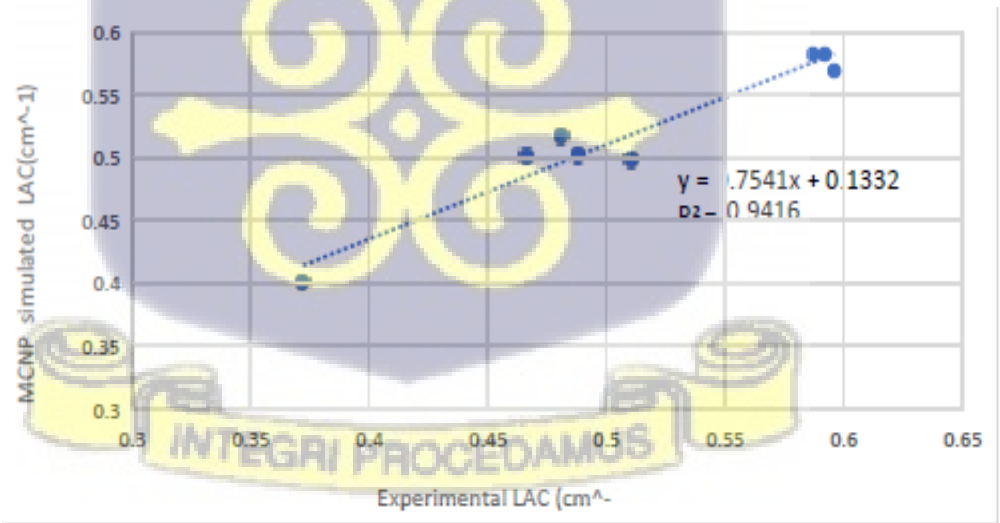

Figure. 4.23b: A graph showing the degree of correlation between experimental and simulated LAC for Am-24

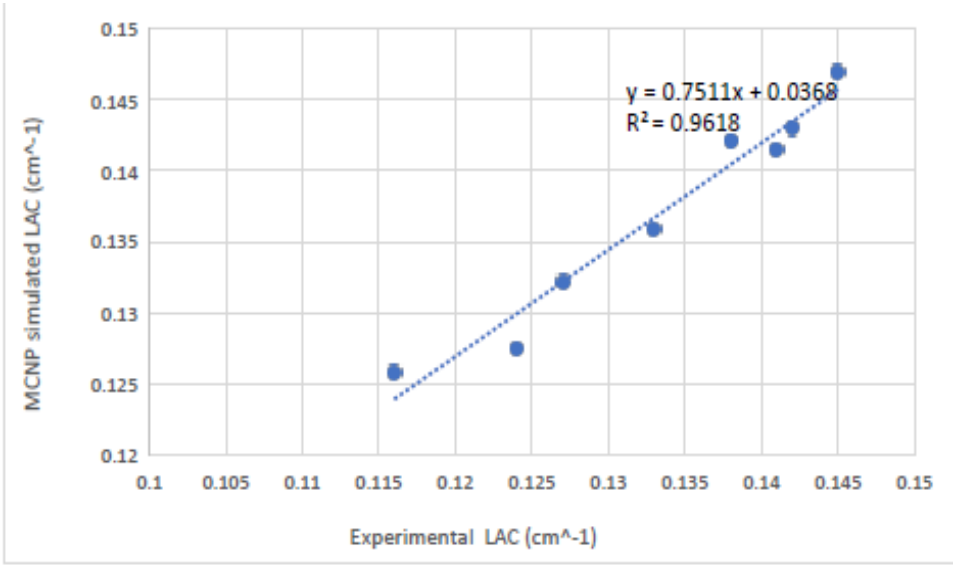

Figure. 4.23c: A graph showing the degree of correlation between experimental and simulated LAC for Cs-137

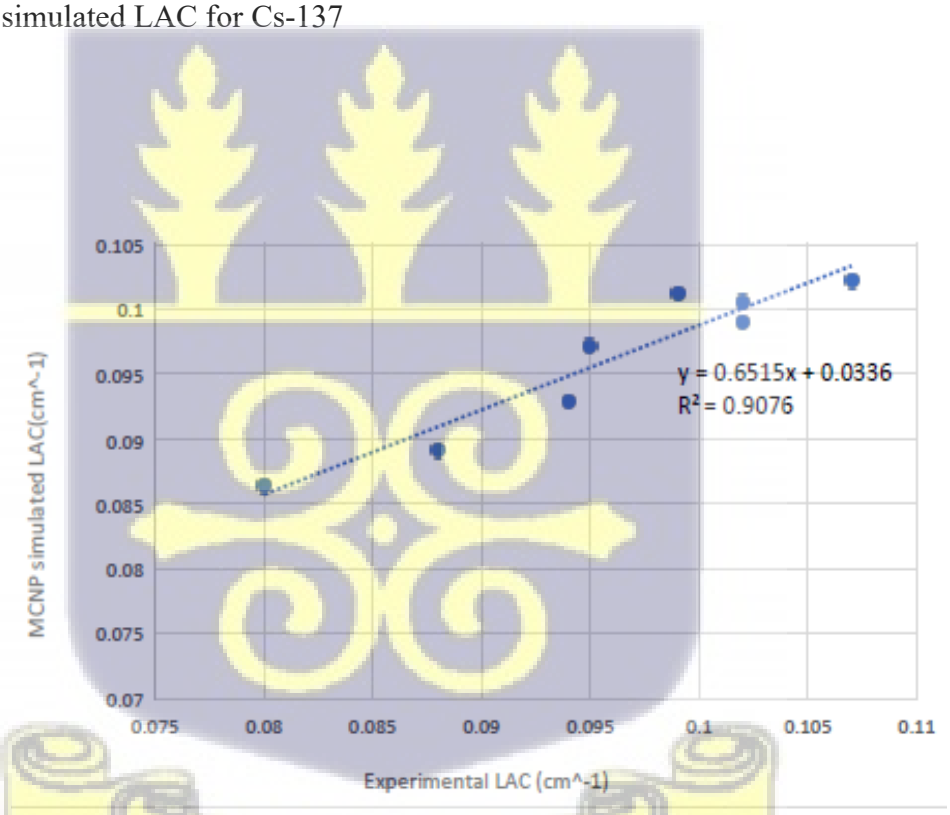

Figure. 4.23d: A graph showing the degree of correlation between experimental and simulated LAC for Co-60

4.3.4.3 Comparison of Experimental and MCNP simulated values of Buildup factors

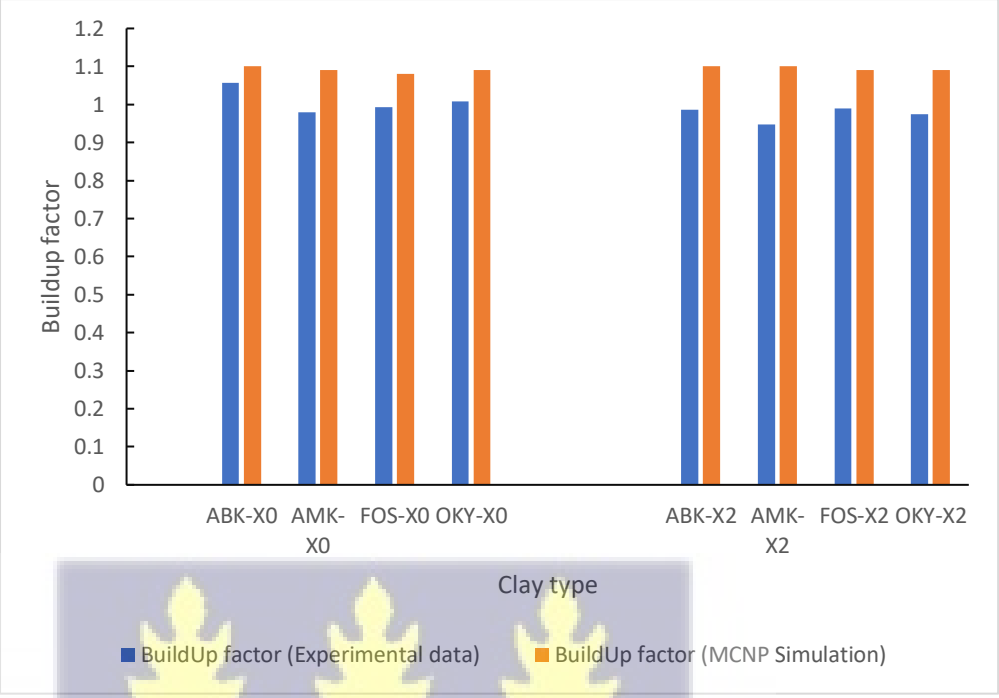

Figure 4.24a: A graph showing the comparison of the results of experimentally determined buildup factor as against MCNP simulated buildup factor for Am-241 radiation through a selection of some the studied clays

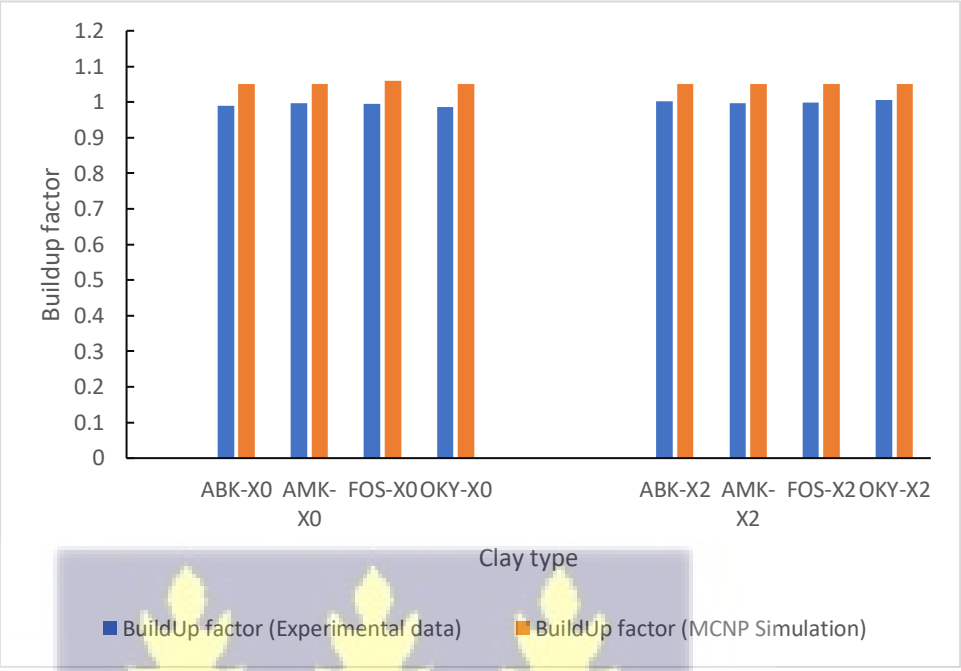

Figure. 4.24b: A graph showing the comparison of the results of experimentally determined buildup factor as against MCNP simulated buildup factor for Cs-137 radiation through a selection of some the studied clay

Figure. 4.24c: A graph showing the comparison of the results of experimentally determined buildup factor as against MCNP simulated buildup factor for Co-60 radiation through a selection of some the studied clays.

Medhat, (2015) conducted a study in which they compared Monte Carlo simulations of photon attenuation in fired clay bricks with experimental measurements using gamma-ray sources. The study revealed a strong correlation between the simulated and experimental results, especially for lower-energy gamma rays. At energies below 1000 keV, the attenuation coefficients predicted by the simulations were within 10% of the measured values. However, at higher energies (above 1250 keV), they observed some discrepancies, with experimental results showing slightly lower attenuation than predicted by the simulations. This could be caused by multiple factors, including the inhomogeneity of the brick material or uncertainties in

the material's exact composition. These findings highlight the importance of refining the material models used in computer simulations. (Medhat, 2015)

Olukotun, et al (2020).and Amin, et al. (2022). also found similar agreement albeit with minimal discrepancies when validating Monte Carlo predictions for the attenuation of gamma radiation in natural materials like fired clay bricks. Their simulations correctly predicted the shielding performance for lower- energy gamma rays, however, the slightly larger variations at higher energies pointed to the need for more studies into the scattering and secondary interactions in the material. It should be noted that, for example, Monte Carlo simulations usually assume idealized conditions, such as perfectly homogeneous materials, which may not be case for the morphology of the fired clay bricks in reality.

This study has demonstrated similar findings in this regard. For the LAC, for all the energies studied, the variation was less than 10% in all cases. However, for the buildup factors for high energies of 1250, the simulated values were on average about 12% higher the experimental values. For mid-range (Cs-137) which is a single energy photon the variation was predominantly about 5.5%. Whereas, for lower energy (Am-241) the variation was mixed with an average variation of about 10%. It could be posited that the simulation was better able to mimic the scenario for single energy photons as against multiple energy peaks for Am-241 and Co-60. On the other hand, the variation could arise from the translation of experimental uncertainties in the final experimental results. These notwithstanding to a very large extent, there is good agreement between experimental and MCNP results

4.3.5 Practical Application and Significance of Results

Given that the LAC for ordinary concrete at 150 keV is 0.3303 cm^{-1} , and using the equations derived from the regression curve fitting in Fig 4.20a, the LAC for ABK-X2 (10% wt doping) which is the best performing clay in this study as well as FOS-X0 (undoped and least dense clay) and Alucobond can be interpolated to produce results in table 4.3.1

In radiation protection, the number of half-value layers (HVLs) required to ensure adequate shielding depends on the radiation type and the specific safety standards set for the application. The HVL is used to quantify the thickness of a material needed to reduce radiation intensity by half.

Table 4.3.1: Parameters used for shielding analysis of hypothetical x-ray facility

Sample	Material Density (g/cm^3)	Doping status -(% by wt)	Shielding parameters					Required Shied Thickness for Radiation Protection (ICRP, 2007)	
			LAC (/cm)	**MAC (cm^2/g)**	**HVL (cm)**	**TVL (cm)**	**mfp**	**5 HVL (cm)**	**7 HVLs (Cm)**
Alucobo	1.1035	N/A	0.1911	0.1732	3.63	12.05	5.23	18.13	25.39
FOS-X0	1.6514	0	0.2359	0.1429	2.94	9.76	4.24	14.69	20.57
ABK-X2	2.0696	10	0.3498	0.1690	1.98	6.58	2.86	9.91	13.87
OC	2.3000	N/A	0.3582	0.1557	1.94	6.43	2.79	9.68	13.55

N/A- not applicable

OC- Ordinary Concrete

For diagnostic radiology, such as chest X-rays or CT scans, shielding typically aims to reduce radiation exposure to safe levels. The required shielding usually ensures that radiation exposure outside the treatment or diagnostic area is reduced by at least 99%, which would generally require 5 to 7 HVLs of shielding material. For instance, a typical barrier for diagnostic X-rays might use lead or concrete and be designed to attenuate the radiation to less than 1 millisievert per year (mSv/year) for personnel working in the vicinity. The 5 to 7 HVLs of a shielding material (e.g., lead or concrete) which are commonly used is meant to achieve a significant reduction in radiation exposure, ensuring that the dose to personnel or bystanders is minimized (Bushberg et al., 2011; Statkiewicz Sherer, et al., 2021).

Similarly, in radiation therapy, the energy levels are much higher, requiring thicker shields. Therefor, 7 to 10 HVLs are generally needed to reduce the dose of radiation sufficiently. Higher-energy radiation from therapeutic sources necessitates a larger number of HVLs for adequate attenuation, especially when treating deep tissue (Statkiewicz Sherer, et al. 2021).

International regulatory agencies such as the International Commission on Radiological Protection (ICRP) together with several national Competent Authorities recommend shielding designs that keep occupational exposure below 1 mSv per year. Achieving this usually involves using shielding with a minimum of 5 to 7 HVLs for typical diagnostic radiation (ICRP, 2006).

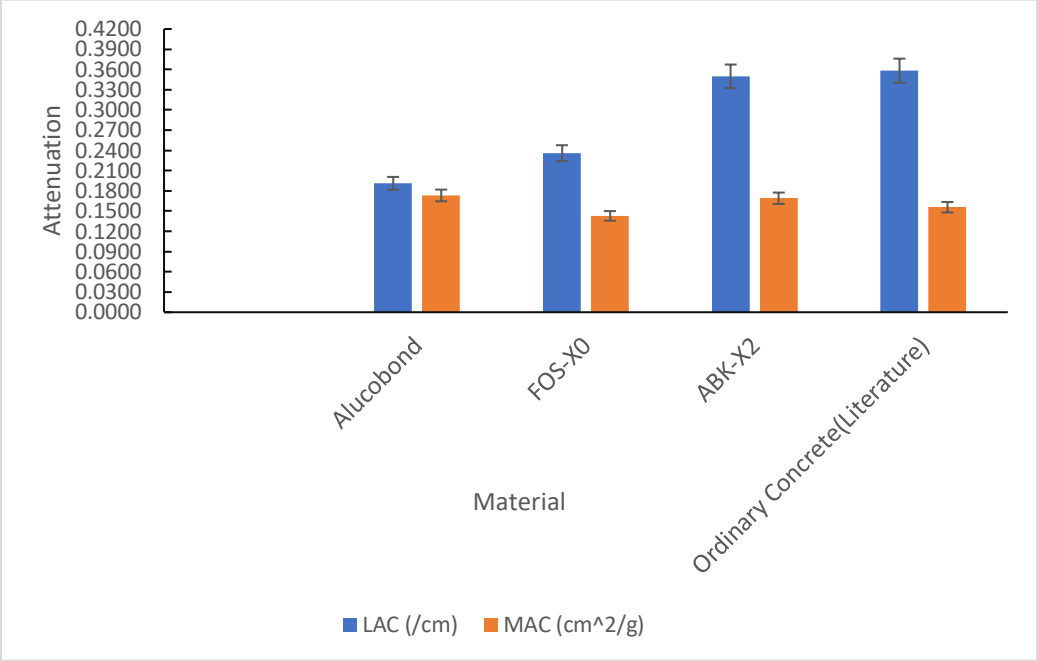

Figure. 4.3.1a: A graph comparing the LAC and MAC for selected materials used in carrying out shielding of 150keV in a hypothetical facility

Figure. 4.3.1b: A graph comparing the thickness of shielding required to ensure the protection of worker and the public

From Fig. 4.3.1a, which were plotted with data from Table 4.3.1, it can be seen that ABK-X2 and Alucobond although have lower LAC as compared to ordinary concrete, on the other hand have higher MAC than ordinary concrete implying Alucobond and ABK-X2 (10% doping) clays have marginally better shielding efficiency for 150keV photons.

To protect workers and persons standing in the vicinity of diagnostic x-ray facility, 10cm of ABK-X2 clay or ordinary concrete will be required to provide 5 HVLs for lower photon(x-ray) energies in the diagnostic energy range and slightly less than 14cm of either ABK-X2 clay or ordinary concrete can provide the 7 HVLs for the higher energy photons which trending towards 150keV in the diagnostic medical facility.

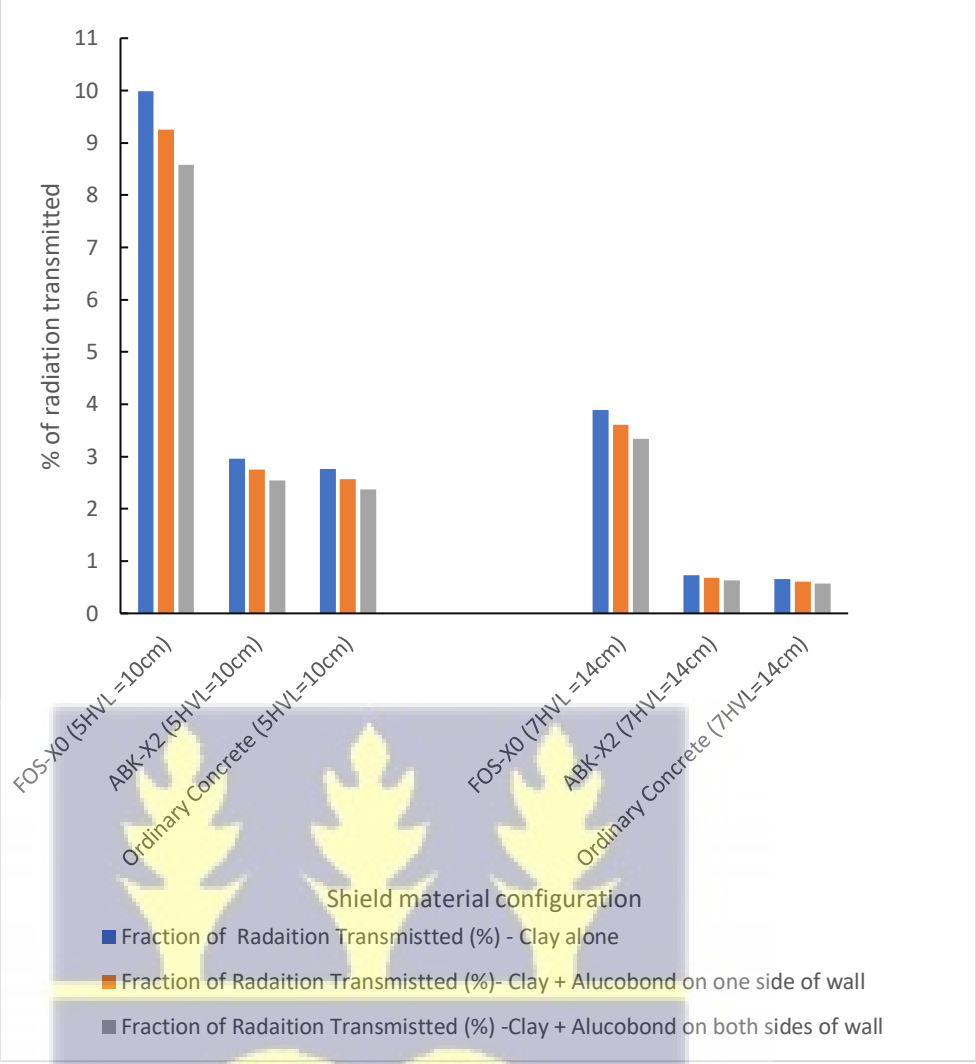

Figure. 4.3.1c A graph showing the attenuation performance of selected shield materials for 150keV photons

From Fig 4.3.1c it can be observed that for 7HVLs both ABK-X2 and ordinary concrete attenuate over 99% of the initial radiation irrespective of the Alucobond panel addition.

From the foregoing, it is clear, that if a hypothetical medical diagnostics facility is to be built by the Ga East Municipal Assembly in Abokobi ,

using locally sourced clay doped at 10% wt of the dopant used in this study which was rich in Fe_2O_3 to the level about 71% purity, all things being equal, the clay can safely be used in place of ordinary concrete to shield expected photon energies in such a facility which would be less than 150keV. Furthermore, adding an Alucobond panel to a fixed thickness of clay would improve the multiple (5 and 7) HVLs shielding performance by 7.3% and 14.1% for one surface paneling and two surface paneling respectively.

CHAPTER FIVE

CONCLUSIONS AND RECOMMENDATIONS

In this final chapter of the thesis, the key outcomes of the research are presented. The impact and implications of the results are summarized and highlighted based on which recommendations are made to specific stakeholders.

5.1 Conclusions

The main objective of the study is to investigate the impact of Fe_2O_3-rich oxide dopant and Alucobond panels on Am-241, Cs-137 and Co-60 gamma radiation shielding effectiveness of selected clays sourced from Ghana.

Sampling was done at six sampling sites known for clay deposits within the study area of the south-eastern part of Ghana. The sites are Okyereko and Assin Fosu in the Central region, Abokobi and Kinbu in the Greater Accra Region and Oframase and Amperkrom in the Eastern region were chosen.

Upon completion of this study, the following conclusions are made in line with the specific objectives and the overall research aim.

Specific Objective 1:

Carry out elemental composition analysis and physico-mechanical tests (i.e., density, porosity and grain size distribution) of the selected clay samples to investigate their influence on some physical and shielding parameters of selected clays.

Research Outcome 1

Elemental composition analysis, grain size distribution and texture confirmed that the samples studied are indeed clays, with one identified as kaolinite. Density measurements showed values between 1.6514±0.0033 and 1.9951±0.0046 g/cm³ for undoped clays. Doping with Fe_2O_3-rich oxides enhanced density, especially at 10% doping, with X1 (5%) and X2 (10%) ranges of 1.6798±0.0042 to 2.0390±0.0057 g/cm³ and 1.7960±0.0028 to 2.0695±0.0039 g/cm³, respectively. These physical properties were found to strongly influence photon interaction behaviour, particularly LAC and MAC, in accordance with theory.

Specific Objective 2:

Carry out shielding performance assessment by radiation transmission tests on sample test pieces – both doped and undoped with the addition of Alucobond panels to obtain shielding parameters (i.e., LAC, MAC, HVL, TVL, mfp, and buildup factor).

Research Outcome 2

Transmission experiments provided LAC, MAC, HVL, TVL, mfp and buildup factors for all samples. The lowest LAC for Am-241 was 0.372±0.0012 cm^{-1} (FOS-X0), while the highest reached 0.596±0.0022 cm^{-1}. As predicted, LAC varied inversely with HVL, TVL and mfp.

Fe_2O_3 doping improved shielding performance, with the 10% doped X2 series yielding MAC values for Am-241 that surpassed those of ordinary concrete, indicating superior attenuation at low photon energies.

Alucobond integration further reduced transmitted photon intensity, with reductions reaching 21% for double-panel configurations (Am-241 shielding) and 2.7% for single-panel shielding of Co-60. Thicker Alucobond panels comprising Al "skin" thickness of 1 mm on both sides as against the. 0.5 mm used in this study are expected to further enhance attenuation.

Curve-fitting models generated in the study provide useful predictive tools for estimating shielding trends and guiding material-selection decisions.

Specific Objective 3

Perform MCNP simulation to compare with some of the shielding parameters (i.e., LAC and B).

Research Outcome 3

MCNP simulations closely matched experimental results for both Linear Attenuation Coefficient and buildup factors, confirming the reliability of the simulation approach and its usefulness as an optimization tool for selecting clay compositions and configurations for photon shielding.

Specific Objective 4:

Demonstrate the feasibility and suitability of using locally sourced raw materials such as clays for photon shielding and radiation protection purposes.

Research Outcome 4

The combined effects of Fe_2O_3-doped clay and Alucobond panels demonstrate that locally sourced Ghanaian clays can serve as effective shielding materials for Am-241, Cs-137 and Co-60 photons. Ghana's significant bauxite reserves (Statistica, 2024; Harbour Aluminum 2024)., its established aluminum production capacity, and growing need for polyethylene recycling present a strategic opportunity for domestic manufacture of aluminum–polyethylene composite panels that can complement or compete with existing proprietary Alucobond products. The clay–Alucobond composite also shows promise for neutron, alpha and beta shielding, supported by the polyethylene core and aluminum skins. Further enhancement is possible by doping clays with neutron-absorbing elements such as carbon. The material's ease of shaping, doping and thermal robustness makes it suitable for shielding and thermal-insulation applications in radiation-sensitive equipment.

Main Objective:

Finally, considering the main objective "To investigate the impact of Fe_2O_3-rich oxide dopant and Alucobond panels on Am-241, Cs-137 and Co-60 gamma radiation shielding effectiveness of selected clays sourced from Ghana."

Overall Research Outcome

The combined experimental and simulation findings confirm that Fe_2O_3-rich oxide doping significantly enhances the photon-attenuation properties

of Ghanaian clays, and that the incorporation of Alucobond panels provides an additional shielding advantage across the evaluated gamma energies. The synergy between these materials presents a practical, locally manufacturable, and cost-effective solution for radiation shielding.

This research not only advances the scientific understanding of clay-based composites for photon shielding but also supports national priorities in resource utilization, environmental sustainability and local industry development. The outcomes directly contribute to United Nations (UN) Sustainable Development Goals SDG 3 (Good Health and Well-being), SDG-11 (Sustainable Cities and Communities), and SDG-13 (Climate Action).

In the light of these, it is concluded that, all the clays can be used as suitable substitutes for photon radiation shields to varying degrees of efficiency and with extra thickness addition, can compare well to ordinary concrete. In particular ABK clay showed good photon shielding performance and can be used in place of concrete in shielding photons (X-rays) with energy lower than 150 keV.

5.2 Recommendations

5.2.1 Recommendations to policy makers

i. The Nuclear Regulatory Authority (NRA) should consider approving hospital building structures designed with clay-based composite materials if they meet the safety standards.

ii. The Ministry of Health in collaboration with other stakeholders must encourage the incorporation of clay brick in the construction of hospital x-ray diagnostic rooms.

iii. The Ghana Geological Survey Authority (GGSA) together with other academic institutions must continue to carry out extensive research on all clay types in Ghana, to characterize them in terms of their physico-mechanical properties to create a pool of suitable deposits that can be exploited later for radiation protection purposes.

5.2.2 Recommendations for further research

i. The investigated clays in this research should be studied for their effectiveness for shielding other nuclear radiations such as neutrons.

ii. Clays from other deposits in Ghana should be investigated to generate a comprehensive map showing their suitability for shielding the various types of radiation.

iii. Further studies must be conducted to confirm the empirical relationships that link the proportions of elements in a material to its shieling properties and to develop predictive equations and models

iv. With respect of further density improvement for any selected clay deposit, and consequently enhancing their photon shielding efficiency, further studies should

a) Focus on development of clay composites from the addition of other suitable dopants/additives – in particular Titanium (Ti) shows promise as it has moderately high coefficient of

correlation with the density of the clays.

b) Explore the use of a much purer elemental constituent of the oxide of interest (i.e. for example, at least 90% pure Fe_2O_3) to enhance the efficiency of their impact on density improvement.

c) Increase the compression pressure used in preparing the test pieces of each deposit before firing to enhance compactness.

d) Fire clay test pieces at higher temperatures, for example 1050°Cand 1100°C.

v. Further research should be carried out on multi-layered radiation shields which incorporate clay bricks.

vi. Where necessary carry out confirmatory research to validate the numerous relationship equations regarding density and LAC, MAC, mfp, elemental concentration, etc. for clays sourced from Ghana generated in this work to establish them as empirical predictive models for use of the scientific community.

To conclude, this research has been extremely successful as the outcomes of the research have contributed to the body of knowledge on clay as a gamma radiation shielding material and highlighted the feasibility of locally-sourced clay-based composite material to support radiation protection and nuclear safety needs for the global community but most especially for the country Ghana.

REFERENCES

3A Composites GmbH. (2024, July 15). The aluminium composite panel achieving versatile results for your architectural projects [Web page]. ALUCOBOND®. Retrieved from https://www.alucobond.com/en/products/

Abdullah, M. A. H., Rashid, R. S. M., Amran, M., Hejazii, F., Azreen, N. M., Fediuk, R., Voo, Y. L., Vatin, N. I., & Idris, M. I. (2022). Recent trends in advanced radiation shielding concrete for construction of facilities: Materials and properties. Polymers, 14(14), 2830.

AbuAlRoos, N. J., Azman, M. N., Baharul Amin, N. A., & Zainon, R. (2020). Tungsten-based material as promising new lead-free gamma radiation shielding material in nuclear medicine. *Physica Medica, 78*, 48–57.

Abubakar, M., Muthuraja, A., Rajak, D. K., Ahmad, N., Pruncu, C. I., Lamberti, L., & Kumar, A. (2020). Influence of firing temperature on the physical, thermal and microstructural properties of Kankara kaolin clay: A preliminary investigation. Materials, 13(8), 1872

Adinkrah-Appiah, K., Adom-Asamoah, M., & Afrifa, R., (2015). Reducing Environmental Degradation from Construction Activities: The use of Recycled Aggregates for Construction in Ghana. J Civil Engineering and Architectural Research. 2.

Adjei, D. N. (2012). Studies of locally available clays for use as radiation shielding (Master's thesis, University of Ghana). International Nuclear Information System.

Ahmad, N., Idris, M. I., Hussin, A., Abdul Karim, J., Azreen, N. M., & Zainon, R. (2024). Enhancing shielding efficiency of ordinary and barite concrete in radiation shielding utilizations. Scientific reports, 14(1), 26029.

Akkurt, I., & Canakci, H. (2011). Radiation attenuation of boron doped clay for 662, 1173 and 1332 keV gamma rays. Iranian Journal of Radiation Research, 9(1), 37–40.

Akkurt, I., Akyildirim, H., Mavi, B., Kilincarslan, S., & Basyigit, C. (2010). Photon attenuation coefficients of concrete includes barite in different rate. Annals of Nuclear Energy, 37(7), 910–914.

Alexander, M. G., & Mindess, S. (2015). Durability of concrete: Design and construction. CRC Press

Amin MN, Ahmad I, Iqbal M, Abbas A, Khan K, Faraz MI, Alabdullah AA, Ullah S. Computational AI Models for Investigating the Radiation Shielding Potential of High-Density Concrete.*Materials*. 2022; 15(13):4573.

Amin, M. N., Ahmad, I., Abbas, A., Khan, K., Qadir, M. G., Iqbal, M., Abu-Arab, A. M., & Alabdullah, A. A. (2022). *Estimating radiation shielding of fired clay bricks using ANN and GEP approaches. Materials*, 15(17), 5908.

Andrade, F.A., Al-Qureshi, H.A., and Hotza, D. (2011) Measuring the plasticity of clays: A review. Applied Clay Science, Volume 51, Issues 1-2, Pg 1-7

Asdrubali, F., Grazieschi, G., Roncone, M., Thiebat, F., & Carbonaro, C. (2023). Sustainability of building materials: Embodied energy and embodied carbon of masonry. Energies, 16(4), 1846.

Asdrubali, Francesco & Grazieschi, Gianluca & Roncone, Marta & Thiebat, Francesca & Carbonaro, Corrado. (2023). Sustainability of Building Materials: Embodied Energy and Embodied Carbon of Masonry. Energies. 16. 10.3390/en16041846.

ASTM International. (2017). ASTM D6913/D6913M-17: Standard Test Methods for Particle-Size Distribution (Gradation) of Soils Using Sieve Analysis. West Conshohocken, PA: ASTM International.

ASTM International. (2018). ASTM C373-18: Standard Test Method for Water Absorption, Bulk Density, Apparent Porosity, and Apparent Specific Gravity of Fired Whiteware Products. West Conshohocken, PA: ASTM International.

Attix, F. H. (1986). *Introduction to radiological physics and radiation dosimetry.* Wiley-Interscience.

Barrett, E. P., Joyner, L. G., & Halenda, P. P. (1951). The determination of pore volume and area distributions in porous substances. Journal of the American Chemical Society, 73(1), 373–380.

Baskar, R., Dai, J., Wenlong, N., Yeo, R., & Yeoh, K.-W. (2014). Biological response of cancer cells to radiation treatment. *Frontiers in Molecular Biosciences, 1*, 24.

Battistoni, G., Broggi, F., Brugger, M., Campanella, M., Carboni, M., Empl, A., Fassò, A., Gadioli, E., Cerutti, F., Ferrari, A., Lantz, M., Mairani, A., Margiotta, A., Muraro, S., Roesler, S., Sala, P. R., & Vlachoudis, V. (2011). Applications of FLUKA Monte Carlo code for nuclear and accelerator physics. Nuclear Instruments and Methods in Physics Research Section B: Beam Interactions with Materials and Atoms, 269(24), 2850–2856.

Benmoussa, H. (2019). Evaluation of physical and mechanical properties of fired-clay bricks incorporating both mineral and organic wastes. Modern Building Materials, Structures and Techniques.

Bergaya, F., & Lagaly, G. (2013). General introduction: Clays, clay minerals, and clay science. In F. Bergaya & G. Lagaly (Eds.), Handbook of clay science (2nd ed., pp. 1–19). Elsevier.

Bevington, P. R., & Robinson, D. K. (2003). Data Reduction and Error Analysis for the Physical Sciences (3rd ed.). McGraw-Hill.

Brindley, G. W., & Brown, G. (Eds.). (1980). *Crystal structures of clay minerals and their X-ray identification* (Monograph No. 5). Mineralogical Society

Bronick, C. J., & Lal, R. (2005**).** Soil structure and management: A review. *Geoderma, 124*(1–2), 3–22

Brouwers, B., van Beeck, J., Meire, D., Lataire, E., (2022). Assessment of the potential of radiography and ultrasonography to record flow dynamics in cohesive sediments (mud). Frontiers in Earth Science. Vol. 10 – 2022.

Bushberg, J. T., Seibert, J. A., Leidholdt, E. M., Jr, & Boone, J. M. (2012). *The essential physics of medical imaging* (3rd ed.). Lippincott Williams & Wilkins.

Chang, Q., Guo, S., Zhang, X., (2023). Radiation shielding polymer composites: Ray-interaction mechanism, structural design, manufacture and biomedical applications, Materials & Design, Volume 233.

Chmielewski, A. G., Haji-Saeid, M., & Ahmed, S. (2005). Progress in radiation processing of polymers. *Nuclear Instruments and Methods in Physics Research Section B: Beam Interactions with Materials and Atoms, 236*(1–4), 44–54

Ciotta, Mariana & Tassinari, Colombo. (2024). Clay minerals and their role in carbon capture and storage. REVISTA DELOS. 17. 10.55905/rdelosv17.n60-050.

Cordella, F., Cappelli, M., Ciotti, M., Claps, G., De Leo, V., Mazzotta, C., Pacella, D., Tamburrino, A. and Panza, F. (2024) Genetic algorithm for multilayer shield optimization with a custom parallel computing architecture. Eur. Phys. J. Plus 139, 150 (2024).

Dana, K., Abdur Rakib, S., Sinhamahapatra, S. (2023). Effect of oxide additives on densification of terracotta. Applied Clay Science, 245, 107147

Danso, H., & Obeng-Ahenkora, N. K., (2018). Major Determinants of Prices Increase of Building Materials on Ghanaian Construction Market. Open Journal of Civil Engineering, Vol.8 No.2,

Das, B. M. (2007). Principles of geotechnical engineering (7th ed.). Thomson.

Delaney, G., Jacob, S., Featherstone, C., & Barton, M. (2005). The role of radiotherapy in cancer treatment: Estimating optimal utilisation from a review of evidence-based clinical guidelines. *Cancer, 104*(6), 1129–1137.

Dhar AK, Himu HA, Bhattacharjee M, Mostufa MG, Parvin F. Insights on applications of bentonite clays for the removal of dyes and heavy metals from wastewater: a review. (2023) Environ Sci Pollut Res Int. 2023 Jan;30(3):5440-5474. doi: 10.1007/s11356-022-24277-x. Epub 2022 Nov 23. PMID: 36418828.

Eisa, M., Ali, M., & Abualreish, M. (2024). Clay and Cement Shielding Behavior from Gamma Sources. Engineering, Technology & Applied Science Research. 14. 16166-16171. 10.48084/etasr.8217.

Eissa, M., Habib, A., AL Houri, A., & Alibrahim, B. (2024). Recent efforts on investigating the effects of recycled rubber content on the mechanical properties of structural concrete. Discover Civil Engineering, 1(1), 16.

El-Nahal, M. A., Elsafi, M., Sayyed, M. I., Khandaker, M. U., Osman, H., Elesawy, B. H., Saleh, I. H., & Abbas, M. I. (2021). Understanding the Effect of Introducing Micro- and Nanoparticle Bismuth Oxide (Bi_2O_3) on the Gamma Ray Shielding Performance of Novel Concrete. *Materials*, *14*(21), 6487.

Elsafi, M., Dib, M. F., Mustafa, H. E., Sayyed, M. I., Khandaker, M. U., Alsubaie, A., Almalki, A. S. A., Abbas, M. I., & El-Khatib, A. M. (2021).

Enhancement of ceramics based red clay by bulk and nano metal oxides for photon shielding features. Materials, 14(24), 7878.

Elsafi, M., Koraim, Y., Almurayshid, M., Almasoud, F. I., Sayyed, M. I., & Saleh, I. H. (2021). Investigation of photon radiation attenuation capability of different clay materials. Materials, 14(21), 6702.

El-Samrah, M. G., Tawfic, A. F., Sallam, F. H., & Omar, A. M. (2023). Investigation of specially designed bentonite samples as potential bricks with better radiation shielding properties. *Progress in Nuclear Energy, 162*, 104778.

Eramo, G. (2020). Ceramic technology: how to recognize clay processing. Archaeological and Anthropological Sciences, 12(8), 164.

García, V. J., Zúñiga-Suárez, A. R., Márquez, C. O., Pérez, J. G., Fernández-Martínez, F., & Hernández-Olivares, F. (2016). Strength developing in clay–andesite brick. Materials Sciences and Applications, 7(8), 403–420

Glasstone, S., & Sesonske, A. (2004). *Nuclear reactor engineering: Reactor design basics* (4th ed., Vol. 1). New Delhi, India: cbspd.

Goorley, J. T., McKinney, G. W., Brown, F. B., et al. (2012). *Initial MCNP6 release overview*. Nuclear Technology, 180(3), 298–315.

Grim, R. E. (1968). Clay mineralogy (2nd ed.). New York, NY: McGraw-Hill.

Gu, X., & Ling, Y. (2024). Characterization and properties of Chinese red clay for use as ceramic and construction materials. Science Progress, 107(1), 00368504241232534.

Guerrero Gómez, G., Afanador Garcia, N., Nolasco Serna, C (2022). Energy evaluation of clay firing process and combustion gases in an intermittent kiln. Journal of Physics: Conference Series. **2163** 012005.

Hall, E. J., & Giaccia, A. J. (2018). Radiobiology for the radiologist (8th ed.). Wolters Kluwer Health.

Harbor Aluminum (2024, August 20) Bauxite Production by Country. HarborAluminum.https://www.harboraluminum.com/en/bauxite-production-bycountry

Harrison, J. D., & Muirhead, C. R. (2003). Quantitative comparisons of cancer induction in humans by internally deposited radionuclides and external radiation. International Journal of Radiation Biology, 79(1), 1–13.

Hubbell, J. H., & Seltzer, S. M. (1995). Tables of X-ray mass attenuation coefficients and mass energy-absorption coefficients 1 keV to 20 MeV for elements Z = 1–92 and 48 additional substances of dosimetric interest (NISTIR 5632). National Institute of Standards and Technology.

Hughes, R.E., DeMaris, P. J., White, W.A., Cowin, D.K. (1985). "Origin of Clay Minerals in Pennsylvanian Strata of the Illinois Basin", Proceedings of the International Clay Conference Denver, 1985, Leonard G. Schultz, H. van Olphen, Frederick A. Mumpton

International Commission on Radiological Protection. (2006). Assessing dose of the representative person for the purpose of radiation protection of the public and the optimisation of radiological protection: Broadening the process (ICRP Publication 101). Annals of the ICRP, 36(3–4), 1–332.

Isfahani, H. S., Abtahi, S. M., Roshanzamir, M. A., Shirani, A., & Hejazi, S. M. (2018). Permeability and gamma-ray shielding efficiency of clay modified by barite powder. Geotechnical and Geological Engineering, 37(2), 845–855.

Issa, A.S., & Al-Asadi, A.K. (2022). Mechanical properties of lightweight expanded clay aggregate (LECA) concrete. Scientific Review Engineering and Environmental Studies (SREES).

Jackson, M. L. (1969). *Soil chemical analysis: Advanced course* (2nd ed.). University of Wisconsin–Madison.

Jock, A. A., Ayeni, F. A., Ahmed, A. S., & Sullayman, U. A. (2013). Evaluation of the refractory properties of Nigerian Ozanagogo clay deposit. Journal

of Minerals and Materials Characterization and Engineering, 1(6), 321–325.

Kamseu, E., Leonelli, C., Boccaccini, D. N., Veronesi, P., Miselli, P., Pellacani, G., & Chinje Melo, U. (2007). Characterisation of porcelain compositions using two china clays from Cameroon. Ceramics International, 33(5), 851–857.

Khattari, Z.Y., Alsaif, N.A.M., Shams, M.S., Elsad, R. A. & Rammah Y. S. (2023) Development of Materials from Natural Clay Minerals and Magnesia Useful for Radiation-Shielding Applications. *Silicon* **15**, 4897–4907 (2023).

Kingery, W. D., Bowen, H. K., & Uhlmann, D. R. (1976). *Introduction to ceramics* (2nd ed.). New York, NY: Wiley-Interscience.

Kullman, J. (2023, October 17). *Curbing concrete's carbon emissions with innovations in cement manufacturing*. ASU News. https://news.asu.edu/20231017-curbing-concretes-carbon-emissions-innovations-cement-manufacturing

Lamarsh, J. R., & Baratta, A. J. (2001). Introduction to nuclear engineering (3rd ed.). Prentice Hall.

Li, J. (2019). Sampling soils in a heterogeneous research plot. Journal of Visualized Experiments, (143), e58519.

Lin, Q., & Wu, H. (2018). Trend analysis of interconnect system for integrated circuit. International Journal of Electronics Communication and Computer Engineering, 9(1), 23–28.

Mahboob, M., Ali, M., Rashid, T. u., & Hassan, R. (2021). Assessment of embodied energy and environmental impact of sustainable building materials and technologies for residential sector. *Engineering Proceedings, 12*(1), 62.

Martin, A., & Harbison, S. A. (2013). An introduction to radiation protection (6th ed.). Boca Raton, FL: CRC Press.

Martin, J. E. (2006). Physics for radiation protection: A handbook (2nd ed.). Wiley-VCH

Masdeu, F.; Carmona, C.; Horrach, G.; Muñoz, J. Effect of Iron (III) Oxide Powder on Thermal Conductivity and Diffusivity of Lime Mortar (2021). Materials, 14, 998.

Massaro, M., Colletti, C. G., Lazzara, G., & Riela, S. (2018). The use of some clay minerals as natural resources for drug carrier applications. *Journal of Functional Biomaterials, 9*(4), 58.

McBride, M. B. (1994). Environmental chemistry of soils. Oxford University Press. (Scribd)

Medhat, M.E. (2015) Comprehensive study of photon attenuation through different construction matters by Monte Carlo Simulation. Radiation Physics and Chemistry, (107), Pages 65-74.

Mitsch, W. J., & Gosselink, J. G. (2007). Wetlands (4th ed.). John Wiley & Sons.

Mokwa, J. B., Lawal, S. A., Abolarin, M. S., & Bala, K. C. (2019). Characterization and evaluation of selected kaolin clay deposits in Nigeria for furnace lining application. *Nigerian Journal of Technology, 38*(4), 936–946.

Montesinos, C. A., Khalid, R., Cristea, O., Greenberger, J. S., Epperly, M. W., Lemon, J. A., Boreham, D. R., Popov, D., Gorthi, G., Ramkumar, N., & Jones, J. A. (2021). Space radiation protection countermeasures in microgravity and planetary exploration. Life, 11(8), 829.

Mori, H., Oku, Y., Mannami, Y., & Kunisada, T. (2020). Iron (III) oxide-based ceramic material for radiation shielding. Ceramics, 3(2), 258–264.

Mousseau, T. A., & Møller, A. P. (2014). Genetic and ecological studies of animals in Chernobyl and Fukushima. Journal of Heredity, 105(5), 704–709.

Murray, H. H. (2007). Applied clay mineralogy: Occurrences, processing and application of kaolins, bentonites, palygorskite-sepiolite and common clays (Developments in Clay Science, Vol. 2). Elsevier

National Council on Radiation Protection and Measurements (NCRP). (1970). Recommendation on Radiation Protection Criteria for Medical X-ray and Gamma-ray Diagnostic Procedures. NCRP Report No. 48. NCRP.

Nzivulu D. K, Hashim N. O, Musila N, Otieno K. E, Wanjala F. O (2024). Investigation of red clay and waste glass composite bricks for ionizing radiation shielding. MethodsX. 2024 May 3; 12:102744.

Ogul, H., Gultekin, B., Yildiz, H., Us, H., Bulut, F., (2024). Novel 3D-Printed lead-free radiation protection apron in the medical X-ray and thermal neutron energy range. Radiation Physics and Chemistry, Volume 219, 111686.

Olukotun, S. F., Gbenu, S. T., Oyedotun, K. O., Fasakin, O., Sayyed, M. I., Akindoyin, G. O., Shittu, H. O., Fasasi, M. K., Khandaker, M. U., Osman, H., & Elesawy, B. H. (2021). Fabrication and characterization of clay–polyethylene composite opted for shielding of ionizing radiation. Crystals, 11(9), 1068.

Olukotun, S.F., Gbenu, S.T., Oladejo, O.F., Sayyed, M.I., Tajudin, S.M., Amosun, A.A., Fadodun, O.G., and Fasasi,M.K.(2020). Investigation of gamma ray shielding capability of fabricated clay-polyethylene

composites using EGS5, XCOM and Phy-X/PSD. Radiation Physics and Chemistry. Volume 177. 109079.

Rahaman, M. N. (2003). *Ceramic processing and sintering* (2nd ed.). New York, NY: Marcel Dekker.

Sathish, K. V., Sowmya, N., Munirathnam, R., Manjunatha, H. C., Seenappa, L., & Sridhar, K. N. (2023). Radiation shielding properties of aluminium alloys. *Radiation Effects and Defects in Solids, 178*(9–10), 1301–1320.

Sato, T., Niita K., Matsuda, N., Hashimoto, S., Iwamoto, Y., Furuta, T., Noda. S., Ogawa, T., Iwase, H., Nakashima, H.,Fukahori, T., Okumura, K., Kai, T., Chiba, S., and Sihver, L. (2015). Overview of particle and heavy ion transport code system PHITS. Annals of Nuclear Energy, Volume 82, 110-115.

Shahzad, K., Kausar, A., Manzoor, S., Rakha, S. A., Uzair, A., Sajid, M., Arif, A., Khan, A. F., Diallo, A., & Ahmad, I. (2023). Views on radiation shielding efficiency of polymeric composites/nanocomposites and multi-layered materials: Current state and advancements. Radiation, 3(1), 1–20.

Shultis, J. K., & Faw, R. E. (2010). Radiation shielding and radiological protection. In D. G. Cacuci (Ed.), *Handbook of nuclear engineering* (pp. 1315–1442). Springer.

Silva, V. J., Taveira, S. K. A., Silva, K. R., Neves, G. A., Lira, H. L., & Santana, L. N. L. (2021). Refractory ceramics of clay and alumina waste. Materials Research, 24(2), e20200485.

Srisuwan, A & Nonthaphong. P., (2020). Physical property and compressive strength of fired clay bricks incorporated with paper waste. Journal of Metals, Materials and Minerals. 30. 10.55713/jmmm.v30i1.598.

Statista. (2024). Production volume of bauxite in Ghana from 2010 to 2022 Graph. Statista. https://www.statista.com/statistics/1270227/production-volume-of-bauxite-in-ghana/

Statkiewicz Sherer, M. A., Visconti, P. J., Ritenour, E. R., & Welch Haynes, K. (2021). *Radiation protection in medical radiography* (9th ed.). Elsevier.

Sullivan, K., & Olson, G. (2022, November 2). *Laying the foundation of cement and concrete decarbonization*. World Resources Institute. https://www.wri.org/update/laying-foundation-cement-and-concrete-decarbonization

Sütçü, M., Alptekin, H., Erdoğmuş, E., Er, Y., & Gencel, O., (2015). Characteristics of fired clay bricks with waste marble powder addition as building materials. Construction and Building Materials. 82. 10.1016/j.conbuildmat.2015.02.055.

Tan, K. H. (2005). *Soil sampling, preparation, and analysis* (2nd ed.). CRC Press.

Thomas, M., Salvador, H., Clark, T., Lang, E., Hattar, K., & Mathaudhu, S. (2023). Thermal and radiation stability in nanocrystalline Cu. Nanomaterials, 13(7), 1211.

Tisserand, R., & Young, R. (2014). Essential oil safety: A guide for health care professionals (2nd ed.). Churchill Livingstone/Elsevier.

Tyagi, G., Singhal, A., Routroy, S., Bhunia, D., & Lahoti, M. (2020). A review on sustainable utilization of industrial wastes in radiation shielding concrete. Materials Today: Proceedings, 32, 746–751.

Uddin, M. N., & Hossain, M., & Mahmud, N., & Alam, S., & Hossain, Md & Mahedi, S., & Ali, A. (2024). Research and applications of nanoclays: A review. SPE Polymers. 5. 507-535. 10.1002/pls2.10146.

Wang, H., Ma, Y., Pratx, G., & Xing, L. (2011). Toward real-time Monte Carlo simulation using a commercial cloud computing infrastructure. *Physics in medicine and biology*,*56*(17), N175–N181.

Winegardner, D.L. (1995). An Introduction to Soils for Environmental Professionals (1st ed.). Routledge.

Zhao, S., Huo, Z., Zhong, G., Zhang, H., & Hu, L. (2021). Research progress of neutron and gamma-ray composite shielding materials. Journal of Functional Materials, 52(3), 3001–3015.

APPENDIXES

Appendix 1: ANOVA TABLES

Table A1.1a: ANOVA table comparing the results of Am-241 LAC for X0 and X1 series

Anova: Single Factor

SUMMARY

Groups	*Count*	*Sum*	*Average*	*Variance*
Column 1	6	2.697	0.4495	0.001816
Column 2	6	2.764	0.460667	0.001985

ANOVA

Source of Variation	*SS*	*df*	*MS*	*F*	*P-value*	*F crit*
Between Groups	0.000374	1	0.000374	0.196836	0.666732	4.964603
Within Groups	0.019005	10	0.0019			
Total	0.019379	11				

Table A1.1b: ANOVA table comparing the results of Am-241 LAC for X0 and X2 series

Anova: Single Factor

SUMMARY

Groups	*Count*	*Sum*	*Average*	*Variance*
Column 1	6	2.697	0.4495	0.001816
Column 2	6	3.412	0.568667	0.001161

ANOVA

Source of Variation	*SS*	*df*	*MS*	*F*	*P-value*	*F crit*
Between Groups	0.042602	1	0.042602	28.61345	0.000324	4.964603
Within Groups	0.014889	10	0.001489			
Total	0.057491	11				

Table A1.1c: ANOVA table comparing the results of Am-241 MAC for X0 and X1 series

Anova: Single Factor

SUMMARY

Groups	*Count*	*Sum*	*Average*	*Variance*
Column 1	6	1.457925	0.242988	8.01E-05
Column 2	6	1.465089	0.244182	7.93E-05

ANOVA

Source of Variation	*SS*	*df*	*MS*	*F*	*P-value*	*F crit*
Between Groups	4.28E-06	1	4.28E-06	0.053667	0.821473	4.964603
Within Groups	0.000797	10	7.97E-05			
Total	0.000801	11				

Table A1.1d: ANOVA table comparing the results of Am-241 MAC for X0 and X2 series

Anova: Single Factor

SUMMARY

Groups	*Count*	*Sum*	*Average*	*Variance*
Column 1	6	1.457925	0.242988	8.01E-05
Column 2	6	1.738858	0.28981	1.78E-05

ANOVA

Source of Variation	*SS*	*df*	*MS*	*F*	*P-value*	*F crit*
Between Groups	0.006577	1	0.006577	134.3974	4.04E-07	4.964603
Within Groups	0.000489	10	4.89E-05			
Total	0.007066	11				

Table A1.2a: ANOVA table comparing the results of Cs-137 LAC for X0 and X1 series

Anova: Single Factor

SUMMARY

Groups	*Count*	*Sum*	*Average*	*Variance*
Column 1	6	0.764	0.127333	6.07E-05
Column 2	6	0.782	0.130333	5.95E-05

ANOVA

Source of Variation	*SS*	*df*	*MS*	*F*	*P-value*	*F crit*
Between Groups	0.000027	1	0.000027	0.449501	0.517756	4.964603
Within Groups	0.000601	10	6.01E-05			
Total	0.000628	11				

Table A1.2b: ANOVA table comparing the results of Cs-137 LAC for X0 and X2 series

Anova: Single Factor

SUMMARY

Groups	*Count*	*Sum*	*Average*	*Variance*
Column 1	6	0.764	0.127333	6.07E-05
Column 2	6	0.825	0.1375	6.27E-05

ANOVA

Source of Variation	*SS*	*df*	*MS*	*F*	*P-value*	*F crit*
Between Groups	0.00031	1	0.00031	5.02702	0.04883	4.964603
Within Groups	0.000617	10	6.17E-05			
Total	0.000927	11				

Table A1.2c: ANOVA table comparing the results of Cs-137 MAC for X0 and X1 series

Anova: Single Factor

SUMMARY

Groups	*Count*	*Sum*	*Average*	*Variance*
Column 1	6	0.413802	0.068967	9.01E-07
Column 2	6	0.415409	0.069235	8.34E-07

ANOVA

Source of Variatio	*SS*	*df*	*MS*	*F*	*P-value*	*F crit*
Between Groups	2.15E -07	1	2.15E-07	0.248259	0.629079	4.964603
Within Groups	8.67E -06	10	8.67E-07			
Total	8.89E-06	11				

Table A1.2d: ANOVA table comparing the results of Cs-137 MAC for X0 and X2 series

Anova: Single Factor

SUMMARY

Groups	*Count*	*Sum*	*Average*	*Variance*
Column 1	6	0.413802	0.068967	9.01E-07
Column 2	6	0.420473	0.070079	3.54E-07

ANOVA

Source of Variatio	*SS*	*d*	*MS*	*F*	*P-value*	*F crit*
Between Groups	3.71E-06	1	3.71E-06	5.913809	0.035339	4.964603
Within Groups	6.27E-06	1	6.27E-07			
Total	9.98E-06	11				

Table A1.3a: ANOVA table comparing the results of Co-60 LAC for X0 and X1 series

Anova: Single Factor

SUMMARY

Groups	*Count*	*Sum*	*Average*	*Variance*
Column 1	6	0.55	0.091667	4.51E-05
Column 2	6	0.566	0.094333	4.39E-05

ANOVA

Source of Variation	*SS*	*df*	*MS*	*F*	*P-value*	*F crit*
Between Groups	2.13E-05	1	2.13E-05	0.47976	0.504298	4.964603
Within Groups	0.000445	10	4.45E-05			
Total	0.000466	11				

Table A1.3b: ANOVA table comparing the results of Co-60 LAC for X0 and X2 series

Anova: Single Factor

SUMMARY

Groups	*Count*	*Sum*	*Average*	*Variance*
Column 1	6	0.55	0.091667	4.51E-05
Column 2	6	0.596	0.099333	4.31E-05

ANOVA

Source of Variation	*SS*	*df*	*MS*	*F*	*P-value*	*F crit*
Between Groups	0.000176	1	0.000176	4.001513	0.073342	4.964603
Within Groups	0.000441	10	4.41E-05			
Total	0.000617	11				

Table A1.3c: ANOVA table comparing the results of Co-60 MAC for X0 and X1 series

Anova: Single Factor

SUMMARY

Groups	*Count*	*Sum*	*Average*	*Variance*
Column 1	6	0.297665	0.049611	4.27E-07
Column 2	6	0.300483	0.050081	6.07E-07

ANOVA

Source of Variation	*SS*	*Df*	*MS*	*F*	*P-value*	*F crit*
Between Groups	6.62E-07	1	6.62E-07	1.281473	0.28404	
Within Groups	5.17E-06	10	5.17E-07			
Total	5.83E-06	11				

Table A1.3d: ANOVA table comparing the results of Co-60 MAC for X0 and X2 series

Anova: Single Factor

SUMMARY

Groups	*Count*	*Sum*	*Average*	*Variance*
Column 1	6	0.297665	0.049611	4.27E-07
Column 2	6	0.303657	0.050609	8.85E-07

ANOVA

Source of Variation	*SS*	*df*	*MS*	*F*	*P-value*	*F crit*
Between Groups	2.99E-06	1	2.99E-06	4.560807	0.058467	4.964603
Within Groups	6.56E-06	10	6.56E-07			
Total	9.55E-06	11				

Appendix 2: Radiation Shielding Parameters

Table A2.1a: Radiation Shielding parameters of Am-241 in various materials

Sample	Density (g/cm^{-3})	Linear Attenuation Coefficient (cm^{-1})	Mass Attenuation Coefficient	HVL (cm)	TVL (cm)	mfp(cm)	BuildUp factor (EXPERIME
ABK-X0	1.995151	0.488	0.244593	1.420381	4.718412	2.049182	1.057
AMK-X0	1.880903	0.466	0.247753	1.48744	4.941172	2.145923	0.9801
FOS-X0	1.651400	0.372	0.225262	1.863295	6.189745	2.688172	0.9934
KBU-X0	1.874181	0.457	0.24384	1.516735	5.038475	2.188184	0.9444
OFM-X0	1.755478	0.433	0.246657	1.600803	5.317742	2.309464	0.9791
OKY-X0	1.925382	0.481	0.24982	1.441054	4.787072	2.079002	1.0086
ABK-X1	2.039091	0.502	0.246188	1.380771	4.586822	1.992031	1.0163
AMK-X1	1.933181	0.481	0.248812	1.441054	4.787072	2.079002	0.9805
FOS-X1	1.679803	0.382	0.227408	1.814521	6.027712	2.617801	1.0143
KBU-X1	1.929921	0.468	0.242497	1.481081	4.920051	2.136751	0.9748
OFM-X1	1.772021	0.438	0.247175	1.582521	5.257042	2.283101	0.9815
OKY-X1	1.948546	0.493	0.253009	1.405978	4.670558	2.028392	1.0238
ABK-X2	2.069571	0.596	0.287982	1.162992	3.863398	1.677852	0.9861
AMK-X2	2.031982	0.587	0.28888	1.180833	3.922632	1.703573	0.9481
FOS-X2	1.796012	0.51	0.283961	1.359113	4.514872	1.960781	0.99
KBU-X2	1.996792	0.582	0.291467	1.190975	3.956332	1.718212	0.9666
OFM-X2	1.880352	0.545	0.289839	1.271837	4.224927	1.834862	0.9551
OKY-X2	1.995096	0.592	0.296728	1.170857	3.889508	1.689181	0.9737
Alucobond-4mm(x75=30cm)	1.1035	0.295	0.267331	2.349651	7.805373	3.389831	1.0002
Polyethylene*	0.93	0.1832	0.196989	3.78355	12.5687	5.45851	1
Ordinary Concrete*	2.3	0.6118	0.266	1.132964	3.763624	1.634521	1
Aluminum*	2.699	0.7498	0.277807	0.924442	3.070932	1.333680	1

*From Literature (Martin (2006))

Table A2.1b: Radiation Shielding parameters of Cs-137 in various materials

Sample	Density (g/cm^{-3})	Linear Attenuation Coefficient (cm^{-1})	Mass Attenuation Coefficient (cm^2/g)	HVL (cm)	TVL (cm)	Mfp (cm)	BuildUp factor (EXPERIMENTAL)
ABK-X0	1.995151	0.138	0.069168	5.0228	16.6854	7.24637	0.989
AMK-X0	1.880903	0.127	0.067521	5.4578	18.1305	7.87401	0.9972
FOS-X0	1.651409	0.116	0.070243	5.9754	19.8498	8.62069	0.995
KBU-X0	1.874181	0.128	0.068297	5.4152	17.9889	7.8125	0.994
OFM-X0	1.755478	0.122	0.069497	5.6815	18.8736	8.19672	0.9918
OKY-X0	1.925383	0.133	0.069077	5.2116	17.3126	7.51879	0.986
ABK-X1	2.039091	0.14	0.068658	4.9510	16.4470	7.14285	0.9928
AMK-X1	1.933184	0.133	0.068798	5.2116	17.3126	7.51879	0.9955
FOS-X1	1.679803	0.118	0.070246	5.8741	19.5134	8.47457	1.0092
KBU-X1	1.92992	0.132	0.068397	5.2511	17.4438	7.57575	1.0035
OFM-X1	1.772024	0.125	0.070541	5.5451	18.4206	8	1.0034
OKY-X1	1.948546	0.134	0.068769	5.172	17.1834	7.46268	0.9989
ABK-X2	2.069571	0.145	0.070063	4.7803	15.8799	6.89655	1.0015
AMK-X2	2.031989	0.142	0.069882	4.8813	16.2153	7.04225	0.9969
FOS-X2	1.796018	0.124	0.069042	5.5898	18.5692	8.06451	0.9983
KBU-X2	1.996793	0.141	0.070613	4.9159	16.3303	7.09219	1.0015
OFM-X2	1.880352	0.132	0.0702	5.2511	17.4438	7.57575	1.0001
OKY-X2	1.995096	0.141	0.070673	4.9159	16.3303	7.09219	1.0053
Alucobond-4mm(x75=30cm)	1.1035	0.093	0.084277	7.453195	24.75898	10.75269	1.0015
Polyethylene*	0.93	0.0823	0.088495	8.4222	27.9779	12.15067	1
Ordinary Concrete*	2.3	0.1822	0.079217	3.80432	12.63768	5.488474	1
Aluminum*	2.699	0.2024	0.074991	3.424	11.3764	4.940711	1

*From Literature (Martin (2006))

Table A2.1c: Radiation Shielding parameters of Co-60 in various materials

Sample	Density (g/cm^3)	Linear Attenuation Coefficient (cm^{-1})	Mass Attenuation Coefficient	HVL (cm)	TVL (cm)	mfp(cm)	BuildUp factor (EXPERIME
ABK-X0	1.995151	0.099	0.04962	7.00148	23.2584	10.1010	0.9945
AMK-X0	1.880903	0.094	0.049976	7.37390	24.4955	10.6383	0.9849
FOS-X0	1.651409	0.08	0.048443	8.6643	28.7823	12.5	0.9914
KBU-X0	1.874181	0.094	0.050155	7.37390	24.4955	10.6383	0.962
OFM-X0	1.755478	0.088	0.050129	7.87667	26.1657	11.3636	0.9983
OKY-X0	1.925383	0.095	0.049341	7.29628	24.2377	10.5263	0.9936
ABK-X1	2.039091	0.102	0.050022	6.79556	22.5743	9.80392	0.9821
AMK-X1	1.933184	0.095	0.049142	7.29628	24.2377	10.5263	1.001
FOS-X1	1.679803	0.083	0.049411	8.35117	27.7419	12.0481	1.0031
KBU-X1	1.92992	0.097	0.050261	7.14584	23.7379	10.3092	0.9986
OFM-X1	1.772024	0.091	0.051354	7.61700	25.3031	10.9890	1.0083
OKY-X1	1.948546	0.098	0.050294	7.0729	23.4957	10.2040	0.9981
ABK-X2	2.069571	0.107	0.051702	6.47801	21.5194	9.34579	0.9939
AMK-X2	2.031989	0.102	0.050197	6.79556	22.5743	9.80392	1.001
FOS-X2	1.796018	0.088	0.048997	7.87667	26.1657	11.3636	0.9993
KBU-X2	1.996793	0.101	0.050581	6.86284	22.7978	9.90099	0.9945
OFM-X2	1.880352	0.096	0.051054	7.22028	23.9852	10.4166	0.9951
OKY-X2	1.995096	0.102	0.051125	6.79556	22.5743	9.80392	0.9987
Alucobond-4mm(x75=30cm)	1.1035	0.073	0.066153	9.494167	31.54226	13.69863	1.0021
Polyethylene*	0.93	0.0604	0.064946	11.4759	38.1222	16.5562	1
Ordinary Concrete*	2.3	0.1336	0.058087	5.188227	17.23492	7.48503	1
Aluminum*	2.699	0.1483	0.054946	4.67395	15.5265	6.74308	1

From Literature (Martin (2006))